# La Théorie des Jeux à Champ-Moyen Appliquée à la Dynamique des Piétons

Butano Matteo

université PARIS-SACLAY

# Mean-Field Games Applied to Pedestrian Dynamics

*La Théorie des Jeux à Champ-Moyen Appliquée à la Dynamique des Piétons*

**Thèse de doctorat de l'université Paris-Saclay**

École doctorale n° 564, Physique en Île-de-France (PIF)
Spécialité de doctorat: Physique
Graduate School : Physique. Référent : Faculté des sciences d'Orsay

Thèse préparée dans l'unité de recherche LPTMS (Université Paris-Saclay, CNRS) sous la direction de **Denis ULLMO**, directeur de recherche CNRS, et la co-direction de **Cécile APPERT-ROLLAND**, directrice de recherche CNRS.

**Thèse soutenue à Paris-Saclay, le 30 Août 2024, par**

**Matteo BUTANO**

## Composition du jury

Membres du jury avec voix délibérative

| | |
|---|---|
| **Bertrand MAURY**<br>Professeur associé au DMA, Ecole Normale Supérieure PSL | Président |
| **Marie-Therese WOLFRAM**<br>Professeur, Mathematics Institute University of Warwick, Coventry, UK | Rapporteuse & Examinatrice |
| **Thierry GOBRON**<br>Chargé de Recherche CNRS (HDR), Laboratoire Paul Painlevé Université de Lille | Rapporteur & Examinateur |
| **Antoine TORDEUX**<br>Assitant Professeur, Bergische Universität Wuppertal | Examinateur |

THESE DE DOCTORAT

NNT : 2024UPASP064

université PARIS-SACLAY | ÉCOLE DOCTORALE Physique en Île-de-France (PIF)

**Titre:** La Théorie des Jeux à Champ-Moyen Appliquée à la Dynamique des Piétons
**Mots clés:** Jeux à Champ-Moyen, Dynamique de Piétons, Physique des Systèmes Complexes

**Résumé:**Cette thèse explore la dynamique des piétons à travers des observations expérimentales et des simulations, en se concentrant sur l'aspect opérationnel. Des expériences avec des foules contrôlées révèlent que les piétons manifestent des comportements anticipatoires qui dévient du comportement granulaire. Cette thèse remet en question deux modèles existants de dynamique des piétons, de complexité différente, en montrant leurs limites à capturer les comportements anticipatoires observés. Ces modèles sont jugés trop myopes, se concentrant sur des décisions à court terme sans tenir compte de manière adéquate des anticipations à long terme. Pour remédier à ces lacunes, ce travail propose un modèle basé sur la théorie des jeux à champ moyen (MFG). Les modèles MFG, qui combinent le contrôle optimal et la théorie des jeux, décrivent les interactions entre un grand nombre d'agents via leur densité moyenne. Le modèle MFG prédit avec succès les schémas d'anticipation expérimentaux en incorporant un taux de réduction qui ajuste l'importance des événements futurs dans le processus d'optimisation. De plus, la thèse présente deux projets corollaires. Le premier a pour but d'integrer les MFG avec des modèles microscopiques basés sur les agents pour traiter des scénarios nécessitant des interactions individuelles détaillées, comme les évacuations. Le second explore l'utilisation des Physics Informed Neural Networks pour résoudre les équations des MFG.

**Title:** Mean-Field Games Applied to Pedestrian Dynamics
**Keywords:** Mean-Field Games, Pedestrian Dynamics, Physics of Complex Systems

**Abstract:** This thesis explores pedestrian dynamics through experimental observations and simulations, focusing on the operational layer of pedestrian movement. Experiments involving a controlled crowd and a moving cylindrical obstacle, reveal that pedestrians exhibit anticipatory behaviors that deviate from granular behavior. The thesis challenges two existing pedestrian dynamics models, of different complexity showing their limitations in capturing the observed anticipatory behaviors. These models are found to be too myopic, focusing on short-term decisions without adequately accounting for long-term anticipations. To address these shortcomings, this work proposes a model based on the theory of Mean-Field Games (MFG). MFG models, which combine optimal control and game theory, describe interactions among a large number of agents via their average density, simplifying the mathematical framework. The MFG model successfully predicts the experimental anticipation patterns by incorporating a discount factor that adjusts the weight of future events in the optimization process. Additionally, the thesis presents two corollary projects. The first has the goal to integrate MFG with agent-based microscopic models to handle scenarios requiring detailed individual interactions, such as evacuations. The second explores using Physics Informed Neural Networks to solve MFG equations.

# Contents

# General Introduction

Many dedicated researchers have recently been trying to provide their best interpretation and contribution to how individuals move. Indeed, pedestrian dynamics models play a crucial role in urban planning, architecture, transportation engineering, and crowd management. These models provide insights into the behavior of individuals in pedestrian environments, helping designers and policymakers create safer, more efficient, and more accessible spaces. By simulating pedestrian movements, these models can predict congestion, identify potential bottlenecks, and optimize layouts to enhance flow and mitigate risks. Moreover, they aid in the design of public spaces that accommodate diverse needs, including those of people with disabilities or mobility challenges. Understanding pedestrian dynamics is essential for creating sustainable, inclusive cities where people can move freely and comfortably, promoting both safety and quality of life. Pedestrian dynamics models are not only instrumental in optimizing urban spaces for efficiency but also in ensuring safety. By accurately simulating pedestrian behavior, these models can anticipate potential incidents such as overcrowding, stampedes, or evacuation scenarios. This predictive capability allows designers and authorities to implement preemptive measures to mitigate risks and enhance safety protocols. Additionally, these models enable the testing of emergency evacuation plans and the assessment of crowd management strategies, ensuring that urban environments are resilient in the face of unforeseen events. Ultimately, the ability to accurately simulate pedestrian dynamics contributes to the creation of environments that prioritize both efficiency and safety, fostering thriving and resilient communities.

To better understand pedestrian dynamics modeling, it is helpful to adhere to the recommendations of [45], who propose that pedestrians' movement can be categorized into three distinct layers. First, the strategic layer, pertaining to the choice of the goal of the motion. Then there is a tactical layer, or which way to take to achieve the objective. Ultimately, the operational aspect of the motion is considered, covering all the minor decisions and adjustments made by pedestrians during their trajectory. In particular, the motivation for our work stems from a consideration that has been circulating for quite some time in the field of pedestrian dynamics. It has been observed that human crowds, especially at the operational level, sometimes resemble granular matter, especially as their density increases. This was first suggested by Helbing in [41]. Here the author affirms that by observing some time-lapse footage of human crowds in motion, it is possible to draw some qualitative resemblances with both fluids and granular matter. In particular, Helbing observations focus on a few features of pedestrians' motion, among

which the formation of streamlines when two crowds of pedestrians moving in opposite directions cross each other, the propagation of shock waves and the oscillation of the passing direction through a narrow choke point where two masses of pedestrian meet. Further examples of the analogy between pedestrians and inert matter was given in [43], where the authors analyzed the video recording of the tragic stampedes of 2006 at the Hajj pilgrimage to explore the onset of phase transitions and turbulence in pedestrian flows during panic movement. Furthermore, [77, 89] study the evacuation times through a bottleneck by three different kinds of crowds, made by humans, animals (sheep) or granular material, to show that the faster-is-slower (FIS) effect, i.e., the fact that individuals all trying to exit a room at a faster speed end up evacuating in more time than calmer crowds, is universal among these types of throngs.

To further investigate the validity of the analogy, Nicolas et al. [75] decided to perform a test with a human crowd that is considered a classic one for grains, the passage of a cylindrical intruder. To achieve this, a conjoint effort between the French team of Alexandre Nicolas and Cécile Appert-Rolland and their Argentinian counterparts Kuperman and Ibañez took place. The two teams organized two identical experimental set-ups in Orsay, France, and Bariloche, Argentina respectively: a crowd of volunteers (35–40 people) was gathered in a controlled environment and arranged to obtain various average densities, then, one staff member, equipped with a cylindrical outfit to simulate a moving obstacle made his/her way through the crowd, keeping a constant velocity and walking as straight as possible. The experiment was initially carried out in two configurations, one with all participants facing the obstacle, and the other where they were randomly oriented, to see if any difference was visible. Contrary to the expectations, the outcome did not bear any resemblance to the granular behavior. In fact, as section 1.1 will show, grains tend to be pushed along by the intruder, whereas participants in the experiment in the two configurations, as reported in section 1.2, showed a radically different response. Indeed, individuals anticipated, in the facing case more than in the random case, the arrival of the obstacle and stepped aside to let it pass.To see if they could recover the granular behavior, the experimenters asked participants to try not to anticipate the intruder's arrival, and to let them be pushed away. However, even in that case, pedestrians still instinctively anticipated, and it was only when they were also asked to give their back to the cylinder that the empirical behavior started to look like grains.

One of the goals of the project I took part into was to prove that the anticipation displayed by pedestrians in the experiment, when participants were facing the obstacles, is a crucial element of pedestrian dynamics, and that nevertheless the most common simulating techniques fail to fully capture it. To show this, we will simulate this experimental scenario using two models for

pedestrians dynamics that are described in chapter 2. There, we will explain the difference between microscopic models, namely those that describe each pedestrian individually, and macroscopic models, that, on the other hand, consider the crowd as a whole and focus on the evolution of the density. In particular, since microscopic models are generally considered more precise, we will only use models of this kind to compare to the experiment. The first of the models we will use is Helbing's social force model [44], described in section 2.1.1. In this model, the preferences of individuals in crowded environments are translated into forces resulting from social constraints. In particular, Helbing considers the desire of people not to be too close to others. The use of forces analogous to natural ones but of social origin in Helbing's model prompted a series of significant contributions in the field of pedestrian dynamics. The majority of these contributions built on Helbing's intuition and proposed novel approaches to comprehend and delineate such societal constraints on human motion. The second we will use is another microscopic model, the one developed by one of the authors of the experiment, A. Nicolas, in collaboration with I. Echeverria-Huarte [33]. This is a very recent model that brings together many of the observations and results in the field, to offer a flexible and realistic simulation tool. As section 2.1.2 will show, this model is based upon the minimization of a cost functional, something that will become interesting later. The results of the comparison are collected in section 4.1, where we will indeed show that neither model can fully reproduce what the experiment shows.

The other objective of this thesis is to show that a model based on a minimal version of the theory of Mean-Field Games can, contrarily to other models, fully capture the experimental behavior. Mean-field games (MFG) are optimally driven stochastic processes. These models, based on the union of optimal control and game theory, describe situations where a multitude of rational agents interact, in a competitive or cooperative way, while trying to reach an objective or a target. Introduced almost two decades ago by the works of Lasry and Lions on one side, and of Huang, Malhamé and Caines on the other, mean-field games suppose that the behavior of each simulated agent can be modeled as a stochastic process using a Langevin equation, where the drift term is obtained minimizing (maximizing) a certain cost (gain) functional. This functional describes the preferences of the agents and the way they interact. In particular, one of the key assumptions of MFG is that when the number of players goes to infinity, these become indistinguishable and the way they interact with each other is via their average density, which makes the mathematics of the problem more tractable. Chapter 3 will be dedicated to a detailed introduction to MFG. In subsection 3.3.2, we will also present an alternative formulation of the problem, allowing us to leverage the knowledge generated in another field of physics, that of the Non-Linear Schrödinger

Equation (NLSE). We will use this analogy to introduce some mathematical tools that will grant us a greater understanding of Mean-Field Games.

Chapter 4 will then present the bulk of the work done during my doctorate. First, in section 4.1, we will show how the Helbing's social force and ANDA simulate the experiment of section 1.2 in the frontal configuration, and how both of them fail to fully capture the empirical anticipation pattern. We will argue that the reason lies in the fact that these models' agents are too myopic, since they choose how to move based only on a small portion of future events. Then, in section 4.2 we prove that indeed the MFG model succeeds where the others fail, predicting an anticipation pattern very similar to the empirical one, and explaining that indeed it is in long-term anticipation that lies the key to explaining the empirical behavior. In section 4.3, we will treat the other two configurations, and show that what causes the change in the empirical behavior is the impairment of pedestrians' forecasting ability, their anticipation. We achieve this by showing that adding only one parameter to our MFG model, namely the *discount factor*, modulating the weight given to future events during the optimization, is enough to simulate the experimental configurations where people were randomly oriented or were giving their back to the intruder.

We will dedicate the last chapter to the presentation of two projects, corollary to the main one, that I have been working on during these years. Section 5.1 will present a simulation software that I developed, and that I baptized *Optimal Crowds*. The intent behind this work is to create a simulation tool that couples the benefits of MFG with the flexibility of the agent-based microscopic models. In fact, although MFG provides an accurate representation of the long-term anticipation of pedestrians, by modeling the crowd via their density, it cannot describe those situations where interactions at a microscopic level play a major role, for example near doors during an evacuation. The model I propose is therefore an agent-based model, where the microscopic part is based on the work of Chraibi and Seyfried [23], a force model where agents have an elliptical form whose dimensions evolve as a function of the speed. The trajectories followed by the pedestrians are given by a velocity floor field, along which each individual tries to align. MFG would therefore enter into play for the definition of said floor field. In fact, the goal of the project was to obtain the velocity field by solving a MFG, to account for the presence of eventual obstacles and for the distribution of the density in the environment, providing the simulated pedestrians with a route ensuring an optimal behavior (in the sense of MFG). However, in the current state of the project we are yet to find a way to properly define and solve such MFG. At the moment in fact, we define the velocity field floor simply by solving a Hamilton-Jacobi-Bellman equation, which is one of the MFG equations. In the most stable form of the algorithm we solve this equation without information about the den-

sity of pedestrians but only with the description of the environment. In this way, we ensure an optimal avoidance of the obstacles but we cannot prevent bottlenecks. However, we are working on periodically including the density in the solution of the HJB equation, to make pedestrians stuck in bottlenecks to find an alternative trajectory, in the spirit of Hoogendoorn's works [45, 46].

Finally, section 5.2 will discuss the second of these corollary projects, done in collaboration with London's Imperial College, namely the one where we use Neural Networks (NN) to solve the MFG equations. In fact, as we will better explain in 4.4, once we will introduce the *discount factor*, the MFG equations will become more complicated to solve. In particular, we will introduce even more non-linearities, and this is where usual finite different numerical schemes start to suffer and give poor results. However, solving any well defined differential equation can be seen as simply finding the zeros of a operator whose arguments are functions. Under this light, we can imagine to approximate the argument of the operator as a Neural Network, which, thanks to a well known theoretical results, are actually universal approximators under certain hypotheses. Therefore, the goal would be to train the NN to become a zero of said operator. In this way, at least in principle, we could deal with equations of any complexity, as long as they are well defined. Unfortunately however, as section 5.2 will show, this is only true in principle, as the reality is that the nature of the equation strongly influences the kind of NN needed to solve it. In this thesis, we will show how we could solve some simpler form of the MFG equations. In particular, we could solve a one-dimensional version of the problem, with and without information about the environment and other agents. Then, we will show our best attempt the complete problem.

# Introduction Générale

De nombreux chercheurs dévoués ont récemment tenté de fournir leur meilleure interprétation et contribution à la compréhension des mouvements des individus. En effet, les modèles de dynamique piétonne jouent un rôle crucial dans la planification urbaine, l'architecture, le génie des transports et la gestion des foules. Ces modèles fournissent des informations sur le comportement des individus dans des environnements piétons, aidant les concepteurs et les décideurs à créer des espaces plus sûrs, plus efficaces et plus accessibles. En simulant les mouvements des piétons, ces modèles peuvent prédire les embouteillages, identifier les goulets d'étranglement potentiels et optimiser les aménagements pour améliorer le flux et réduire les risques. De plus, ils aident à concevoir des espaces publics qui répondent à des besoins divers, y compris ceux des personnes handicapées ou ayant des difficultés de mobilité. Comprendre la dynamique piétonne est essentiel pour créer des villes durables et inclusives où les gens peuvent se déplacer librement et confortablement, favorisant à la fois la sécurité et la qualité de vie. Les modèles de dynamique piétonne sont non seulement instrumentaux pour optimiser l'efficacité des espaces urbains, mais aussi pour garantir la sécurité. En simulant avec précision le comportement des piétons, ces modèles peuvent anticiper des incidents potentiels tels que la surpopulation, les bousculades ou les scénarios d'évacuation. Cette capacité prédictive permet aux concepteurs et aux autorités de mettre en œuvre des mesures préventives pour atténuer les risques et renforcer les protocoles de sécurité. De plus, ces modèles permettent de tester des plans d'évacuation d'urgence et d'évaluer des stratégies de gestion des foules, garantissant que les environnements urbains soient résilients face aux événements imprévus. En fin de compte, la capacité de simuler avec précision la dynamique piétonne contribue à la création d'environnements qui priorisent à la fois l'efficacité et la sécurité, favorisant des communautés prospères et résilientes.

Pour mieux comprendre la modélisation de la dynamique piétonne, il est utile de suivre les recommandations de [45], qui proposent que le mouvement des piétons peut être catégorisé en trois couches distinctes. Tout d'abord, la couche stratégique, concernant le choix de l'objectif du mouvement. Ensuite, il y a la couche tactique, ou la manière de choisir le chemin pour atteindre l'objectif. Enfin, l'aspect opérationnel du mouvement est pris en compte, couvrant toutes les petites décisions et ajustements effectués par les piétons au cours de leur trajet. En particulier, la motivation de notre travail découle d'une considération qui circule depuis un certain temps dans le domaine de la dynamique piétonne. Il a été observé que les foules humaines, surtout au niveau opérationnel, ressemblent parfois à de la matière gran-

ulaire, surtout lorsque leur densité augmente. Cela a été suggéré pour la première fois par Helbing dans [41]. Ici, l'auteur affirme qu'en observant certaines séquences vidéo accélérées de foules humaines en mouvement, il est possible de dégager quelques similitudes qualitatives avec à la fois des fluides et de la matière granulaire. En particulier, les observations d'Helbing se concentrent sur quelques caractéristiques du mouvement des piétons, parmi lesquelles la formation de lignes de courant lorsque deux foules de piétons se déplaçant dans des directions opposées se croisent, la propagation des ondes de choc et l'oscillation de la direction de passage à travers un point d'étranglement étroit où deux masses de piétons se rencontrent. D'autres exemples de l'analogie entre les piétons et la matière inerte ont été donnés dans [43], où les auteurs ont analysé l'enregistrement vidéo des bousculades tragiques de 2006 lors du pèlerinage de Hajj pour explorer l'apparition de transitions de phase et de turbulences dans les flux piétons en situation de panique. En outre, [77, 89] étudient les temps d'évacuation à travers un goulot d'étranglement par trois types de foules différents, composés d'humains, d'animaux (moutons) ou de matière granulaire, pour montrer que l'effet plus-vite-est-plus-lent (FIS), c'est-à-dire le fait que des individus essayant tous de sortir d'une pièce à une vitesse plus rapide finissent par évacuer en plus de temps que des foules plus calmes, est universel parmi ces types de groupes.

Pour approfondir la validité de l'analogie, Nicolas et al. [75] ont décidé de réaliser un test avec une foule humaine qui est considéré comme un classique pour les grains : le passage d'un intrus cylindrique. Pour y parvenir, un effort conjoint entre l'équipe française d'Alexandre Nicolas et Cécile Appert-Rolland et leurs homologues argentins Kuperman et Ibañez a eu lieu. Les deux équipes ont organisé deux configurations expérimentales identiques à Orsay, en France, et à Bariloche, en Argentine respectivement : une foule de volontaires (35-40 personnes) a été rassemblée dans un environnement contrôlé et disposée pour obtenir différentes densités moyennes, puis un membre de l'équipe, équipé d'une tenue cylindrique pour simuler un obstacle en mouvement, s'est frayé un chemin à travers la foule, en maintenant une vitesse constante et en marchant aussi droit que possible. L'expérience a été initialement menée dans deux configurations, l'une avec tous les participants face à l'obstacle, et l'autre où ils étaient orientés aléatoirement, pour voir si une différence était visible. Contrairement aux attentes, le résultat ne ressemblait en rien au comportement granulaire. En fait, comme la section 1.1 le montrera, les grains ont tendance à être poussés par l'intrus, alors que les participants à l'expérience dans les deux configurations, comme rapporté dans la section 1.2, ont montré une réponse radicalement différente. En effet, les individus anticipaient, dans le cas face à l'obstacle plus que dans le cas aléatoire, l'arrivée de l'obstacle et s'écartaient pour le laisser passer. Pour voir s'ils pouvaient retrouver le comportement granulaire, les expérimenta-

teurs ont demandé aux participants d'essayer de ne pas anticiper l'arrivée de l'intrus et de se laisser pousser. Cependant, même dans ce cas, les piétons anticipaient encore instinctivement, et ce n'est que lorsqu'on leur a également demandé de tourner le dos au cylindre que le comportement empirique a commencé à ressembler à celui des grains.

Un des objectifs du projet auquel j'ai participé était de prouver que l'anticipation affichée par les piétons dans l'expérience, lorsque les participants faisaient face aux obstacles, est un élément crucial de la dynamique piétonne, et que néanmoins les techniques de simulation les plus courantes échouent à le capturer pleinement. Pour montrer cela, nous allons simuler ce scénario expérimental en utilisant deux modèles de dynamique piétonne décrits dans le chapitre2. Nous y expliquerons la différence entre les modèles microscopiques, c'est-à-dire ceux qui décrivent chaque piéton individuellement, et les modèles macroscopiques, qui, en revanche, considèrent la foule dans son ensemble et se concentrent sur l'évolution de la densité. En particulier, puisque les modèles microscopiques sont généralement considérés comme plus précis, nous n'utiliserons que des modèles de ce type pour comparer avec l'expérience. Le premier modèle que nous utiliserons est le modèle de force sociale de Helbing [44], décrit dans la section 2.1.1. Dans ce modèle, les préférences des individus dans des environnements encombrés sont traduites en forces résultant de contraintes sociales. En particulier, Helbing considère le désir des gens de ne pas être trop proches des autres. L'utilisation de forces analogues à des forces naturelles mais d'origine sociale dans le modèle de Helbing a suscité une série de contributions significatives dans le domaine de la dynamique piétonne. La majorité de ces contributions se sont appuyées sur l'intuition de Helbing et ont proposé de nouvelles approches pour comprendre et décrire ces contraintes sociétales sur le mouvement humain. Le deuxième modèle que nous utiliserons est un autre modèle microscopique, celui développé par l'un des auteurs de l'expérience, A. Nicolas, en collaboration avec I. Echeverria-Huarte [33]. Il s'agit d'un modèle très récent qui rassemble de nombreuses observations et résultats dans le domaine, pour offrir un outil de simulation flexible et réaliste. Comme la section 2.1.2 le montrera, ce modèle est basé sur la minimisation d'une fonction de coût, ce qui deviendra intéressant par la suite. Les résultats de la comparaison sont rassemblés dans la section4.1, où nous montrerons en effet qu'aucun modèle ne peut reproduire pleinement ce que l'expérience montre.

L'autre objectif de cette thèse est de montrer qu'un modèle basé sur une version minimale de la théorie des jeux à champ moyen (Mean-Field Games, MFG) peut, contrairement à d'autres modèles, capturer pleinement le comportement expérimental. Les jeux à champ moyen sont des processus stochastiques optimisés. Ces modèles, basés sur l'union du contrôle optimal et de la théorie des jeux, décrivent des situations où une multitude d'agents ra-

tionnels interagissent, de manière compétitive ou coopérative, tout en essayant d'atteindre un objectif ou une cible. Introduits il y a près de deux décennies par les travaux de Lasry et Lions d'une part, et de Huang, Malhamé et Caines d'autre part, les jeux à champ moyen supposent que le comportement de chaque agent simulé peut être modélisé comme un processus stochastique utilisant une équation de Langevin, où le terme de dérive est obtenu en minimisant (maximisant) une certaine fonction de coût (gain). Cette fonction décrit les préférences des agents et la manière dont ils interagissent. En particulier, l'une des hypothèses clés des MFG est que lorsque le nombre de joueurs tend vers l'infini, ceux-ci deviennent indiscernables et la manière dont ils interagissent entre eux est via leur densité moyenne, ce qui rend les mathématiques du problème plus traitables. Le chapitre 3 sera consacré à une introduction détaillée aux MFG. Dans la sous-section 3.3.2, nous présenterons également une formulation alternative du problème, nous permettant de tirer parti des connaissances générées dans un autre domaine de la physique, celui de l'équation de Schrödinger non linéaire (NLSE). Nous utiliserons cette analogie pour introduire certains outils mathématiques qui nous permettront de mieux comprendre les jeux à champ moyen.

Le chapitre 4 présentera ensuite l'essentiel du travail effectué durant mon doctorat. Tout d'abord, dans la section 4.1, nous montrerons comment le modèle de force sociale de Helbing et l'ANDA simulent l'expérience de la section 1.2 dans la configuration frontale, et comment ils échouent tous les deux à capturer pleinement le schéma d'anticipation empirique. Nous soutiendrons que la raison réside dans le fait que les agents de ces modèles sont trop myopes, car ils choisissent comment se déplacer en se basant uniquement sur une petite partie des événements futurs. Ensuite, dans la section 4.2, nous prouverons que le modèle MFG réussit là où les autres échouent, en prédisant un schéma d'anticipation très similaire à celui empirique, et en expliquant que c'est en fait l'anticipation à long terme qui est la clé pour expliquer le comportement empirique. Dans la section 4.3, nous traiterons les deux autres configurations, et montrerons que ce qui cause le changement dans le comportement empirique est l'altération de la capacité de prévision des piétons, leur anticipation. Nous y parviendrons en montrant que l'ajout d'un seul paramètre à notre modèle MFG, à savoir le *taux d'actualisation*, modulant le poids donné aux événements futurs lors de l'optimisation, suffit pour simuler les configurations expérimentales où les personnes étaient orientées aléatoirement ou tournaient le dos à l'intrus.

Nous consacrerons le dernier chapitre à la présentation de deux projets, corollaires au principal, sur lesquels j'ai travaillé au cours de ces années. La section 5.1 présentera un logiciel de simulation que j'ai développé et que j'ai baptisé *Optimal Crowds*. L'intention derrière ce travail est de créer un outil de simulation qui combine les avantages des MFG avec la flexibilité des modèles

microscopiques basés sur les agents. En effet, bien que les MFG fournissent une représentation précise de l'anticipation à long terme des piétons en modélisant la foule via leur densité, ils ne peuvent pas décrire les situations où les interactions au niveau microscopique jouent un rôle majeur, par exemple près des portes lors d'une évacuation. Le modèle que je propose est donc un modèle basé sur les agents, où la partie microscopique est basée sur les travaux de Chraibi et Seyfried [23], un modèle de force où les agents ont une forme elliptique dont les dimensions évoluent en fonction de la vitesse.

Les trajectoires suivies par les piétons sont données par un champ de vitesse, le long duquel chaque individu essaie de s'aligner. Les MFG interviennent donc pour la définition de ce champ de vitesse. En fait, l'objectif du projet était d'obtenir le champ de vitesse en résolvant un MFG, pour tenir compte de la présence d'éventuels obstacles et de la distribution de la densité dans l'environnement, fournissant ainsi aux piétons simulés une route assurant un comportement optimal (au sens des MFG). Cependant, dans l'état actuel du projet, nous n'avons pas encore trouvé un moyen de définir et de résoudre correctement un tel MFG. À l'heure actuelle, nous définissons le champ de vitesse simplement en résolvant une équation de Hamilton-Jacobi-Bellman, qui est l'une des équations des MFG. Dans la forme la plus stable de l'algorithme, nous résolvons cette équation sans information sur la densité des piétons mais uniquement avec la description de l'environnement. De cette manière, nous assurons une évitement optimal des obstacles mais nous ne pouvons pas prévenir les goulets d'étranglement. Cependant, nous travaillons à inclure périodiquement la densité dans la solution de l'équation HJB, pour permettre aux piétons coincés dans des goulets d'étranglement de trouver une trajectoire alternative, dans l'esprit des travaux de Hoogendoorn [45, 46].

Enfin, la section 5.2 discutera du deuxième de ces projets corollaires, réalisé en collaboration avec l'Imperial College de Londres, à savoir celui où nous utilisons des réseaux de neurones (NN) pour résoudre les équations des MFG. En fait, comme nous l'expliquerons mieux dans la section 4.4, une fois que nous aurons introduit le *taux d'actualisation*, les équations des MFG deviendront plus compliquées à résoudre. En particulier, nous introduirons encore plus de non-linéarités, et c'est là que les schémas numériques classiques aux différences finies commencent à souffrir et à donner de mauvais résultats. Cependant, résoudre toute équation différentielle bien définie peut être vu comme simplement trouver les zéros d'un opérateur dont les arguments sont des fonctions. Sous cet angle, nous pouvons imaginer approximativement l'argument de l'opérateur comme un réseau de neurones qui, grâce à un résultat théorique bien connu, sont en fait des approximations universelles sous certaines hypothèses. Par conséquent, l'objectif serait de former le NN à devenir un zéro de cet opérateur. De cette manière, en principe du moins,

nous pourrions traiter des équations de toute complexité, tant qu'elles sont bien définies. Malheureusement cependant, comme la section 5.2 le montrera, cela n'est vrai qu'en principe, car la réalité est que la nature de l'équation influence fortement le type de NN nécessaire pour la résoudre. Dans cette thèse, nous montrerons comment nous avons pu résoudre certaines formes plus simples des équations des MFG. En particulier, nous avons pu résoudre une version unidimensionnelle du problème, avec et sans information sur l'environnement et les autres agents. Ensuite, nous montrerons notre meilleure tentative pour résoudre le problème complet.

# 1 - Context and Motivation

Our work is motivated by the findings of an experiment performed some years ago by Nicolas et al. [75], that challenged a belief shared by many, that, especially at high densities, the behavior of human crowds would be similar to that of granular matter. Therefore, Nicolas et al. decided that a good way to further inquire into this matter would be to perform a test using pedestrians that would be a standard one for amorphous media, the passage of an intruder. Much to their surprise, the behavior of pedestrians they observed differed substantially from what they would expect if the comparison with granular matter held through. In section 1.1 of this chapter, we will use a method created by A. Seguin to show how a cylindrical intruder moves through an amorphous medium. This model will be used to replicate the experimental setup and demonstrate how granular particles react to obstacles. This will set the benchmark against which we will compare the results of the experiment, which will be described in details in section 1.2, where we will explain why Nicolas et al. were surprised by their findings.

## 1.1 . Passage of an Intruder in a Granular Medium

The crossing by an intruder is a classical test in the field of granular matter. In fact, various experimental results can be found in the literature [19], where, as we can see from Figure 1.1, a cylinder is dragged with various forces through an assembly of smaller cylinders, representing grains, with different density configurations. Similar to when using a finger to draw into sand, most of the grains accumulate in front of the intruder along its direction of motion, leaving a wake promptly filled by the excess material escaping on the sides of the intruder. In this section, we will introduce a numerical model, first conceived by Antoine Seguin in his Ph.D. thesis [82], that simulates this scenario. This model was not first conceived to simulate pedestrians, although it could serve as a starting point to create a model with that intent. Nevertheless, it accurately represents granular matter, and our goal now is to show what the results of the experiment of Nicolas et al. would be if it were performed in such material. These models are based on the principle that two grains, should not overlap. This means that a purely theoretical approach would suggest choosing the grains' velocities only among those that ensure that no overlap will occur. Although it being technically implementable, such a method quickly becomes cumbersome when many grains are to be simulated. This is the reason the way these simulations are actually carried out allows for at least some amount of overlap in the form of the relaxation of

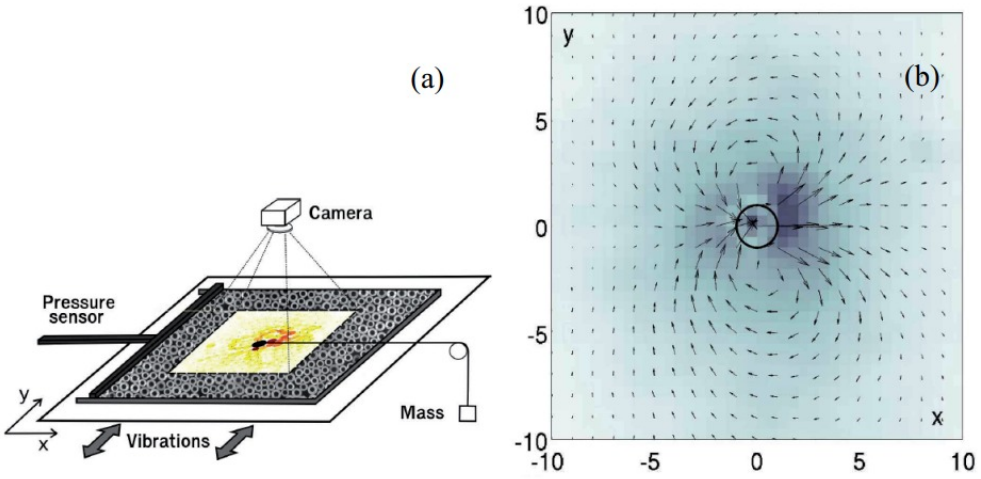


Figure 1.1: **Left**: Experimental setup where a cylindrical intruder is dragged through a granular medium. **Right**: velocity field measured in the experiment. Particles are pushed by the cylinder and circulate around it due to the vibration of the plate. Note that the cylinder moves from left to right. Figures extracted from [19].

the rigidity hypothesis of the grains, which physically means that if two grains overlap they are actually deforming one into the other, and they will both feel a repelling force related to the amount of the deformation following an elastic potential. More specifically, the force felt by two penetrating particles comes from Hertz's theory and reads:

$$F_n = -ka^{\frac{3}{2}} \tag{1.1}$$

where $a$ is the penetration's depth and $k$ is a constant expressing the sphere's rigidity and depends on its elastic properties. At this point, one can use any kind of algorithm to integrate the equation of motion and use the expression of the force (1.1) to simulate the motion of a particle. Most importantly, the choice of the time step is particularly delicate in this context. In fact, let us visualize the act of one particle impacting into another. When they touch each other, they deform and their velocity is reduced until, at some maximum penetration $a_{max}$ they halt. This happens when the kinetic energy $E_{kin}$ of the particles equals the elastic potential energy $E_{el}$. Then, both particles are repelled away from each other via the Hertz force. Now, if we want to accurately simulate this, since the particles' motion is discrete, we have to make sure that during one time step $\Delta t$ neither particle moves more than $a_{max}$. To do so, let us compute the elastic energy at maximum penetration. During the impact, the Hertz force $F_n$ performs a work

$$E_{el} = \int_0^{a_{max}} kx^{\frac{3}{2}} dx \sim ka_{max}^{\frac{5}{2}} \tag{1.2}$$

As we said, at $a_{max}$ the elastic energy equals the kinetic energy $E_{kin} \sim mv^2$ therefore we have

$$mv^2 \sim k a_{max}^{\frac{5}{2}}.$$

Moreover, since an estimate of $a_{max}$ can be obtained as $v\tau$ where $v$ is the velocity of the particle we are following just before impact and $\tau$ the time it takes to arrive at maximum penetration, we can finally write $mv^2 \sim k(v\tau)^{\frac{5}{2}}$, from which we get that one can choose safely the time step for the simulation by making sure that

$$\Delta t \ll \left(\frac{m^2}{vk^2}\right)^{\frac{1}{5}} \tag{1.3}$$

Now that we settled this, one last consideration is in order. This method is used by Seguin [12] to reproduce the passage of an obstacle with fixed velocity through granular matter. In this case however, the intruder would keep hitting other particles without being impacted, thus continuously adding energy to the system. One way to make up for this, as suggested again in [82], is to introduce a damping term in the expression of the force, which now becomes

$$F_n = -kx^{\frac{3}{2}} - \lambda_d \frac{da}{dt} \tag{1.4}$$

where $\lambda_d$ is linked to the coefficient of restitution, i.e., the ratio between the velocity of a particle before and after the collision, such that $e_n = \exp(-\lambda_d \tau / m)$.

As we said, this model was used to simulate how granular matter is impacted by the passage of an intruder. To this end, we choose the grains' diameter is $d = 0.37m$, a measure comparable with that of humans. The simulated tank containing the grains is of size $L_x = 25d$ along the $x$-direction and of $L_y = 200d$ along $y$-direction. Then, the damping coefficient $\lambda_n$ is chosen so that the restitution coefficient $e_n = 0.5$. The initial state is prepared by first positioning the intruder, of size $2d$, at the point of coordinates $(L_x/2, 2.5d)$. Then, the other grains' positions are initialized, uniformly chosen at random to respect the target average density of $2.5ped/m^2$ to reproduce the experimental ones, and making sure that no overlap is present from the beginning. The intruder will then make its way through with constant velocity $s = 0.6ms^{-1}$ for a distance of approximately $80d$, to feel the least the wall pressure on the top and the bottom. Most importantly, a Gaussian white noise is added to the grains motion, so that particles fill up through diffusion the wake caused by the intruder's passage. Figure 1.2 shows the density and velocity fields, obtained as an average over 10 realizations, of the simulation of granular particles crossed by an intruder. By observing the left panel of Figure 1.2, we can see how the passage of the intruder through the granular medium causes an accumulation of mass in front of it along the direction of its motion. This is quite intuitive to understand, since the grains are subjected to purely mechanical forces and have no idea of the intruder's arrival. The velocity field shows

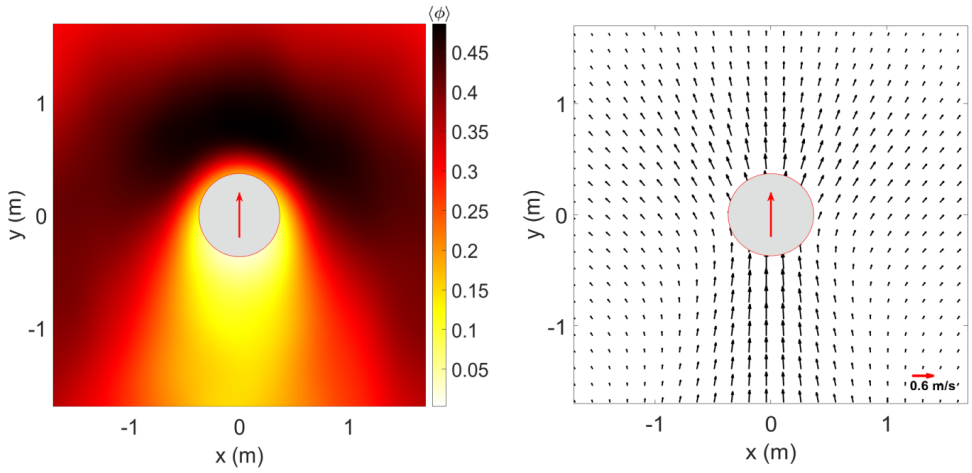


Figure 1.2: **Left**: Density field (Expressed in packing fraction) of the granular simulation obtained as an average over 10 repetitions. The most prominent features are the accumulation of the density in front of the intruder and the trail behind it. Average density equivalent is $2.5 ped/m^2$ **Right**: velocity field of the granular simulation, again obtained as an average over 10 repetitions. We observe how the grains are pushed along by the intruder. Figure extracted from [12].

that, indeed, grains are pushed along the direction of motion of the obstacle. Moreover, we observe some differences between the simulated velocity field and the experimental one showed in Figure 1.1. Indeed, in the experiment the density is higher, close to the jamming transition, and circulation around the obstacle is present. On the other hand, the simulation is performed for a density well below this value, and circulation is less visible. In fact, when the density is high, once impacted by the cylinder, grains have no way to go but to slowly diffuse and wait for some space to free up thanks to the occupation of the cylinder's wake. When the density is lower, grains have instead more space to travel when they are pushed. Nevertheless, both setups show a similar pattern for the density, because in either case no anticipation is present.

## 1.2 . Passage of an Intruder through a Crowd of Pedestrians

Now that we know what happens when a cylindrical intruder passes through an amorphous medium, we turn our attention to the findings of the experiment performed by Nicolas et al. [75]. The experiment was performed by gathering a group of around 40 individuals used to assemble crowds of different average densities in a controlled environment. After equipping each participant with a colored hat, a member of the staff wore a cylinder and

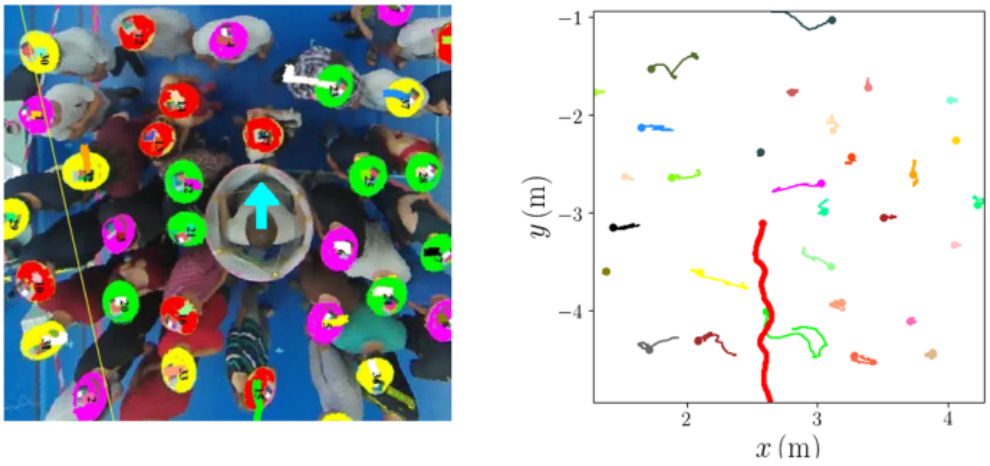


Figure 1.3: Experimental configuration of [75]. Crowds of different densities were assembled in a controlled environment, and a cylindrical obstacle impersonated by a staff member made its way through them (left panel). The motion of the individuals was recorded using a high-resolution camera placed above the crowd and a software capable of detecting the colored hats participants were equipped with (right panel). Image taken from [75].

made his/her way through the crowd, trying to keep its velocity and direction as constant as possible, as can be seen in the left panel of Figure 1.3 The motion of the individuals was registered using a high-resolution camera and a software capable of detecting the colored hats so that the trajectories could be recorded and analyzed. The right panel of Figure 1.3 shows a snapshot of the trajectories of both the intruder and the pedestrians.

The experiment was initially conducted in two configurations: with participants facing the incoming obstacle, or oriented randomly with respect to the cylinder's direction of motion. For each configuration, the experiment was repeated multiple times and the average density and velocity fields were obtained. The density field was computed as follows. At each time step, given a snapshot of the participants' position, a tessellation of the convex hull containing all individuals was created, with each region being a Voronoi cell with seed a pedestrian's position, i.e., the region of space of all points closer to that position than to any other. Then, for each point in a Voronoi cell, the density was defined as the inverse of the cell's area. The velocity field, on the other hand, was computed by dividing the difference between two successive positions by the time step and then each point of a regular grid was assigned a velocity obtained by interpolating the velocities nearby. Figure 1.4 summarizes the findings of the experiment, for average densities of $2.5 ped/m^2$, $3.5 ped/m^2$ and $6 ped/m^2$ in the frontal and random configurations. What this

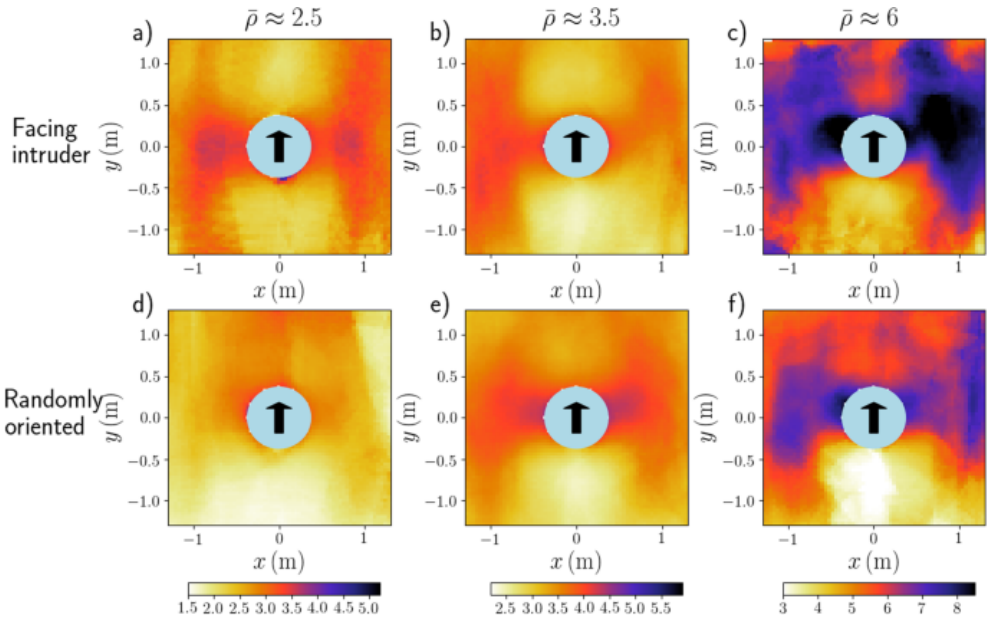


Figure 1.4: **Top row**: density plots with averages $2.5ped/m^2$, $3.5ped/m^2$ and $6ped/m^2$ for the experimental configuration where participants were all facing the intruder. **Bottom row**: same as top row, but for the configuration where pedestrians were randomly oriented. Image taken from [75].

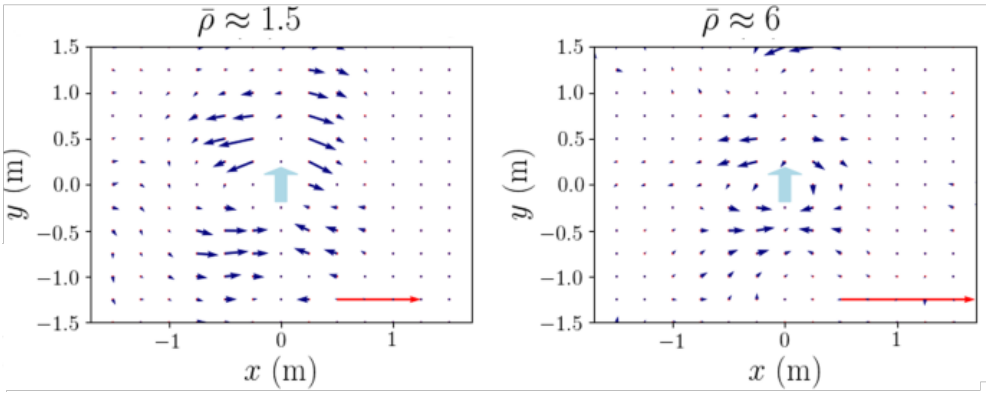


Figure 1.5: Experimental velocity field obtained with the configuration where pedestrians were all facing the incoming intruder. Regardless of the average density ($1.5ped/m^2$ on the left, $6ped/m^2$ on the right) we observe a clear anticipation patter with pedestrians moving laterally well in advance. Image taken from [75].

Figure shows is that, regardless of the value of the density, and to an extent of the disposition of pedestrians, we observe a wing-shaped density field with an increase on the sides of the obstacles and a decrease in front of and behind it. This behavior radically diverges from the one observed in granular matter, where grains would be pushed along by the intruder and accumulate in front of it. Instead, pedestrians in the experiment anticipated the arrival of the intruder, choosing the right moment to step into a denser area, accepting a temporary increase in discomfort to be able to return to a calmer area sooner. From the perspective of a pedestrian in front of the cylinder and observing it getting closer, it is evident how any move with a component parallel to the intruder motion would not be beneficial. This is further confirmed by the velocity plots in Figure 1.5. In fact, here we can see how pedestrians move laterally in front of the obstacle and well in advance before its arrival. They understand that any step with a backward component would simply delay the impact, whereas any step with a forward component does not give them any advantage. This is, whether unbeknownst to pedestrians or not, an optimization process, which does not simply involve how the cylinder will move, but also how other people will react to it while knowing that everyone is trying to achieve the same goal. What is even more striking is that this behavior is observed independently fro the value of the average density, and regardless of the intensity of the physical contacts.

Once they realized how the empirical behavior differed from their granular expectation, the experimenters asked participants to try not to anticipate, to see if they could recover the granular behavior. However, even in this case, participants displayed some sign of anticipation, showing how strongly hard-

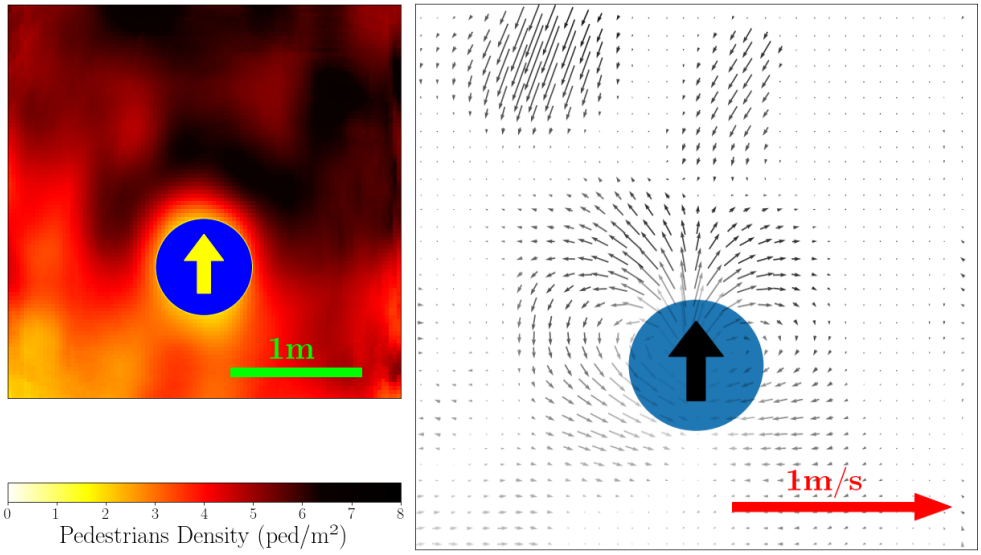


Figure 1.6: Density plot (left panel) and velocity field (right panel) for the experimental configuration where pedestrians were giving their back and were told not to anticipate. The average density is of $4ped/m^2$. Image taken from [16].

wired in our brains the urge to move away is. Finally, the experimenters decided to perform the trial with a new disposition of the participants. This time they asked them to give their back to the obstacle and not to anticipate. In this case, the empirical density and velocity plots started to look more like those of an amorphous medium. The results of this configuration are shown in Figure 1.6. Here, indeed, we observe something reminiscent of the granular case of section 1.1. In fact, by looking at the density plot, we see how participants accumulate in front of the cylinder. By observing at the velocity field, we also see how in front of the obstacle pedestrians did not move laterally as in the other configuration, but rather they were pushed along by it. It should also be observed that the circulation pattern observed in the experiment with pedestrians is not as strong as the observed in the experiment with grains, showed in Figure 1.1. In fact, for reasons of safety, it is difficult to approach the jamming limit with pedestrians if one wants to avoid accidents. Nevertheless, it is evident that the one observed in Figure 1.6 is a behavior more similar to granular matter than in the other two experimental configurations. Finally, the velocity plot observed here differs from the one of Figure 1.2, because in that case the average density was lower, allowing the grains to be pushed along by intruder.

At this point, it is evident why Nicolas et al. were surprised by the results they obtained. In fact, pedestrians in their experiments showed a clear anticipatory dynamics, by not waiting to be impacted by the obstacle before mov-

ing, reacting well in advance and efficiently to avoid it. The key takeaway from this experiment is that pedestrians do not always exhibit granular behavior. In contrast to grains, humans possess self-propulsion and possess the ability to devise a strategy to effectively evade incoming obstacles, irrespective of the average density in their vicinity. Therefore, although there might be situations where individuals indeed qualify as grains, this is generally not the case and failing to properly account for this difference could lead to faulty methods and inaccurate simulation tools. In particular, what emerges from this experiment is that one important aspects of pedestrian motion is indeed anticipation, and that this, in situations that are simple and familiar enough, can happen on time and length scales that could be longer than what previously thought. One of the goals of this thesis is to prove that the way pedestrian models have been designed through the years, usually only provide a short-term anticipation that is not enough to reproduce what was observed in this experiment. In chapter 2 we will give an overview of various pedestrian dynamics models, providing more details about those that will later be used in chapter 4 to compare against the experiment and the MFG model.

# 2 - Modelling Pedestrian Dynamics

In the previous chapter we have seen that, even though this might be the case under certain circumstances, it is generally not true that pedestrians crowds behave like granular matter. Indeed, when the situation is familiar and simple, individuals can anticipate obstacles and behave very differently from amorphous media. For this reason, we stressed the importance of having simulation tools that correctly take this anticipation capability into account to ensure accurate prediction. However, as will be apparent in chapter 4, where we will compare them to the experimental data, most pedestrian dynamics models simulate pedestrians without an adequate level of foresightedness. In this chapter, we want to give an overview of the most important attempts at simulating pedestrian motion produced in the last decades. These models can be divided into two distinct categories, namely microscopic and macroscopic models. Section 2.1 will deal with microscopic models, that describe each pedestrian separately and simulate their motion using a fixed rule applied at each time step using to each individual's current position and velocity. These models have been widely used and are also at the base of various commercial simulation software tools. Then, in 2.2 we will focus on macroscopic models, that describe pedestrians as a whole, and study the evolution of aggregate quantities like their average density. These models usually inherit the knowledge coming from other fields where densities are the object of study, such as fluid dynamics. In particular, macroscopic models sacrifice some accuracy about the details of the interaction between pedestrians, but are usually more flexible and can handle more numerous crowds.

## 2.1 . Microscopic Models

Microscopic models have the advantage of more accurately describing the configurations where the granularity of pedestrians' crowds plays a crucial role, such as near a door or a narrow passage. However, these models' drawback lies in their inability to scale efficiently, since modelling a large number of individuals often is limited by computational capabilities. Microscopic models can be divided into force-based models and velocity-based. Force-based models simulate the motion of individuals using Newton's equations of motion, and introducing various force terms to reproduce what have been called first by Helbing [44] *social forces*. These forces emerge from the consideration that although all of us want to reach their target as fast as possible, consuming the least amount of energy, we generally refrain from bumping into other people, especially if they are a protected category (disabled, old folks, preg-

nant women etc.), and we generally try to respect others' personal space and preserve our own. These are social constraints, that are not straightforwardly described into a mathematical expression, therefore each iteration of a force-based model expands on the characterization of these so-called social forces. Velocity-based models, on the other hand, who were first developed in the field of robotics [88, 28], prescribe to each simulated pedestrian a velocity chosen among those ensuring no collision in the motion. If this is done in a fully decentralized way [83], it is common that, especially at high densities, finding a suitable velocity becomes so hard that the motion of the crowd stops altogether. Adopting a centralized approach [50, 28] partly solves this, but it also makes it harder to scale for a large number of pedestrians, and it may also lead to unrealistic motion such as sharp turns or freezing. In subsections 2.1.1 and 2.1.2 respectively, we will describe in details the two microscopic models we will use in chapter 4 to compare against the experiment, Helbing's social force [44], and the model of Echeverria et al. [33], a hybrid between a velocity and force-based model. We will observe how these two models present two different levels of anticipation. Helbing's social force prescribe no knowledge of future events to simulated individuals, whereas Echeverria's model use the concept of time-to-collision, a type of anticipation mechanism that, in the spirit of velocity-based models, only reaches to the near-future. We will explain these models in detail, especially focusing on the way interactions between pedestrians are dealt with and what kind of anticipation dynamics they entail.

### 2.1.1 . Helbing's Social Force Model

In its first paper of 1995, Helbing presented an innovative concept, trying to describe an aspect of pedestrian motion that many overlooked at. In fact, let us for a moment consider our personal experience. When we move in spaces where other people are present, reasonably we do not wait to impact into someone else before changing our operational strategy, i.e., our direction and velocity. We, on the other hand, try to move ahead of time to avoid getting too close, as this would be considered awkward and unpleasant, or, more generally, unwelcome in society. Hence, we act as if there were a personal space that extends beyond the volume occupied by other individuals' bodies, resulting in a repulsive interaction that intensifies with increasing proximity, emulating the repulsion forces observed for electrically charged particles, i.e., a field of forces. This idea, although more general, was first captured by Lewin in [65], where the author asserts that individuals, when living in the world, are constantly subject to a series of *stimuli*, of different nature and coming from all directions, which cause a *behavioral response*, chosen by maximizing the personal benefit while trying to cope with social expectations. In the case of pedestrians, we could clearly tramp over other people and push them away

to enter the train car first. However, depending on how much we worry about their reaction, we might refrain ourselves and behave more gently, effectively balancing between the urge to reach our goals and the consequences we are prepared to face for our behavior. The first to translate this into a mathematical model was Helbing, in his seminal paper [44], where he introduced the concept of *social forces*. His model is a force-based model, its dynamics given by Newton's equation of motion where, among the force terms, one represents these social forces, actively inducing local repulsion whose intensity increases exponentially with the decrease in distance. More specifically, the motion of pedestrian $i \in \{1 \dots N\}$ is given by

$$m_i \frac{d\vec{v}_i}{dt} = \frac{m_i}{\tau_i}(\vec{v}_i^* - \vec{v}_i) + \sum_{i \neq j} \vec{F}_{i,j}^{contact} + \sum_{i \neq j} \vec{F}_{i,j}^{social} + \vec{\xi}_i(t). \tag{2.1}$$

The first term of the right-hand side of the equations simulates the effort of pedestrian $i$ to maintain a certain desired velocity $\vec{v}_i^*$. Then, the second term includes the contact forces $\vec{F}_{i,j}^{contact}$, analog to those used for the granular model in section 1.1, describing the collision between two pedestrians when their bodies overlap. Finally, the term $\vec{F}_{i,j}^{social}$ describes the local repulsion felt by individuals induced by social norms and the desire to respect each other's personal space, and in more precise terms it reads, in one possible formulation proposed by Pinsard [78],

$$F_{i,j}^{social} = -F_i^{social} \left( \alpha_i + (1 - \alpha_i) \frac{1 + \cos\theta_{i,j}}{2} \right) e^{-\frac{d_{i,j}}{l_i}} \tag{2.2}$$

This formula includes $F_i^{social}$, the maximum intensity of the force felt by pedestrian $i$, which models how strong each individual feels the repulsion away from others close to their personal space. Then, the term in the parenthesis describes the anisotropy of the force, with $\alpha_i \in [0, 1]$ being a coefficient measuring how much a pedestrian differentiates between obstacles in front of and behind him. In fact, when $\alpha_i = 1$, pedestrian $i$ will give the same importance to all interactions regardless of their relative position. On the other hand, if $\alpha_i = 0$, the intensity of the interaction will decrease with the angle, meaning that only obstacles in front of pedestrian $i$ will be given full attention, and this will decrease as the cosine of the relative angle, finally vanishing for obstacles behind the individual's back. Finally, the last term in the multiplication $\exp\{d_{i,j}/l_i\}$, where $d_{i,j}$ is the distance between pedestrians $i$ and $j$, and $l_i$ is a length scale, describes how the intensity of the social force decreases with the distance, with $l_i$ giving the scale of the personal space perceived by pedestrian $i$. Note that although all the parameters of this force term could change from one pedestrian to another, allowing for greater realism, one would almost always choose them all the same because in the limit of a large number of pedestrians their effect would average out.

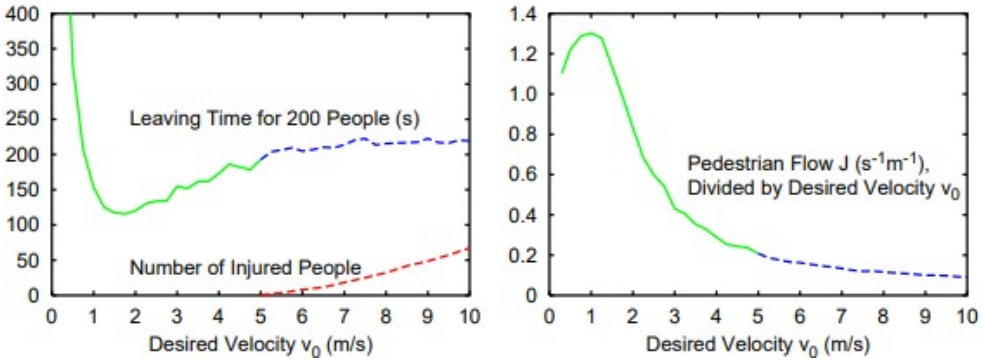


Figure 2.1: Reproduction of the **faster-is-slower effect** using the social force model: for desired velocities higher than $1.5m/s$ the evacuation is performed worse, with the leaving time (left panel) increasing and the pedestrian flow decreasing (right panel). Image taken from [42].

This model represented a break-through, allowing for an accurate quantitative and qualitative description of many of the phenomena observed in pedestrian dynamics. For example, Helbing et al. [42] were able to reproduce the faster-is-slower effect, the well-known empirical fact that the efficiency of the evacuation of a room decreases when individuals try to go too fast. This is because when everyone tries to move fast, they simply end up bouncing one into the other, creating a flow that escapes more slowly from the room. As Figure 2.1 shows, the evacuation performance decreases for desired velocities higher than $1.5m/s$ with an increase in evacuation time and a decrease in the flow of pedestrians through the exit. This is something well known to experts in building security, since a typical faster-is-slower scenario occurs when people have to evacuate a building in a hazardous situation. Moreover, Helbing et al. were able to describe the clogging effect appearing when a uniform flow of pedestrians walking in a corridor passes through an area where the corridor is enlarged and then restricted again, creating something similar to a funnel. In this case, the disruption of the flow is due to a sudden change in the surrounding constraints, to which the flow of individuals has to adjust. Finally, they were able to use their social force model to investigate the best strategy between following the group or individually looking for an exit in case of an evacuation where the presence of smoke blinds pedestrians, making the escapes invisible to them. They showed indeed that an optimal strategy would be a mix of the two, meaning that one should observe where the mass of people is moving, but also not disregard the information acquired independently.

However, social force models also have some limitations. In fact, one problematic aspect of this approach is that the contribution to the social force

repulsion of all pedestrians are summed together, which sometimes is not a good idea. For example, imagine you are facing one pedestrians, moving towards you, and then there is another person behind him, moving in the same direction, like a queue. Clearly, you would react to the first of the two, the one you actually see. However if you sum the contributions of the social forces, simulated pedestrians would also react to the second one, which they are supposed to ignore. Moreover, as pointed out in [59], Helbing's social force, in its original implementation, leads to a choice of certain parameters resulting in a totally nonphysical behavior to ensure a realistic crowd behavior. For example, in order to prevent pedestrians to overlap too much, a very high elastic constant, which produces elastic repulsion forces of the order of several times the mass of a body. Or, a very short cutoff of the social force interaction range. Finally, in [76], it is observed that the social force model pedestrians do not possess any kind of self-slowing mechanism, meaning that their behavior is always competitive, which in practice means that they will always be pushing, even when this is detrimental.

In the years after the first introduction of Helbing's model, many have worked on it and, using the same idea, improved it. Others have decided to deviate from the use of forces to determine the pedestrians trajectories, instead directly choosing their velocity from a set of admissible ones. In the next section, we will discuss a very recent model that takes many of the advancements the community of pedestrian dynamics realized and blend them into one time-to-collision model.

### 2.1.2 . ANDA - A Time-to-Collision Model

We now turn our attention to describing the model recently introduced by Echeverria-Huarte and Nicolas in [33]. This model, named ANDA, ANticipatory Dynamics Algorithm, at each time step $\Delta t$ divides the simulation of pedestrians' motion into various layers, summarized in Figure 2.2, each dealing with the simulation of a segment of a pedestrian's motion. First, agents find their preferred velocity via a decision-making layer by minimizing a cost functional, inspired by the suggestion of Moussaid et al.[74]. This functional is made of various terms such as the shortest path to the target, a biomechanical term representing the physical cost of motion, a term incorporating the desire to respect the one's private sphere and then a time-to-collision term inspired by Karamouzas et al.[49] to avoid collisions, giving more importance to the most imminent. Then, a mechanical layer handles the case where a collision occurs. Finally the agents' positions are updated. Most of the novelty in this model is contained in their choice of a cost functional $\mathcal{E}$ to be minimized to find the desired velocity. For each agent, for any velocity function $u(s) \in \mathbb{R}^2$,

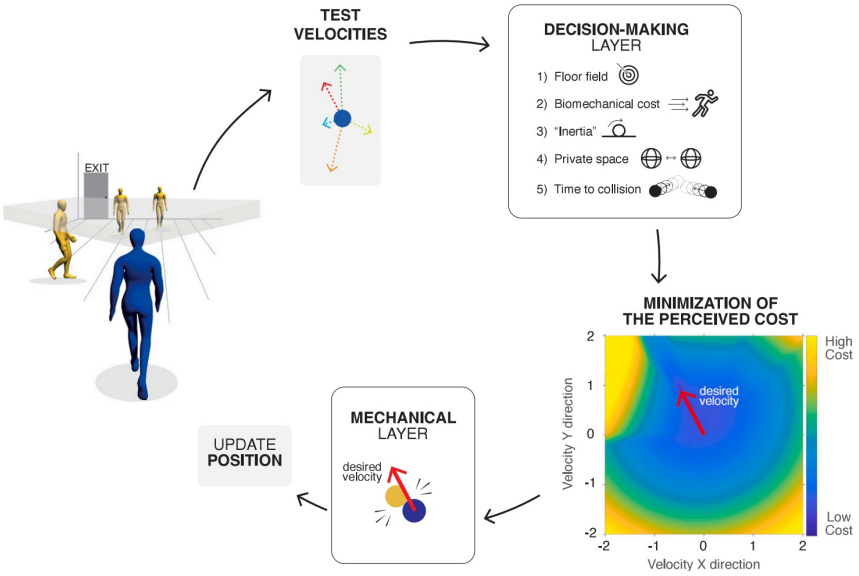


Figure 2.2: Schematic representation of the flow of operation in the ANDA model. A decision-making layer gives the energetic landscape, where pedestrians follow the direction of steepest descent to reach their goal. Then, if needed, a mechanical layer handles collisions. Image taken from [33].

$s \in [t, t + \Delta t)$, the cost functional $\mathcal{E}$ reads

$$\mathcal{E}[\vec{u}] = \int_t^{t+\Delta t} e(\tau, \vec{r}(\tau), \vec{u}(\tau))d\tau + \mathcal{E}^T(\vec{r}(t + \Delta t)).$$

where $r(t)$ is the position of the agent. The term $e(\tau, \vec{r}(\tau), \vec{u}(\tau))$ is a Lagrangian cost that contains the preferences of the agent for its motion towards the target, specified by $\mathcal{E}^T(\vec{r}(t + \Delta t))$, a driving term, prescribing the direction towards the shortest path to the target. The authors of ANDA then consider the limit for $\Delta t \to 0$, so that the functional becomes

$$\mathcal{E}(\vec{u}) \simeq e(t, \vec{r}(t), \vec{u})\Delta t + \mathcal{E}^T(\vec{r}(t) + \vec{u}\Delta t).$$

and now the optimization is performed on $\mathcal{E}(\vec{u})$, a function of the number $\vec{u} \in \mathbb{R}^2$. Thus, given $r(t)$, the position of an agent at time $t$, the position at time $t + \Delta t$ is given by the velocity $\vec{u}^*$ obtained solving

$$\vec{u}^* = \inf_{\vec{u} \in \mathbb{R}^2} \mathcal{E}(\vec{u}), \tag{2.3}$$

that in [33] is done with a using a Nelder–Mead algorithm. The first thing we notice is that the decision-making process considers only what will happen between the time $t$, let us say the present, and the very near future up to time $t + \Delta t$, where $\Delta t$ can be interpreted as a reaction time.

Let us now explain the terms that compose the running Lagrangian cost. First, a bio-mechanical cost is considered, inducing individuals to limit their velocity. This term comes from the measurements of [68], where the energy expenditure of a human body was linked to the speed of motion, and reads

$$e^{\text{speed}}(u) = \begin{cases} 7.6u - 35.4u^2, & u < 0.1m/s \\ 0.4 + 0.6u^2, & u \geq 0.1m/s \end{cases}. \tag{2.4}$$

Then, another biomechanical aspect considered in ANDA is the fact that abruptly changing one's velocity is uncomfortable. Thus, an inertial term

$$e^{\text{inertia}}(\vec{u}\,) = \mu(\vec{u} - \vec{v}(t))^2 \tag{2.5}$$

is included in the cost functional. In this expression $\vec{v}$ represents the present velocity, i.e., the velocity of the agent at time $t$. The terms introduced until now only consider the individual aspects of pedestrian motion. In the following, we will define how pedestrians in ANDA interact with each other. This interaction occurs on two scales. First, a cost term describes the tendency of pedestrians to preserve a personal space. This is modeled similarly to what Helbing does, with a repulsive term depending on the distance between two pedestrians, and activates up to a value $R_i$, the size of the personal space of pedestrian $i$. More precisely, this term reads

$$\mathcal{E}^{\text{pers}}(\vec{u}) = \sum_{j \in \text{fov}(i)} \frac{\eta}{R_i + R_j} V^{\text{rep}} \left( \frac{||r_i(t) + \vec{u}(t)\Delta t - \vec{r}_{\,j}(t + \Delta t)||}{R_i + R_j} \right), \tag{2.6}$$

where $\vec{r}_{\,j}(t + \Delta t) = r_j(t) + \vec{v}_j(t)\Delta t$ is the position of neighbor $j$ at time $t + \Delta t$ assuming that it maintains the current velocity $\vec{v}_j(t)$. Then, a sum over all the neighbors in the field of view (fov) of pedestrian $i$, extending from $-\theta$ to $\theta$ from the direction of its current velocity $\vec{v}(t)$, is performed, with $V_{rep}$ giving the intensity of the repulsion

$$V^{\text{rep}}(d\,) = \begin{cases} \frac{1}{d} - \frac{1}{1+\varepsilon^*}, & d < 1 + \varepsilon^* \\ 0, & d \geq 1 + \varepsilon^* \end{cases}. \tag{2.7}$$

The repulsion therefore decreases with the inverse of ration between the future relative position and the sum of the personal space radii and vanishes when the ratio is equal to $1 + \varepsilon^*$. This term means that the contribution to the choice of the velocity $\vec{u}^*$ made by the desire to respect the personal space is given by observing where neighbors will be after a time step assuming they will maintain the same velocity they had at time $t$. In particular, this terms does not describe interactions with pedestrians whose future relative position enters the personal space. To describe interactions with agents further than this distance it was proved by [74] and [49] that instead of positional variables, considering the time to collision $\tau_{i,j}$ between pedestrians is much

more effective to simulate how people react to incoming dangers. The time-to-collision with an other pedestrian $j$ is a function on the velocity $\vec{u}$ and is calculated using $j$'s current velocity $\vec{v}_j(t)$. The function that was found to better reproduce the anticipation based on the TTC is

$$V^{\text{ttc}}(\tau) = K^{\text{ttc}} \frac{e^{-\tau/\tau^c}}{\tau^p}, \tag{2.8}$$

with $p = 2$ and $\tau = 3.0s$ and $K^{\text{ttc}}$ giving the intensity of this interaction term. The authors of ANDA consider the time to the most imminent collision, based on the empirical findings of [72] showing that individuals tend to focus on the greatest danger when they choose how to move. Moreover, they average the intensity of the TTC potential $V^{\text{ttc}}$ over pedestrian $i$'s personal space, to extend the anticipation radius. The TTC term of the cost then reads

$$e^{TTC} = \frac{1}{\varepsilon^*} \int_0^{\varepsilon^*} V^{ttc}(\tau_j(\varepsilon)) d\varepsilon. \tag{2.9}$$

For a more detailed explanation of the derivation of this term we refer to [33]. Combining all the terms introduced the ANDA cost functional reads

$$\mathcal{E}(\vec{u}) = [e^{\text{speed}}(u) + e^{\text{inertia}}(\vec{u}) + e^{\text{TTC}}(\vec{u})]\Delta t + \mathcal{E}^T(\vec{r}(t) + \vec{u}\Delta t) + \mathcal{E}^{\text{pers}}(\vec{u}). \tag{2.10}$$

Once this is minimized, see [33] for details, for all the agents, the movement is performed. At this point, it is not assured that no collision occurs. However, this is not pathological, but a price to pay to keep the algorithm away from the deadlocks and the unnatural motion otherwise affecting most of the so-called velocity-based models. If two pedestrians overlap as a result of their motion after the decision-making step, a mechanical layer in spirit and in theory very similar to the one described for the granular model in section 1.1 kicks in and repels the agents away from each other.

With their model, the authors of ANDA were able to obtain a vast array of results validating their approach. First, they were able to simulate the avoidance of two pedestrians walking one towards the other in a narrow corridor, then, they performed various simulation to test their model's performance in unidirectional and bidirectional flows, obtaining a fundamental diagram comparable to multiple experimental databases, as Figure 2.3 shows. Moreover, they were able to apply their simulation tool to reproduce the navigation of pedestrians throughout a complex environment, reproducing the Montparnasse train station in Paris. Finally, the ANDA model was used to simulate the changes in level of attention or lack thereof when individuals walk with while using their smartphone, something common nowadays. They were able to do so by modifying the decision time of pedestrians by giving a longer one to those simulating a person walking and looking at the phone. The results they obtained were in good agreement with empirical studies, testifying even

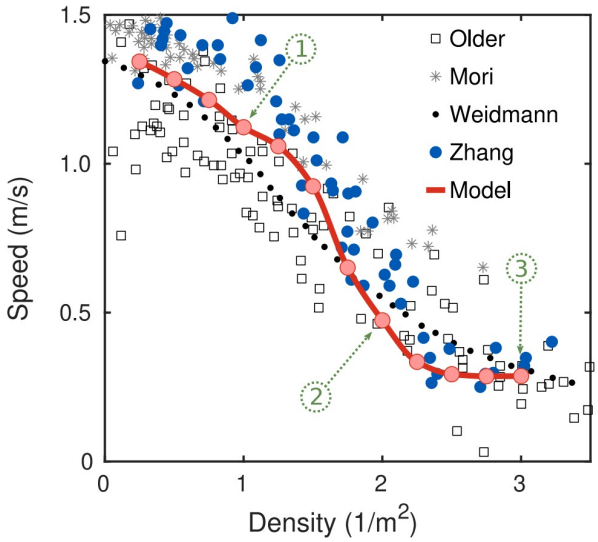


Figure 2.3: Comparison between the fundamental diagram predicted by the ANDA model, in solid red, against various empirical databases. Image taken from [33].

further to the validity of this simulation method. As we said, the reason we introduced both ANDA and Helbing's social force in detail, is to understand how they work before comparing them to the experiment in chapter 4. Of course, we could have chosen many other models to perform this comparison, however we believe that these two models represent well enough two attempts, of radically different complexity, at describing pedestrian dynamics. In fact, Helbing's model builds on a granular model, and simply add some longer-ranged repulsion. In this case no anticipation is present, and any avoidance begins once a certain threshold distance is reached. On the other hand, ANDA is a very complete model, taking the best of a wide range of advances in the field occurred over the three decades that separate it from the social force model. Most importantly, ANDA's time-to-collision avoidance mechanisms perfectly represents the short-time anticipation many models have started including to account for pedestrians' forecasting capabilities. As will see in in chapter 4, no matter the complexity of the simulation scheme, both models lack an essential element to reproduce the experimental findings: long term anticipation.

## 2.2 . Macroscopic Models

The use of macroscopic models to describe human behavior dates back to the 1950s, when models of traffic dynamics were developed that described the ensemble of cars on a road as a continuum characterized by the local density.

Then, in the 70s, Fruin [34] proposed an approach consisting in schematizing the rooms of a building as the nodes of a graph, with each node being associated with the density in the room and each edge with the flow between connected rooms. Although very simple, this model can be useful to simulate buildings with many small rooms, however, when applied to large premises the graph description becomes less effective. In general, macroscopic models focus on the description of the density of pedestrians, rather than trying to capture each individual's motion. In this section, we will describe two macroscopic models that describe the motion of pedestrians through their density. The first is the *Lighthill-Whitham-Richards* model, invented in 1955 and used to describe car traffic in a one-dimensional environment, simulating a road. The other is the *Hughes* model, a more recent one that introduces the passage to two dimensions, making it suitable for simulating pedestrians. Although with some differences, these two models use the same equation to describe the evolution of the density. This equation is the conservation law much used in other disciplines such as fluid dynamics. Its derivation is intuitive, and can be described as follow. For simplicity, we consider the one-dimensional case. Let us consider a point in space $x$ and a small space element $dx$ at time $t$. After a small time element $dt$, the quantity of fluid (or anything else we want to describe with this equation) that entered the space element from point $x$ is given by $j(x,t)dt$, where $j$ is the current. The amount that at the end of $dt$ left the same space is given by $j(x+dx,t)dt$. Thus, to know how much fluid accumulated or dispersed in $dx$ during $dt$, we can take $j(x,t)dt - j(x+dx,t)dt$. However, the same amount of fluid can be given by considering the density $\rho$. In fact, if we take $dx$ small enough that $\rho(x,t)$ is constant over it, then to know the amount of fluid that accumulated or dispersed in $dx$ after $dt$ we can simply take $\rho(x,t+dt)dx - \rho(x,t)dx$. Equating the two ways of obtaining the accumulated or dispersed fluid gives the following conservation law, generalized to more than one dimensions,

$$\partial_t \rho + \vec{\nabla} \cdot \vec{j} = 0 \tag{2.11}$$

When we observe that $\vec{j} = \rho\vec{v}$, where $\vec{v}$ is the velocity of the fluid, this law now gives us the evolution in time of the density. In the following we will explain what hypotheses can be made on this equation to simulate different scenarios. In particular, we will show how it is the choice of the current $j$ to determine the dynamics of the density.

### 2.2.1 . Lighthill-Whitham-Richards Model

The first macroscopic model we are going to explore is the Lighthill-Whitham-Richards model, first introduced in 1955 in two papers [66, 67]. In a nutshell, this model describes the motion of cars along a one-dimensional road with no curves. It aims to accurately describe how the changes in local densities

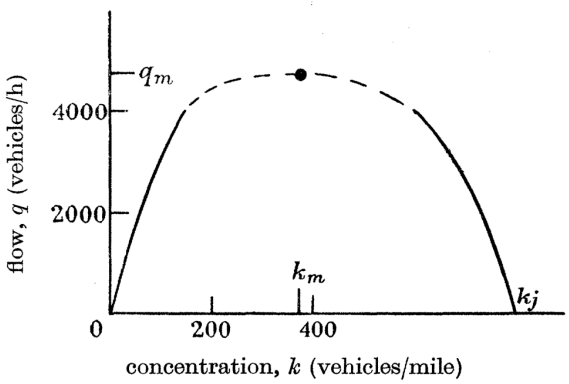


Figure 2.4: Example of flow-density relation used in LWR model. Although empirical ones may differ, this picture serves to give the idea that when density is low, the flow is low because there are few cars. Then, when the density is very high, nobody moves anymore, thus stopping the motion. It follows that there must be a value of the density where the flow is at its maximum. Image taken from [67].

propagate along through the traffic. For example, if a current of cars is interrupted by a traffic light that turns red, how does the information about the difference in speed and consequently the increase in density reach all drivers.

In this model, the density of vehicles evolves following the conservation law (2.11), with the assumption that the current $j = j(\rho) = f(\rho)$ depends *only* on the density $\rho$ following a fundamental diagram as in Figure 2.4. This shape of the fundamental diagram is commonly found empirically by experimenters, and although LWR specifically treats the case of vehicles, this relation still holds for pedestrians. In this model, equation (2.11) is solved by considering a curve $(\hat{x}(t), t)$ parameterized by $t$. Let us now solve the equation along this curve, and then we will be able to say something about its nature. First, let us define $\hat{\rho}(t) = \rho(\hat{x}(t), t)$, the density along the curve. Now, if we take its time-derivative we have

$$\frac{d\hat{\rho}}{dt} = \partial_{\hat{x}}\hat{\rho}\frac{d\hat{x}}{dt} + \partial_t\hat{\rho}, \tag{2.12}$$

and if we choose $\frac{d\hat{x}}{dt} = \frac{df(\hat{\rho})}{d\hat{\rho}}$ we have, from (2.11), that $\hat{\rho}$ is constant along the curve, meaning that $\hat{\rho} \equiv const$. If this is the case, though, $\frac{df(\hat{\rho})}{d\hat{\rho}}$ also is constant along the curve $(\hat{x}(t), t)$, meaning that $\frac{d\hat{x}}{dt}$ is constant as well. This leads to the fact that $(\hat{x}(t), t)$ is a straight line. This means that, for a given initial value of the density $\rho_0$, one can follow the line with angular coefficient given by $df(\rho)/d\rho$ evaluated in $\rho_0$ and the density would be constant along that line.A useful way to visualize this is by using a representation of the solution where the position $x$ is plotted against the time $t$.

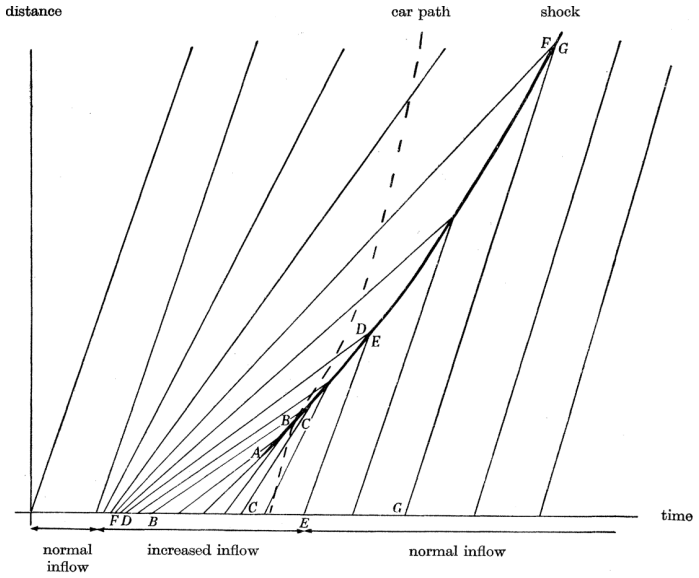


Figure 2.5: Characteristic curves of the LWR model. Each curve represents a locus of points where the solution of equation (2.11) is constant. These curves carry the information about the fact that at time $t = 0$ at point $x_0$ the density had a certain value $\rho_0$. When two curves intersect, a shock is produced. Image taken from [67].

This is what Figure 2.5 shows, where the different lines are the curves along which the solution of equation (2.11) is constant, with different initial conditions. To understand what these lines represent in practice, let us imagine that at time $t$, at a certain position $x = 0$, the value of the density is $\rho_0$. Then, we can follow the line of constant density to see where the value $\rho_0$ will be after some time. If two lines intersect, this means that at the same time there should be two values of the density, clearly something impossible, and this is called a shock. Although this model was purely conceived having car traffic in mind, it can be adapted to human motion provided that the fundamental diagram is chose accordingly, in particular in one-dimensional unidirectional flows of pedestrians.

### 2.2.2 . Hughes's Model

Another important macroscopic model is Hughes's model. This describes the crowd of pedestrians using the continuity equation (2.11), making the assumption that all individuals are aware of a common goal, typically a certain area to reach, that could represent, for example, an exit. The desire to achieve the goal is described using a *potential* $\phi(x, y)$, indicating at each location in space the time required to reach the final destination. In this model, the velocity of the simulated pedestrians is parallel to $-\vec{\nabla}\phi$. Moreover, Hughes describes the effect of interactions among pedestrians through the local density,

introducing a term $g(\rho)$ penalizing speed in congested areas. This term is then multiplied to the potential gradient and finally the continuity equation of the model reads

$$\partial_t \rho - \vec{\nabla} \cdot (\rho g(\rho) \vec{\nabla} \phi) = 0. \tag{2.13}$$

This model was used by Hughes in [48] to simulate the approaching of a pedestrian crowd to the pillars on the Jamarat bridge in Mina, Saudi Arabia, during the stoning ritual. In this event, millions of pedestrians cross a multi storey bridge that has at the center three pillars going through all the floors, approaching them to throw stones. Hughes used his model to simulate the situation upstream a pillar, showing how the velocity decreases near it, due to congestion effects. Moreover, Hughes introduces some variations to its model such as the possibility to treat different populations of pedestrians and how they interact. This model is particularly interesting for us because it uses some elements which we will find later. In the following chapter, in fact, we will introduce the theoretical foundation of the MFG model, and we will find again the continuity equation. However, what will differ is the choice of the term corresponding to the flux. In fact, this term is chosen arbitrarily, although as consequence of certain assumptions, in both the macroscopic models we have described. On the other hand, in MFG this term comes from the solution of another differential equation and is a consequence of the microscopical description of individuals.

# 3 - Mean-Field Games

Mean-Field Games (MFG) are a branch of applied mathematics that developed during the last decade under the impulse of the seminal works of Lasry and Lions [61, 60] on one side and of Huang, Malhamé and Caines [47] on the other. MFG are optimally driven diffusion processes, used to find the optimal strategy for an agent to reach a certain goal while being affected by a multitude of other agents trying to do the same thing and subject to interference with his/her plan. MFG has been since applied in various fields, ranging from finance [20, 22], to economics [1, 2], problems of social nature such as pedestrian dynamics, segregation, and epidemics [3, 54, 14], and engineering [53, 52]. This demonstrates the flexibility and adaptability of the method, which can be used to find the right balance between costs and benefits in situations of competition.

The theory of MFG is built upon two other successful mathematical theories, that of Optimal Control and Game Theory. In fact, MFG are in essence an optimization process, based on the concept of *utility*, the total satisfaction gained by performing a certain action, as well as what is paid in the process, in terms of consumption or discomfort. Therefore, to obtain the optimal course of action one simply needs to maximize the utility, and this would indeed be an optimization process, as explained in section 3.1. But it is often the case that such decisions are made in a competitive context, where many people are trying to solve the problem at the same time. In that case, it is necessary to assess how the presence of others impacts on the decision process and on its outcome. This is where Game Theory comes into play. Developed in the 1950s by a group of scientist of the RAND corporation to estimate the likelihood of nuclear war with the Soviet Union, this theory studies the consequences of the interaction, competitive or collaborative, on decision processes, as we will see in section 3.2. However, when the number of interacting agents grows, this becomes very difficult to solve, if not impossible.

This is where the theory of Mean-Field Games is most effective. MFG assumes the interaction with a multitude of agents can be reduced to the interaction against an aggregate of the others' behavior. In the case of pedestrians, for example, one does not record the position of all the people in the crowd to decide how to move, but instead focuses on their average density. This reduces the complexity of the problem at the expense of some accuracy, a trade-off that has proven to be beneficial in many instances. Section 3.3 will delve into the mathematical structure of MFG and will provide all the necessary tools to simulate the experimental configuration of chapter 1, together with additional context about the use of MFG.

## 3.1 . Optimal Control

Optimal Control is the branch of applied mathematics dealing with the description of systems whose dynamics can be modified via one or more parameters, called *control parameters*, to maximize (minimize) a certain gain (loss) function. Although this concept found most of its applications to systems of recent appearance, such as in the economy or industrial production, its origin is actually more remote and related to a concept familiar to physicists. In fact, it is well known that in classical mechanics, when a body of mass $m$ changes its position from $q_1$ at time $t_1$ to $q_2$ at time $t_2$, the trajectory is given by Newton's second law

$$\ddot{q} = -\frac{d}{dx}U. \tag{3.1}$$

However, it is also possible to describe the particle's dynamics as the minimization of the action associated with the motion

$$S = \int_{t_1}^{t_2} \mathcal{L}(q, \dot{q}, t)dt, \tag{3.2}$$

where $\mathcal{L}$ is called the Lagrangian of the motion. All in all, it is the shape of the Lagrangian that determines the motion. Abstractly, any form could be chosen, however, in classical mechanics, a series of considerations fix the Lagrangian to be

$$\mathcal{L}(q, \dot{q}, t) = \frac{\dot{q}^2}{2} - U(q). \tag{3.3}$$

Then, it can be proven that

$$\frac{\delta S}{\delta q} = 0 \implies \frac{d}{dt}\frac{\partial \mathcal{L}}{\partial \dot{q}} - \frac{\partial \mathcal{L}}{q} = 0 \tag{3.4}$$

is equivalent to Newton's law (3.1). In this case, we interpret the Lagrangian as a running cost of the process, the total cost, or utility, being the action functional. The control parameter of the system is the position $q$ and optimizing the utility amount to finding the dynamics of the body.

In a more general way, optimal control can also be applied to stochastic dynamics, i.e., where the dynamics contains a random part, described by a random variable. Let us consider $\vec{x} \in \mathbb{R}^n$ the position of a body moving with a random component from time $t$ to time $T$, then this kind of dynamics is described by the *Langevin equation*

$$\dot{\vec{x}} = \vec{a}(t) + \sigma\vec{\xi}(t), \tag{3.5}$$

where $\vec{a}(t) \in \mathbb{R}^n$ is called the *drift* term, whereas $\vec{\xi} \in \mathbb{R}^n$ is a Gaussian white noise representing the random component of the motion, and $\sigma$ its intensity. Now, a typical problem in optimal control would be to find the best drift term

to optimize a certain cost functional. In this case, $\vec{a}(t)$ is the control parameter and the cost functional to be minimized can be written as

$$\mathcal{C}[\vec{a}](\vec{x},t) = \mathbb{E}\left\{\int_t^T \mathcal{L}[\vec{a}_\tau](\vec{x}_\tau,\tau)d\tau + \mathcal{C}_T(\vec{x}_T)\right\}. \tag{3.6}$$

Analogously to the classical mechanics case, we will call Lagrangian the function $\mathcal{L}[\vec{a}](\vec{x},t)$ giving the running cost of the motion governed by $\vec{a}$ between time $t$ and $T$, with initial position $\vec{x}$. The running cost is used to describe the preferences of the underlying motion. The second term of the cost functional is the final cost $\mathcal{C}_T(\vec{x}_T)$, telling where it will be more or less expensive to be at the end of the motion, describing eventual areas of attractions or repulsion. Finally, since the motion is random, as expressed by the Langevin equation (3.5), to obtain a deterministic quantity we must take the expected value. At this point, let us introduce the *value function*, the value the cost functional takes at its minimum

$$u(\vec{x},t) = \inf_{\vec{a}} \mathcal{C}[\vec{a}](\vec{x},t). \tag{3.7}$$

The goal is therefore to find the optimal control, which is the $a$ that minimizes $\mathcal{C}$. For this, we can use Bellman's *Dynamic Programming Principle* [9]. This principle states that, if the trajectory from point A to point B, given by an optimal policy, passes through point C, then the trajectory from point C to point B would still be optimal with respect to the cost functional. In practice, this means that it is possible to divide the integral in the definition of the cost functional and still obtain the same value function

$$\begin{aligned} u(\vec{x},t) &= \inf_{\vec{a}} \mathbb{E}\left\{\int_t^{t+dt} \mathcal{L}[\vec{a}](\vec{x},\tau)d\tau + \int_{t+dt}^T \mathcal{L}[\vec{a}](\vec{x},\tau)d\tau + \mathcal{C}_T(\vec{x}_T)\right\} \\ &= \inf_{\vec{a}} \{\mathcal{L}[\vec{a}](\vec{x},t)dt + u(\vec{x}+d\vec{x},t+dt)\} \end{aligned} \tag{3.8}$$

Now, $u(\vec{x}+d\vec{x},t+dt)$ can be written as

$$u(\vec{x}+d\vec{x},t+dt) \simeq u(\vec{x},t) + \frac{du}{dt}dt, \tag{3.9}$$

where the total derivative of $u$ with respect to $t$ is given by Ito's chain rule [35]

$$\frac{du}{dt} = \vec{\nabla}u \cdot \vec{a} + \partial_t u + \frac{\sigma^2}{2}\Delta u. \tag{3.10}$$

Finally, we can plug (3.10) in (3.9) and this into equation (3.8) to obtain the *Hamilton-Jacobi-Bellman* (HJB) equation

$$0 = \inf_{\vec{a}}\{\mathcal{L}[\vec{a}](\vec{x},t) + \vec{\nabla}u \cdot \vec{a}\} + \partial_t u + \frac{\sigma^2}{2}\Delta u. \tag{3.11}$$

This is a backward differential equation that is solved starting from the terminal condition

$$u(\vec{x},t) = \mathcal{C}_T(\vec{x}(T)). \tag{3.12}$$

Moreover, the final form of (3.11) equation is determined once the Lagrangian is specified.

| | 1 betrays (1B) | 1 cooperates (1C) |
|---|---|---|
| 2 betrays (2B) | -7/-7 | -1/-10 |
| 2 cooperates (2C) | -10/-1 | -3/-3 |

Table 3.1: Payoffs of the *prisoner's dilemma* as formalized by Tucker [79]. Values are negative because they represent jail time in years. The Nash equilibrium of the game is the situation where both prisoners betray, although this is not the set of strategy granting them the lowest number of years in prison.

## 3.2 . Game Theory

The other pillar at the foundation of the theory of Mean-Field Games is Game Theory, a branch of applied mathematics that studies how to find the best strategy in competitive situations where two or more players interact and have something to gain and something to lose. The best way to illustrate the kind of situations Game Theory deals with is with an example. Let us consider the situation where two accomplices to an armed robbery are arrested and interrogated at the same time but in separate rooms by the police. The evidence against them is enough to arrest both for robbery, however, not definitive to prove their guilt for a homicide that occurred during the robbery. The only way for the police to link the criminals to the homicide is if one betrays the other, causing the other a worse punishment and gaining a small discount for his/her sentence. Otherwise, if the two cooperate remaining silent, they will both be given a lighter sentence. This situation is called the *prisoner's dilemma*, and its first formalization dates to 1950 by Tucker [79]. In table 3.1 we quantify the aforementioned situation, by adding numerical values to each set of strategies. In fact, each player, called 1 and 2 here, has in practice 2 choices, the strategies, betray (B) or cooperate (C), and each choice will give him a certain number of years of jail, the payoffs. In Game Theory agents are supposed to act rationally, meaning that they will act according to the mathematical optimization of the payoffs associated to the strategies, while keeping in mind that all the opponents are trying to do the same. By reasoning only in terms of payoffs, it is possible to identify the so-called Nash-equilibrium (NE), i.e., the set of strategies ensuring that, if the other player does not modify his/her behavior, then one should not change his/her own neither. To find the NE, one should therefore not simply look for the strategy allowing for the best payoffs, but also the one from which nobody deviates. If we now go back to the prisoner's dilemma, to find the Nash-equilibrium we focus on one of the two players, let us say player 1, and try to find an answer to each move of player 2.

- Let us assume player 2 betrays (2B), then player 1 would get fewer years of prison if he betrays (1B), rather than if he cooperates (1C) because he/she allows the police to put the other criminal away for longer.

- On the other hand, if player 2 cooperates (2C) and does not denounce player 1, the latter's best choice would still be to betray (1B) because he/she is rewarded for his confession to the police.

If we apply the same reasoning to player 2 we realize that the strategy they both end up playing, reasoning in terms of payoffs and accounting for the other player, is to betray. The set of strategies (1B,2B) is therefore the Nash-equilibrium of the game.

We can formalize this in general as follows. Let us consider a game played by $N$ players, and let us call $s_i$ the strategy of player $i$ and $w_i(s_1, \dots, s_N)$ the payoff for player $i$. We define the N-tuple $\vec{s}^*$ the Nash-equilibrium if

$$w_i(s_1^*, \dots, s_i^*, \dots, s_N^*) \geq w_i(s_1^*, \dots, s_i, \dots, s_N^*), \quad \forall i \tag{3.13}$$

meaning that for any given player $i$, it is not convenient to change strategy if everyone else is sticking to the NE strategy.

In the prisoner's dilemma, we have found that the NE is when both players betray the other, although this is not the strategy providing a lighter sentence for both players. In fact, if the two were able to agree on not denouncing the other, they would be better off. In general, the NE is stable with respect to the mathematical optimization of the outcomes, but in the real world, it might be hard identify it. However, in the experiment of the cylinder, as we will later see, individuals show a level of spontaneous coordination that allow them to get really close to the theoretical NE given by the MFG model. Although being also at the base of much of the economic research, rationality is subject to controversy [70], especially when assumed in contexts where the players, or agents, have to deal with complex situations with uncertain outcomes. Shedding light on this topic is clearly out of the scope of the present work, however the author of this thesis believes that, at least in some cases, simple and familiar enough, humans can actually be rational and find, maybe not intentionally, the best option. The experiment with pedestrians this thesis is dealing with, testifies to that. In fact, since humans start taking their first steps as newborns, obstacle-avoidance strategies are hardwired into the brains and, in a more advanced stage of development, so is the self positional-awareness with respect to others. The goal of the present work is therefore to illustrate how an approach based on a macroscopic description of pedestrians' motion coupled with the game-theoretical nature of their strategy allows for an accurate representation of certain instances of pedestrian dynamics.

### 3.2.1 . Differential Games

We have introduced Game Theory using an example with only two players, choosing among a discrete number of strategies. However, the same reasoning can be done in a case where the number of players is larger than two, let us say N, choosing from a continuum of alternatives at every time step between an initial time $t$ and a final time $T$. We imagine that we can associate to each player a *state variable* $\vec{x_i}$, which evolves following a Langevin equation

$$\dot{\vec{x}}_i = \vec{a}_i + \sigma\vec{\xi}_i(t). \tag{3.14}$$

Analogously to what we discussed for optimal control models, $\vec{a}_i$ is the *control parameter*. Then, in this case we reasons in terms of a cost, and not of payoffs, which we want to minimize. The cost associated to a strategy is given by a cost functional analog to (3.6).

$$\mathcal{C}_i[\vec{a}_i](\vec{X}, t) = \mathbb{E}\left\{\int_t^T \mathcal{L}_i[\vec{a}_{i,\tau}](\vec{X}_\tau, \tau)d\tau + \mathcal{C}_T(\vec{X}_T)\right\}, \tag{3.15}$$

where $\vec{X} = (\vec{x}_1, \ldots, \vec{x}_N)$ contains the state variables of all players. Like for normal games (3.13), it is possible to introduce the notion of Nash-equilibrium $\vec{A}^* = (\vec{a}_1^*, \ldots, \vec{a}_N^*)$ so that

$$\mathcal{C}_i[\vec{A}^*] \leq \mathcal{C}_i[(\vec{a}_1^*, \ldots, \vec{a}_i, \ldots, \vec{a}_N^*)], \quad \forall i. \tag{3.16}$$

Differential games constitute the addition of the game theoretical component to an optimization process. Using the procedure of section 3.1 one would obtain a system of $N$ coupled Hamilton-Jacobi-Bellman equations, one for each player, that once solved would give the Nash equilibrium of the differential game. However, this is often very difficult to do, especially when $N$ becomes large. In the next section, we will introduce the assumptions at the base of MFG that are crucial to be able to solve these problems.

## 3.3 . Quadratic Mean-Field Games

Mean-Field Games build upon differential games, extending them and finding a way to actually solve them, in the limit $N \to \infty$. Everything we defined until now applies to a generic optimization problem. However, the first MFG models ever introduced use a running cost that reads

$$\mathcal{L}_i[\vec{A}_t](\vec{X}_t, t) = \frac{\mu_i}{2}\vec{a}_i^2(t) - V(\vec{X}_t, t). \tag{3.17}$$

Models using this Lagrangian are called Quadratic Mean-Field Games, and they are the first type of models initially studied by MFG founders [61, 60, 62, 47]. This kind of MFG has also been the subject of multiple studies such as

[87, 40], giving us more profound understanding about their functioning. In this thesis, we will only deal with quadratic MFG. We observe that the running cost (3.17) is composed of a quadratic term, depending solely on the strategy of player $i$, and a term $V(\vec{X}_t, t)$ that depends on the state variables of all other players. This term couples the agents together, therefore representing the competitive, game-theoretical side of the optimization process. Through the potential, one could possibly model various forms of interaction. However, as we said, describing the interaction between agents through their individual position would be computationally unfeasible once their number $N$ becomes large. Thus, the core simplification of MFG is to consider that individuals interact via the empirical density

$$\hat{m}(\vec{x}, t) = \frac{1}{N} \sum_{i=1}^{N} \delta(\vec{x} - \vec{x_i}(t)) \tag{3.18}$$

that, using the Central Limit Theorem, for $N \to \infty$, is equivalent to its expected values $m(\vec{x}, t) = \mathbb{E}[\hat{m}(\vec{x}, t)]$. This approximation, at the basis of the definition of Mean-Field Games, is what finally renders the problem treatable, giving us a chance to solve it. Moreover, when the number of agents becomes large, we can consider their differences fading, to the point that they become indistinguishable. Thus, we will drop the index from our equations and the running cost, after these simplifications becomes

$$\mathcal{L}[\vec{a}_t](\vec{x}_t, t) = \frac{\mu}{2}\vec{a}^2(t) - V[m](\vec{x}_t, t). \tag{3.19}$$

Then, although other choices are possible, we decide to use a potential of the form

$$V[m](\vec{x}_t, t) = gm(\vec{x}, t) + U_0(\vec{x}, t) \tag{3.20}$$

where $g$ is a constant giving the intensity and the nature of the interaction. A negative sign of $g$ means a repulsive interaction, and in this case, we call this a MFG with *negative coordination*, whereas a positive $g$ means an attractive interaction, thus *positive coordination*. On the other hand, $U_0(\vec{x}, t)$ is an external potential describing eventual additional constraints and the interaction with the environment.

Now that we have defined the running cost, we can introduce the cost functional of our MFG model

$$\mathcal{C}[\vec{a}](\vec{x}, t) = \mathbb{E}\left\{ \int_t^T \frac{\mu}{2}\vec{a}_\tau^2 - V[m](\vec{x}_\tau, \tau)d\tau + \mathcal{C}_T(\vec{x}_T) \right\}. \tag{3.21}$$

At this point, if we follow the same path as in section 3.1, we obtain that (3.11) with our choice of running cost becomes

$$0 = \inf_{\vec{a}} \left\{ \frac{\mu}{2}\vec{a}^2(t) + \vec{\nabla} u \cdot \vec{a} \right\} - V[m](\vec{x}, t) + \partial_t u + \frac{\sigma^2}{2}\Delta u \tag{3.22}$$

If then minimize the term in the curly brackets we observe that the potential, that does not depend on the control parameter, exits the brackets, and from what is left we obtain that the optimal control is given by

$$\vec{a}^* = -\frac{\vec{\nabla} u}{\mu} \tag{3.23}$$

This is therefore the optimal control parameter that guides the dynamics of the stochastic process given by equation (3.14). Intuitively, this tells agents to perform a descent along the gradient of the value function, reaching as fast as possible the most desirable areas in the state variable space. Moreover, once we have obtained (3.23), we can plug it back in (3.22) and finally obtain the Hamilton-Jacobi-Bellman equation of our MFG as

$$\begin{cases} \partial_t u = -\frac{\sigma^2}{2}\Delta u + \frac{1}{2\mu}(\vec{\nabla} u)^2 + V[m] \\ u(\vec{x}, t = T) = c_T(\vec{x}) \end{cases} . \tag{HJB}$$

As previously observed, this equation is solved backwards, as also hinted at by the minus sign in front of the Laplacian, starting from a terminal condition $u(\vec{x}, t = T) = c_T(\vec{x})$. Finally, given that each player's state variable follows a stochastic evolution described by the Langevin equation (3.14), the corresponding average density evolves following the Kolmogorov-Fokker-Plank equation

$$\begin{cases} \partial_t m = \frac{\sigma^2}{2}\Delta m + \frac{1}{\mu}\nabla \cdot (m \nabla u) \\ m(\vec{x}, t = 0) = m_0(\vec{x}) \end{cases} , \tag{KFP}$$

a forward equation solved starting from an initial density profile. The key aspect of Mean-Field Games lies in the fact that the drift term in the KFP equation is given by the optimal control, obtained by solving the HJB equation. The fact that the latter is solved backwards is crucial, in that the information about the future is winded back up to the initial start of the process. MFG agents have full knowledge of everything that will happen along the process, making them able to anticipate and act efficiently.

### 3.3.1 . The Stationary or Ergodic Regime of MFG

As we said, a MFG is calculated over a time that goes from $0$ to $T$. As pointed out by [21], however, what happens near the beginning or the end of this interval and what happens during intermediate times, namely when $t \ll \tau \ll T$, differ substantially. In fact, it can be shown that under certain hypotheses, among which the fact that the potential term $V[m](\vec{x}, t)$ does not depend on time explicitly, during this intermediate period, the observables of the system become time-independent, meaning that we can write

$$\partial_t \vec{a}^*_e(\vec{x}, t) = -\frac{1}{\mu}\partial_t \vec{\nabla} u^e(\vec{x}, t) = 0 \qquad \Longrightarrow \qquad u^e(\vec{x}, t) = u^e(\vec{x}) + u^e(t) \ . \tag{3.24}$$

and that $m^e(\vec{x},t) = m^e(\vec{x})$. In particular, always in [21], it is shown that

$$m(\vec{x},t) \simeq m_e(\vec{x}), \quad u(\vec{x},t) \simeq u^e(\vec{x}) - \lambda t \tag{3.25}$$

where $\lambda$ is a constant that varies depending on the problem at hand. We call this regime of the system the *ergodic* or *stationary* state. We will use the two definitions interchangeably. Having established this fact means that we can cast equations (KFP) and (HJB) in a time independent form. In fact, by substituting expressions (3.25) into these equations we obtain the time-independent ergodic system

$$0 = \frac{\sigma^2}{2}\Delta u^e - \frac{1}{2\mu}(\vec{\nabla}u^e)^2 - \lambda - V[m^e]\,, \tag{3.26}$$

$$0 = \frac{\sigma^2}{2}\Delta m^e + \frac{1}{\mu}\nabla\cdot(m^e\nabla u^e)\,. \tag{3.27}$$

This is useful because in many instances one is more interested in what happens during the majority of the time of the game, i.e. the ergodic or stationary regime, than near the beginning or the end, i.e. the transient regime.

### 3.3.2 . The Schrödinger Formulation

Another technical detail that we wish to introduce is the possibility to cast the Mean-Field Games equation in a form familiar to physicists. In fact, following the work of Ullmo et al. [87, 86], let us define the following change of variables

$$u(\vec{x},t) = -\mu\sigma^2 \log\Phi(\vec{x},t), \tag{3.28}$$

that is called *Cole-Hopf transformation*. Moreover, let us define $m = \Phi\Gamma$. By substituting these expressions into the time-dependent equations of MFG (KFP) and (HJB) we obtain

$$\mu\sigma^2\partial_t\Phi = -\frac{\mu\sigma^4}{2}\Delta\Phi - V[m]\Phi \tag{3.29}$$

for the Hamilton-Jacobi-Bellman equation and

$$\mu\sigma^2\partial_t\Gamma = \frac{\mu\sigma^4}{2}\Delta\Gamma + V[m]\Gamma \tag{3.30}$$

for the Kolmogorov-Fokker-Planck equation. At this point we observe that, besides the missing imaginary factor associated with time derivation, these equations have exactly the structure of the Non-Linear Schrödinger Equation, with formal correspondence $\Psi \to \Gamma$, $\Psi^* \to \Phi$ and $\rho \equiv ||\Psi||^2 \to m \equiv \Phi\Gamma$. Therefore, all the knowledge pertaining to this subject can be applied to the context of quadratic MFG. In the following, we will refer to this formulation of the problem as the Schrödinger Representation (SR). One of the first advantages of using the SR becomes apparent when we consider the stationary

state of MFG. In fact, in SR the ergodic value function and density are transformed into

$$\Phi^e = e^{-\frac{u^e}{\mu\sigma^2}}, \quad \Gamma_e = \frac{m^e}{\Phi^e}, \tag{3.31}$$

and it can be easily shown that they both follow the same differential equation

$$\frac{\mu\sigma^4}{2}\Delta\Psi^e + V[m^e]\Psi^e + \lambda\Psi^e = 0. \tag{3.32}$$

It is also possible to show that once equation (3.32) is solved, then it is possible to have access to the entire solution because

$$\Phi = e^{\frac{\lambda}{\mu\sigma^2}t}\Psi^e, \quad \Gamma = e^{-\frac{\lambda}{\mu\sigma^2}t}\Psi^e$$

solve equations (3.29) and (3.30).

Always in the spirit of quantum mechanics, it is possible to define operators that, once evaluated on a state of the system, correspond to physical quantities. First, let us introduce the position operator $\hat{X} = (\hat{X}_1, \ldots, \hat{X}_n)$, corresponding to the multiplication to the $i$-th component. Then, we define the momentum operator $\hat{P} = -\mu\sigma^2\vec{\nabla}$. Finally, for any operator $\hat{O}$ defined in terms of $\hat{X}$ and $\hat{P}$ we define its average as

$$\langle\hat{O}\rangle(t) = \langle\Phi(t)|\,\hat{O}\,|\Gamma(t)\rangle = \int \Phi(\vec{x},t)\hat{O}\Gamma(\vec{x},t)d\vec{x}, \tag{3.33}$$

with $\Phi$ and $\Gamma$ evolving according to equations (3.29) and (3.30) respectively. We observe that, with this definition, whenever $\hat{O}$ does not depend on $\hat{P}$, its average is actually

$$\langle\hat{O}\rangle(t) = \int m(\vec{x},t)\hat{O}(\vec{x})d\vec{x}. \tag{3.34}$$

Then, it is possible to show that by taking the time derivative of (3.33), one recovers

$$\frac{d}{dt}\langle\hat{O}\rangle = \langle\partial_t\hat{O}\rangle - \frac{1}{\mu\sigma^2}\langle[\hat{O},\hat{H}]\rangle, \tag{3.35}$$

where $\hat{H}$ is the Hamiltonian that reads

$$\hat{H} = -\frac{\hat{P}^2}{2\mu} - V[m](\hat{X}), \tag{3.36}$$

by using (3.35) to the position and momentum operators one has

$$\frac{d}{dt}\langle\hat{X}\rangle = \frac{\langle\hat{P}\rangle}{\mu}, \quad \frac{d}{dt}\langle\hat{P}\rangle = \langle\hat{F}[m]\rangle, \tag{3.37}$$

where $\hat{F}[m] = -\vec{\nabla}V[m](\hat{X})$ is the *force operator*. Moreover, if

$$V[m](\hat{X}) = U_0(\vec{x}) + f(m), \tag{3.38}$$

the mean force depends uniquely on the external potential $\langle \hat{F} \rangle = \langle \hat{F}_0 \rangle = -\langle \vec{\nabla} U_0 \rangle$. Finally, reconnecting with what we discussed at the beginning of section 3.1, it is possible to introduce an action functional

$$S[\Phi, \Gamma] = \int_0^T dt \int_{R^d} d\vec{x} \left( \frac{\mu\sigma^2}{2} (\Phi \partial_t \Gamma - \Gamma \partial_t \Phi) - \frac{\mu\sigma^4}{2} \vec{\nabla}\Phi \cdot \vec{\nabla}\Gamma + \Phi U_0(\vec{x})\Gamma + F[\Phi\Gamma] \right), \tag{3.39}$$

and it can be shown that finding a couple $(\Phi^*, \Gamma^*)$ so that

$$\frac{\delta S}{\delta \Phi}(\Phi^*, \Gamma^*) = 0, \quad \frac{\delta S}{\delta \Gamma}(\Phi^*, \Gamma^*) = 0, \tag{3.40}$$

means that $(\Phi^*, \Gamma^*)$ solve equations (3.29) and (3.30) respectively.

### 3.3.3 . Understanding the Ergodic Regime - Solitons

We now wish to use the SR to explore in more depth the concept of ergodic or stationary state of MFG we introduced in subsection 3.3.1, following the footsteps of Ullmo et al.[87]. Let us consider a simple example of a one dimensional system with linear local interactions given by $V[m](x) = U_0(x) + gm(x)$ in the limit of a strong attractive interaction $g \to +\infty$, and with a quartic external potential

$$U_0(x) = -\frac{x^2}{2} - \frac{x^4}{4}. \tag{3.41}$$

Moreover, let us imagine an initial density profile which is localized and that could be described by its mean and variance, such as, for example, a Gaussian, with a short characteristic length $\eta$. In the strongly attractive limit, as reported in [87], what is found is that agents soon stick together and move coherently forming what is called, again in analogy with the NLS nomenclature, a *soliton*. This behavior appears after a certain time $\tau^{erg}$ from the beginning $t = 0$ and disappears before the end $T - \tau^{erg}$ of the time interval. Here, we are interested in describing the dynamics of the soliton during this intermediate time, thus its stationary or ergodic state. Using relations (3.37), the fact that interactions are local, and the assumption that the density to be compact and narrow over a short length, the position $X_t = \langle X \rangle (t)$ and momentum $P_t = \langle P \rangle (t)$ operators follow

$$\begin{cases} \frac{d}{dt} X_t = \frac{P_t}{\mu} \\ \frac{d}{dt} P_t = -\vec{\nabla} U_0 \end{cases} \tag{3.42}$$

This is the dynamical system giving the dynamics of the position and the momentum of the density's center of mass. Its motion is therefore that of a classical particle of mass $\mu$ in the potential $U_0$. However, unlike classical mechanics, the dynamics is not fixed by the choice of the initial position and momentum. In fact, with a MFG we have to satisfy both an initial and terminal conditions. The initial position is given by

$$X_{t=0} = \int dx\, x\, m_0(x), \tag{3.43}$$

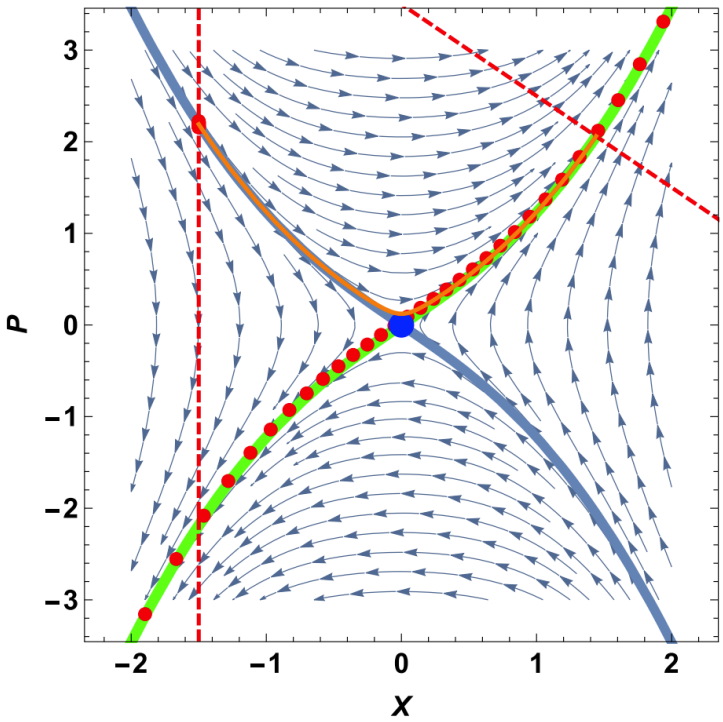


Figure 3.1: Phase space of a one dimensional MFG model, evolving with local interactions and a quartic potential $U_0(x) = -x^2/2 - x^4/4$. Along the vertical dashed line $x_0 = -3/2$ are the allowed initial position, whereas the slanted dashed line is the terminal condition $p_T = -x_T + 7/2$. Trajectories for small $T$ are further away from the unstable fixed-point $(x \equiv 0, p \equiv 0)$ whereas when $T$ grows trajectories spend a long time in a neighborhood of the fixed point, reaching the ergodic state. Image taken from [87].

whereas for the terminal condition we observe that

$$P_{t=T} = \langle \hat{P} \rangle (t = T) = \mu\sigma^2 \int dx\, \Gamma(x, T)\, \partial_x \Phi(x, T),$$

can be written, by multiplying and dividing by $\Phi$, as

$$P_T = -\int dx\, m_T(x)\, \partial_x u_T(x) = -\langle \partial_x c_T(x) \rangle \simeq -\partial_x c_T(x_T), \tag{3.44}$$

again assuming that the density stays localized on a shorter scale than the variation of $c_T$. Let us deal with a more concrete example. The authors of [87] deal with the case where the initial position is $x_0 = -3/2$ and the terminal condition reads $c_t(x) = x(x-7)/2$. The dynamics of the soliton's center of mass is given by equations (3.42), where the potential $U_0$ is given by equation (3.41). In this case, we observe that the system has one fixed point, given by

$(x \equiv 0, p \equiv 0)$, and by performing a simple stability analysis we find that this fixed point is unstable, with one attractive and one repulsive direction. Figure 3.1 gives us the entire phase space of the dynamics, which confirms that $(x \equiv 0, p \equiv 0)$ is an unstable fixed point, with the stable manifold colored in blue and the unstable manifold in green. Moreover, in this figure we see a vertical dashed line representing all points of the phase space compatible with the initial condition $x_0 = -3/2$. The slanted dashed line is given from the expression of $c_t(x)$ that combined with (3.44) gives us all points compatible with the terminal condition, i.e. all points satisfying $p_T = -x_T + 7/2$. This means that only the trajectories starting above the two manifolds in the picture are compatible with these two conditions. What differentiates between them would therefore be $T$. In fact, when $T$ is small, the trajectory stays further from the fixed point, whereas for large $T$, trajectories approach the fixed point very fast, spend a long in its vicinity reaching a stationary or ergodic state, before leaving the neighborhood of the fixed point to reach the terminal condition. The author of this thesis finds this example simple but informative enough to better understand the concept of ergodic state. This will become particularly relevant in chapter 4, where we will show the MFG simulation of the experiment described in section 1.2. In fact, during the experiment, data were collected when the cylinder was halfway through the crowd, neglecting what happens when the obstacle enters or leaves the crowded area. For this reason, we will use the ergodic state of the MFG to simulate the experiment, and the simple example treated here can be a good way to better grasp what will be shown in the following.

## 3.4 . Overview on MFG Applications

Before discussion of a more specific type of MFG to use for simulating the experiment of chapter 1, we want to provide more insight into the various directions along which the research on MFG has evolved during the past two decades.

**MFG with Big Players** As we mentioned, the key assumption of MFG is that the interaction between agents happens via the average density of all other players, that are considered indistinguishable. However, it could be interesting to have one or few "big players", whose strategy and behavior influences other small players, therefore their density. One case this behavior could be observed in a real-life scenario is in finance, as the work of Lehalle et al. [55] proves. In this case, few large investors enter a market populated a large number of small retail high frequency traders. While the moves of a single big investor impact the market decisively, only a large group of small investors can have any direct effect on it. Another example can be found in

the field of opinion dynamics, where Stella et al. [85] show that the impact of a "stubborn" big agent is enough to pull the average of the other small players towards a neighborhood of its opinion. In this case, the big agent is integrated into the MFG by choosing for him a running cost different from the one of other agents, and solving a dedicated set of equations to obtain its strategy and motion. Including a big agent into the MFG entails a large deal of complications in the model, most importantly the fact that its motion is stochastic and cannot be averaged out. Being able to solve the MFG system with a stochastic element presents a big challenge and is a topic yet to be fully understood.

**MFG on Networks** MFG can also be extended to situations where individuals are in contact through a more or less organized structure, for example a graph. It could, for example, be the case that many graphs are then in contact between them, as in the work of [7]. Here, the authors use a mix of repeated games and mean-field games to study the interaction of different networks where individuals are rewarded for herding towards a shared common opinion. For a more mathematical explanation of mean-field games on networks we refer to [4], where existence and uniqueness results are obtained.

**MFG in Different Populations** Another possible application of MFG is the description of populations each composed of indistinguishable rational agents, that are in contact with each, usually with different overall preferences. This scenario is considered, for example, by Lachapelle et Wolfram in [54], where they treat the case of two different groups of pedestrians moving towards two different targets trying not to mix with the other group. Another instance of MFG between populations can be found in [3], where the case of segregation in cities is treated.

**MFG in Epidemiology** MFG models have found their territory in the field of epidemic models. On notable work in the field is the one of Laguzet and Turinici [58], where the decision of individuals to be vaccinated is analyzed, and the model is compared with the 2009/10 vaccination campaign. Interestingly, the authors observe that when a term attenuating future risk is introduced in the model, agents may choose to wait before getting vaccinated to better estimate the actual need for it. This anticipates the introduction of the discount factor we will discuss in section 4.3. Another important and recent contribution to the epidemiology field is that of Bremaud et al. [14, 13], where a MFG model is coupled to the SIR (Susceptible, Infected, Recovered) model to find the optimal way to enforce a lockdown and how this affects various classes of individuals among an interacting population. Moreover, they also

discuss the case where each individual only interacts with a limited number $k$ of neighbors, organized on a graph.

**MFG in Economics and Finance** Applications of MFG to finance date soon after the introduction of the model. Among the main contributions on the topic, we register that of Lehalle et al. [20], where the problem of trade crowding, meaning the effects of transactions of the dynamics of the price of the traded object, using mean-field games, and obtaining the optimal trading rate to liquidate a position during regular trading hours. Moreover, another example of MFG applied to economics are the works of of Gomes et al. [36, 37], where the authors study an economy where agents have to balance between capital gain and consumption.

### 3.4.1 . MFG in Pedestrian Dynamics

One of the first attempts to build a model using differential games can was made by Hoogendoorn in [45, 46]. In these works, however, the model proposed does not fully correspond to a Mean-Field Game. In fact, although in Hoogendoorn's models the minimization of a subjective cost functional is already present, the actual motion of pedestrians is not performed by the evolution of their density but through a microscopic model, where the desired velocity is obtain from said optimisation, computed not over the entire duration of the motion but repeatedly over time. Indeed, in the various scenarios simulated with this model, pedestrians reevaluate their trajectory based on the current traffic condition, whereas, in a fully MFG approach, the optimal behavior would be available to all individuals from the beginning.

The use MFG to describe pedestrian dynamics was at first suggested by Guéant et al. [39, 25], Lachapelle [56] and Dogbé [32]. In particular, in [32], Dogbé describes how to model a crowd of individuals using the MFG formalism, starting with the case of one pedestrian, whose state variable is its position, whose dynamics is given by the minimizing a cost functional describing the environment. Then, it passes to the problem with $N$ pedestrians and finally, taking the limit $N \to \infty$, arrives to the actual definition of the Mean-Field Game. Although introducing the technical tools of MFG, Dogbé does not solve the system of equations nor presents any simulation. For the first actual implementation of MFG for describing pedestrian motion, we refer to the work by Lachapelle and Wolfram [54]. In this paper the authors they treat the case where more than one population exist in the same simulation space, with different levels of aversion towards agents of the same or of the other population. They do this by adding a coupling term to the MFG cost functional they choose for their model, giving the intensity of the aversion between populations of different kind. In addition to this, Lachapelle and Wolfram address the problem of the description of congestion, which is the fact that moving fast

in high density areas is harder. This is particularly important to try and recover a realistic fundamental diagram, in connection with the Hughes model were the current depends on the density. The relation between MFG and the Hughes' model is explored even further in the work by Burger et al [15], that describes the scenario where a group of pedestrians tries to evacuate a room as fast as possible. In particular, in this work the authors show that through an accurate choice of the MFG's running cost it is possible to draw a mapping between the two models.

Another and more recent contribution to the field of MFG model for simulating pedestrian dynamics is the one proposed by Cristiani et al. [26, 27]. In particular, in the first of these two papers, [27], the authors delve into the categorization of pedestrian models based on the anticipation abilities of the simulated individuals, ranging from irrational, where pedestrians move erratically, to rational and highly rational, where pedestrians move following a trajectory obtained from the analysis of the surrounding environment and other people's behavior. In the case of MFG, as we will see in section 4.3, the anticipation abilities of the agents can be modulated using what is called a *discount factor*, however Cristiani et al. propose in [27] an alternative way to do this, by reducing the time interval of the agents' optimization. Then, in [26], the authors extend this by considering a MFG model where agents constantly recompute their optimization over a moving time interval.

Finally, we acknowledge the work of Arjmand and Mazanti [5, 6] where the authors explore the mathematical properties of a general form of MFG applied to a pedestrian dynamics scenario, namely the one where pedestrians have to evacuate a room as fast as possible. In this work, they study the well-posedness of the problem, look for the uniqueness of Lagrangian equilibria. Then, they bring their attention on models where constraints are presents, usually to describe obstacles like walls, fences etc.

# 4 - Simulation of the Experiment

The goal of this chapter is to convince the reader that a MFG description is a good way to simulate the experiment introduced in chapter 1 and that it can provide a good framework to understand its results, in all three experimental configurations, summarized in Figure 4.1. Since, as we explain in 1.2, the main empirical features are present regardless of the average density, we decide to work with a value of $3.5ped/m^2$, because for this density we possess the cleanest experimental data. First, we focus on the case where pedestrians were facing the obstacle, displayed on the left-most column of Figure 4.1. We refer to this as the complete information configuration, since in that case, all pedestrians could assess the cylinder's position and velocity, anticipating it at their best. Under these circumstances, we want to show that models of pedestrian dynamics based on short-term anticipation fail at reproducing the empirical data. Thus, in section 4.1 we show how two of the microscopic models of chapter 2, namely Helbing's social force and ANDA, perform at the task. We will discover that none of them fully captures the dynamics at play because they both fail to provide long-term anticipation, the ability to anticipate the obstacle well ahead of its arrival, and to deal with its passage until the subsequent rearrangement of the crowd. In section 4.2 we want to convince the Reader that, on the other hand, a model based on the minimal version of MFG described in section 3.3 can simulate agents with a sufficiently long anticipation time-frame to adequately reproduce the experimental configuration where pedestrians had complete information about the intruder. Then, we deal with the other two experimental setups, displayed in the central and right-most columns of Figure 4.1, with participants randomly oriented, or giving their back to the obstacles and trying not to anticipate. In section 4.3 we show how by adding only one parameter to our MFG model, namely the *discount factor*, we can modulate the anticipation time-window of the simulated agents to correctly reproduce these configurations as well. What follows is a synthesized version of the work contained in the two journal papers [12, 16], attached to this thesis in the Published Papers chapter, and in the preprints [17, 18]. We invite the Reader to consult them to have more details about what we present here.

## 4.1 . Microscopic Models - Complete Information

In chapter 2 we gave an overview of various pedestrian dynamics simulation models and divided them into microscopic and macroscopic models. As we said, each type of model has drawbacks and advantages. In particular,

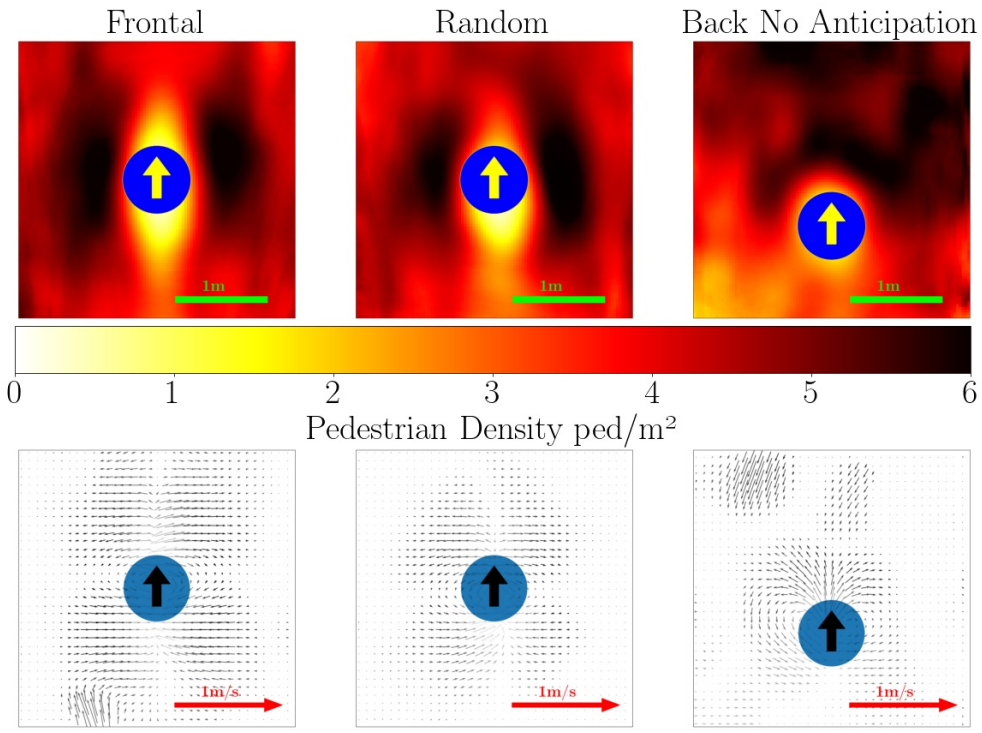


Figure 4.1: Experimental results of the passage of a cylindrical intruder (blue disc) through a static dense crowd for an average density of $\sim 3.5 ped/m^2$ for the three different configurations of the experiment of section 1.2. **Top row**: densities plots. **Bottom row**: velocity fields. Data from [75]. Figures extracted from [16].

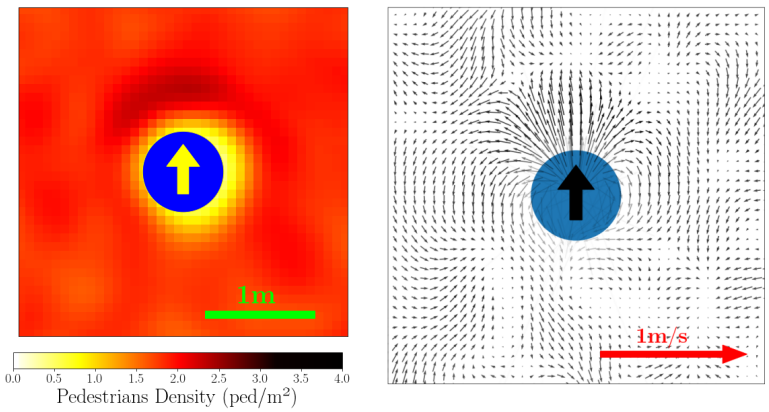


Figure 4.2: Density (left panel) and velocity (right panel) fields of the social force simulation. An accumulation is present in front of the obstacle, and the velocity field displays the agents moving around the intruder.

as was reported in [78], macroscopic model perform particularly well when used to describe situations with a very large number of pedestrians, such as the evacuation of large buildings. On the other hand, macroscopic models are less precise in reproducing situations where the interactions between the agents have an important role on the behavior of the crowd, especially at the operational level. In a direct comparison between a microscopic and a macroscopic model, Maury et al. [69] showed how the behavior of the simulated flow near a door during an evacuation can widely differ between the two types of models, with macroscopic one unable to predict some of the features observed in the microscopic simulation. We therefore expect microscopic models to be accurate at capturing the interactions between the individuals around the incoming intruder. Here we will show how the Helbing's social force model of subsection 2.1.1 and the ANDA model explained in subsection 2.1.2 perform at reproducing the experimental configuration where participants were facing the obstacle. We test the models on this configuration because it is the one where long-term anticipation is more clearly involved in the pedestrians' behavior, thus providing us with a valuable benchmark against which we will compare the MFG model.

As shown in section 2.1.1, Helbing's social force model has proved very valuable in numerous situations and still constitutes a valid tool implied in some of the state-of-the-art simulation software. However, when it comes to reproducing the frontal configuration of the experiment of chapter 1.2, it appears that this method fails at capturing the dynamics at play. In fact, as the left panel of Figure 4.2 shows, in the density plot simulated using this model we observe an accumulation, although slight, of pedestrians in front of the

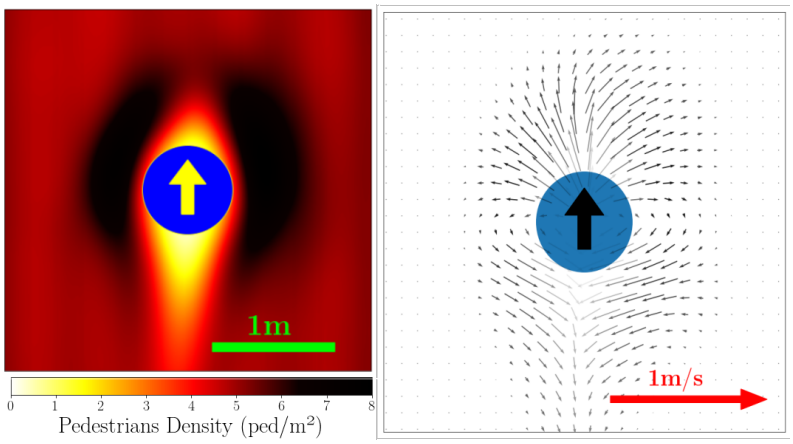


Figure 4.3: Density (left panel) and velocity (right panel) fields of the ANDA simulation. Although the density fields display a clear improvement, with more wing-shaped distribution, the velocity field still lacks the lateral motion ahead of the intruder observed empirically. Figures extracted from [12].

obstacle, similarly to the granular simulation of 1.1. Moreover, in the right panel of Figure 4.2 we can see how the velocity field simulated with the social force model does not show any sign of anticipatory behavior, with most motion being the rotation of individuals around the incoming intruder. Although having represented a milestone in the field of pedestrian dynamics, the social force model struggles to capture the complex anticipatory behavior observed in the experiment we refer to here. The reason for this is the locality of the social force interaction, whose scale in space and time is too short to inform the simulated individuals of the intruder's arrival.

The second model we want to use to simulate the experiment is ANDA. This is a complex simulation tool that puts together decades of advancements in the field of simulating pedestrians and, as we showed in section 2.1.2, it can reproduce a wide array of pedestrian dynamics empirical facts. However, when used to reproduce the experimental configuration of complete information, although achieving a better overall result than the social force model, it still cannot fully reproduce it. As we can see, the density field, on the left of Figure 4.3 shows a decisive improvement with respect to both the granular model, in Figure 1.2, and the social force model, showed in Figure 4.2. Indeed, in ANDA agents accumulate at the sides of the moving intruder. However, the opening in front of the obstacle is not at all comparable to the empirical one, as if the simulated agents did not anticipate enough. In fact, by looking at the right panel of Figure 4.3, we see that the displacement in front of the intruder is alongside its direction of motion, meaning that agents were pushed along by it without anticipating. In conclusion, we have observed how ANDA, al-

though being way more technologically advanced than the simple social force model, cannot reproduce the entirety of the empirical features displayed by the experimental figure. We insist that the reason for this is the lack of long term anticipation in both models. In fact, in the social-force model no anticipation is considered, whereas ANDA uses a short-term time-to-collision anticipation mechanism, clearly not enough to reproduce the timely avoidance maneuver displayed by pedestrians in the experiment.

## 4.2 . MFG Simulation of Complete Information

We have tested both the social force model and ANDA finding that neither of them can fully reproduce the complete information experiment. This is because they only allow for short-time anticipation. Although this experiment is of a simple conception, it entails something crucial to understand how far into the future individuals plan their motion. Indeed, in the configuration where participants were facing the obstacle, the situation was familiar enough that they could estimate the location and timing of their collision with the intruder as well as understand others behavior. Therefore, they could anticipate its arrival in advance and choose a strategy allowing them the least amount of displacement, given that moving in a crowded space is uncomfortable. However, this optimization takes place on a timescale longer than that of the aforementioned models, exceeding the operational layer of motion. In the following, we prove that using a minimal MFG model, we can extend the anticipation horizon and include some tactical planning.

### 4.2.1 . Adapting MFG to the Experiment

We describe each pedestrian motion through the Langevin equation (3.14), where the state variable $\vec{x}$ represents the position at time $t$. Then, the optimal control $\vec{a}$ is the optimal velocity at time $t$. We use the running cost (3.19), where the square of the velocity means that pedestrians try not to go too fast and, in general, the optimal strategy would be not to move. However, the presence of the potential (3.20) forces them to move. Moreover, we choose the terminal cost $c_T \equiv 0$ because we only want to simulate the avoidance of the intruder. The external potential $U_0$ is used here to describe the moving cylinder

$$U_0(\vec{x}, t) = \begin{cases} +\infty & \|\vec{x} - \vec{s}t\| < R \\ 0 & \text{otherwise} \end{cases} . \tag{4.1}$$

Then, the density term of potential (3.20) represents the interactions among pedestrians, mediated by the average density. Since we want pedestrians to avoid congested areas, we choose negative coordination $g < 0$.

In practice, we decide that we want to simulate the experimental configuration using the ergodic state of the MFG model. This is for two reasons:

first, the empirical data of the experiment were collected when the moving intruder was halfway along its path; second, solving the stationary state is faster, although not easier, than solving the time-dependent MFG. However, the choice of external potential 4.1 presents two issues:

1. As section 4.4.1 will better explain, the value function $u$ would be infinite for all points under the cylinder, something unpleasant to implement numerically. Fortunately, using the Schrödinger representation solves this, since where $u$ is infinite we have that $\Phi \equiv 0$ and $\Gamma \equiv 0$.

2. $U_0(\vec{x}, t)$ explicitly depends on time, preventing the existence of the ergodic state, as we mentioned in subsection 3.3.1. We solve this by passing from the reference frame of the experimenters to the frame of the cylinder, defining

$$\hat{\Phi}(\vec{x} - \vec{s}t, t) = \Phi(\vec{x}, t), \quad \hat{\Gamma}(\vec{x} - \vec{s}t, t) = \Gamma(\vec{x}, t),$$
$$\hat{u}(\vec{x} - \vec{s}t, t) = u(\vec{x}, t), \quad \hat{m}(\vec{x} - \vec{s}t, t) = m(\vec{x}, t).$$

With these assumptions, the MFG equations we solve to simulate the experiment are

$$\frac{\mu\sigma^4}{2}\Delta\hat{\Phi} - \mu\sigma^2\vec{s}\cdot\vec{\nabla}\hat{\Phi} + [U_0(\vec{x}) + g\hat{m}]\hat{\Phi} = -\lambda\hat{\Phi} \tag{4.2}$$

$$\frac{\mu\sigma^4}{2}\Delta\hat{\Gamma} + \mu\sigma^2\vec{s}\cdot\vec{\nabla}\hat{\Gamma} + [U_0(\vec{x}) + g\hat{m}]\hat{\Gamma} = -\lambda\hat{\Gamma} \tag{4.3}$$

where $\lambda$ is the same as the one in equation (3.25). These equations differ only for the sign of the term with the cylinder's velocity $\vec{s} = (0, s)$. The value of $\lambda$ in this case is given by observing what happens far from the obstacle, in what we call the asymptotic regime.In fact, at a certain distance from the intruder, pedestrians are not impacted by its presence. Thus, the optimal strategy is not to move, so that $\vec{a}^* = 0$ and the average density would be constant, equal to $m_0$. Using this information and the definition of the cost functional (3.21) we get, far from the cylinder,

$$u(\vec{x}, t) = -\int_t^T (gm_0)d\tau = -gm_0T + gm_0t\ , \tag{4.4}$$

and thus $\lambda = -gm_0$. Moreover, to solve equations (4.2) and (4.3) we need to specify the boundary conditions. To this end, we need to introduce the velocity field, given by the KFP equation in the moving frame

$$\partial_t\hat{m} - \vec{s}\cdot\vec{\nabla}\hat{m} = \frac{\sigma^2}{2}\Delta\hat{m} + \frac{1}{\mu}\vec{\nabla}\cdot(\hat{m}\vec{\nabla}\hat{u})$$
$$\partial_t\hat{m} = \vec{\nabla}\cdot\left[\frac{\sigma^2}{2}\vec{\nabla}\hat{m} + \vec{s}\hat{m} + \frac{1}{\mu}\hat{m}\vec{\nabla}\hat{u}\right] = -\vec{\nabla}\cdot\vec{j}$$

from which, since $\vec{j} = m\vec{v}$, we have that

$$\hat{\vec{v}} = -\frac{\vec{\nabla}\hat{u}}{\mu} - \vec{s} - \frac{\sigma^2\vec{\nabla}\hat{m}}{2\hat{m}}. \tag{4.5}$$

Of course, this definition is still valid in particular for the ergodic regime. We observe now that passing to the moving frame means that we now look at the experiment standing on top of the cylinder. In this case, we see distant pedestrians moving with relative velocity $-\vec{s}$, and, as we already mentioned, having a constant density $m_0$. Using these facts, we can say that in the asymptotic regime, in the ergodic state, it must hold

$$\hat{\vec{v}}_{asy} = -\frac{\vec{\nabla}\hat{u}_{asy}}{\mu} - \vec{s} = -\vec{s}$$

from which we obtain $\nabla\hat{u}_{asy} = 0$ and $\nabla\hat{\Phi}_{asy} = 0$, leaving us with $\hat{\Phi}_{asy} = C$. To fix $C$ we recall that $\hat{\Phi}_{asy}\hat{\Gamma}_{asy} = m_0$, meaning that one can take $C \equiv \sqrt{m_0}$, and this is the boundary condition for both equations (4.2) and (4.3).

Interestingly, it is possible to choose another set of boundary conditions. In fact, let us consider the change of variables $\hat{u} = \bar{u} - \mu\vec{\nu}\cdot\vec{r}$, with $\vec{\nu}$ generic velocity. Substituting (4.5) gives

$$\bar{\vec{v}} = -\frac{\nabla\bar{u}}{\mu} - (\vec{s} - \vec{\nu}) - \frac{\sigma^2\nabla\hat{m}}{2\hat{m}}, \tag{4.6}$$

that, considering the asymptotic behavior, when put equal to $-\vec{s}$ gives, $\nabla\bar{u}_{asy} = \mu\vec{\nu}$, from which $\nabla\bar{\Phi}^e_{asy} = -(\mu\nu)/\sigma^2\bar{\Phi}^e_{asy}$, that, when solved gives

$$\bar{\Phi}^e_{asy} = \sqrt{m_0}e^{-\frac{\mu\vec{\nu}\cdot\vec{r}}{\sigma^2}}, \quad \bar{\Gamma}^e_{asy} = \sqrt{m_0}e^{\frac{\mu\vec{\nu}\cdot\vec{r}}{\sigma^2}}, \tag{4.7}$$

that, in the Schrödinger formalism, can be considered a Gauge transformation.

### 4.2.2 . Phase Space MFG

Another useful property of the Schrödinger formulation is that, as it was shown in [11], the MFG solutions are entirely specified by two dimensionless parameters. In fact, the intruder is characterized by its radius $R$ and its speed $s$. Similarly, the crowd is characterized by a length scale

$$\xi = \sqrt{\left|\frac{\mu\sigma^4}{2gm_0}\right|} \tag{4.8}$$

the distance over which the crowd density tends to recover its bulk value from a perturbation, the *healing length*, and a velocity scale

$$c_s = \sqrt{\left|\frac{gm_0}{2\mu}\right|} \tag{4.9}$$

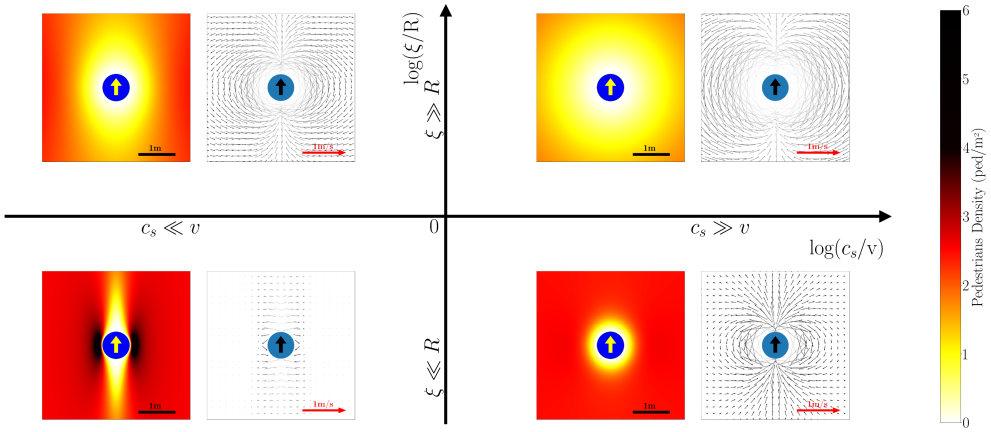


Figure 4.4: Typical density and velocity fields induced by the crossing intruder in the permanent regime, as predicted by the MFG model in different regions of the parameter space. Parameters taken in the small $c_s/s$ and small $\xi/R$ quadrant display good visual agreement with the experimental data. Figure taken from [12].

the typical speed at which pedestrians tend to move, that, in analogy with NLS formalism, we call the *sound velocity*. Note that $\mu\xi c_s = \mu\sigma^2$ has the dimension of an action and plays the role of $\hbar$ in the original nonlinear Schrödinger equation. Up to a scaling factor, solutions of (4.2) and (4.3) can be expressed as a function of the two ratios $\xi/R$ and $c_s/s$ instead of depending on the full set of parameters $(R, v, \mu, \sigma, m_0, g)$, which facilitates the exploration of the parameter space and makes modeling more robust. Figure 4.4 presents the typical density and velocity fields simulated in the ergodic regime, for each quadrant of the reduced parameter space. Intuitively, one understands that $c_s$ governs the cost of motion for the agents while $\xi$ gives the extent of the perturbation caused by the presence of the intruder. The main difference between large and small $c_s/s$ is the change in rotational symmetry, which reflects a fundamental change in strategy. For large values of $c_s/s$ pedestrians do not mind moving, and they rather try to avoid congested areas for as long as possible, thus creating circulation around the intruder, as shown in the velocity plots. On the other hand, for small values of $c_s/s$, moving fast costs more; therefore, to avoid the intruder, pedestrians have to move earlier, and accept to temporarily side-step into a more crowded area, thereby stretching the density along the vertical direction.

### 4.2.3 . MFG Simulation of the Complete Information Case

We now present the MFG simulation of the experimental configuration where pedestrians were facing the arriving cylinder. Under these circumstances, participants could efficiently estimate the cylinder's size and velocity,

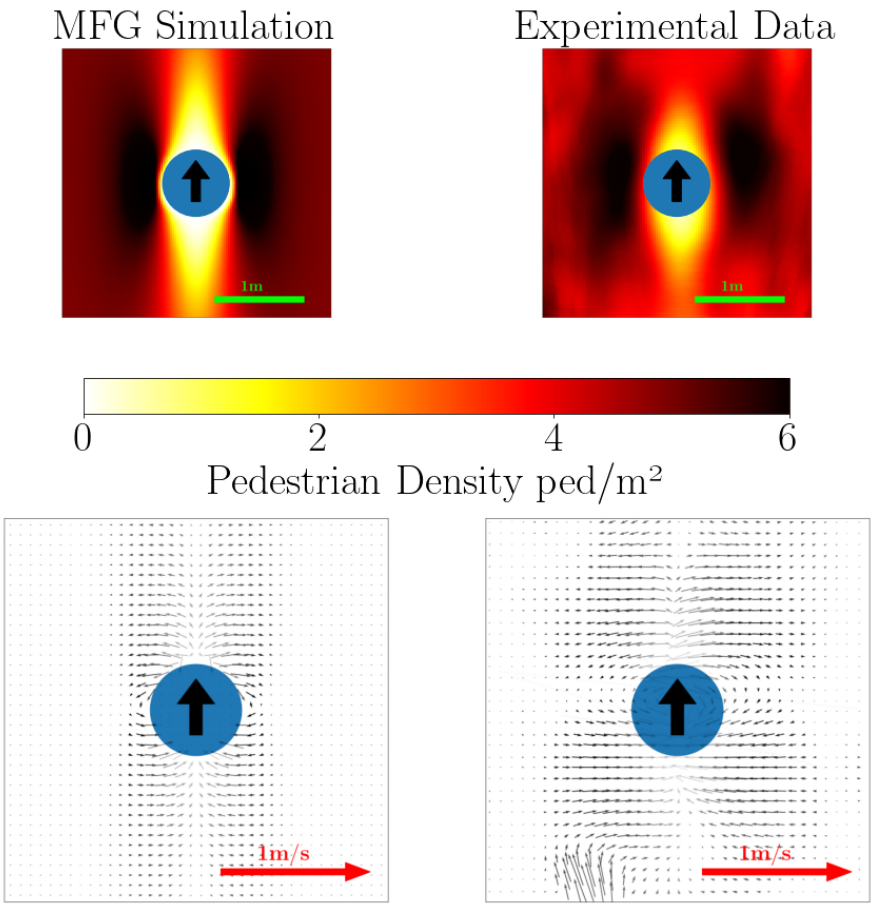


Figure 4.5: Qualitative comparison between density, first row, and velocity plots, second row, between the experiment, right column, and the ergodic state of the MFG model, with parameters $\xi = 0.2$, $c_s = 0.1$, left column, for the case where all pedestrians were facing the incoming intruder. Figures extracted from [16].

thus the time it would take for the obstacle to reach them. The simulation is shown on the left column of Figure 4.5. Here we see how striking the resemblance to the experiment is. Starting from the density plot, we clearly see the vertically symmetric distribution of pedestrians, with a depletion prior and posterior to the obstacle passage and with an increase on the sides. Moreover, the velocity field obtained from the MFG model correctly displays the lateral motion of pedestrians stepping aside to make room for the intruder. We believe MFG good performances should be attributed to long-term anticipation, naturally hardwired to the very structure of MFG. In fact, the back-propagation of information in the HJB equation (HJB) allows MFG agents to optimally anticipate the obstacle's arrival.

We have achieved a good qualitative agreement to the experimental data,

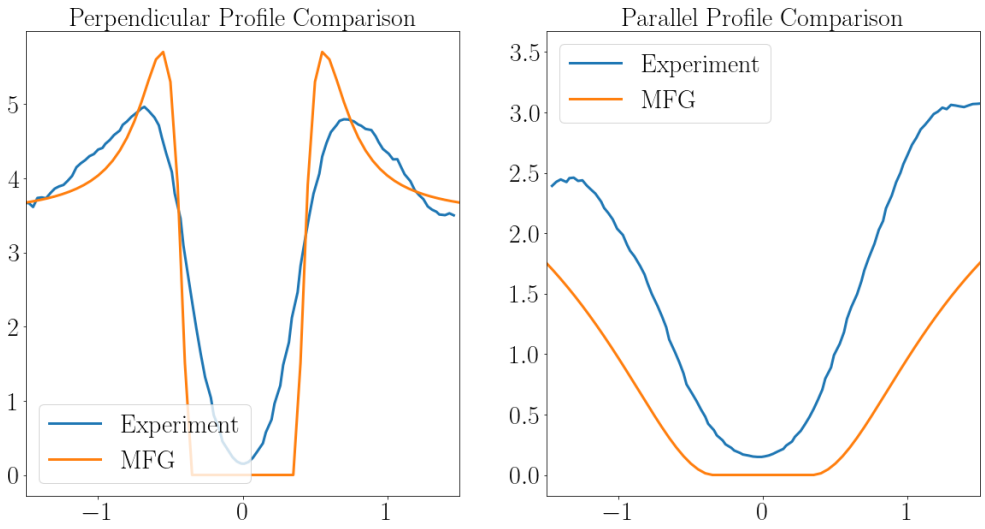


Figure 4.6: Profile comparison between the MFG simulation and the experimental data for the frontal configuration. The left panel shows the profile perpendicular to the intruder's direction of motion, whereas in the right panel the profile parallel to the intruder's direction of motion is shown.

using a model inspired on a minimal version of Mean-Field Games. This points to the fact that what is needed to accurately capture the empirical behavior, is already present in the vary basics of MFG. In particular, the long-term anticipation present in this kind of model is what makes it a good choice to reproduce scenarios such as the one considered here. However, attempting to reach a perfect quantitative agreement was out of the scope of our work. In fact, let us take a look at Figure 4.6, where the MFG and experimental density profiles are compared. The left and right panels represent the comparison of the density profiles cut along the directions perpendicular and parallel to the intruder's motion respectively. As we can see, the agreement in this case is not perfect, with a clear difference in the maximum density in the left panel, and a visible discrepancy of the parallel profile. It should be noted that the data at our disposal is very coarse grained, which makes it hard to accurately tune the parameters of the MFG model. We hope the future experiments will bring to the table even more data that will allow for a more precise calibration of the model.

### 4.3 . Reduced Information

Now we turn our attention to the other two configurations the experiment was performed in, namely the center column, where pedestrians were

oriented randomly, and the right-most column, where pedestrians were giving their back to the obstacle and were told not to anticipate, of Figure 4.1. To simulate them, we first need to understand what changes from the frontal configuration. The difference is indeed the quantity and quality of information individuals in the crowds had depending on their orientation. When they were facing the obstacle, participants had perfect knowledge of its trajectory. On the other hand, in the other configurations, only some, or in the third case, no one, could directly see the approaching intruder. This means that these people had to rely on other elements, like the pressure of the crowd or the noise, to choose an avoidance strategy, and their knowledge of the intruder's future trajectory was less certain than before. To incorporate this into our MFG we choose to add an exponential term $e^{\gamma(t-\tau)}$ that multiplies the running cost, much like a continuous interest rate on a cash flow, with $\gamma$ being called a *discount factor*. We expect the consequences to be that future events will be more or less disregarded, depending on the value of $\gamma$. This term therefore acts as a measure of the knowledge of pedestrians. After this addition, the model's cost functional is defined as

$$c[\vec{a}](\vec{x},t) = \mathbb{E}\left\{\int_t^T \mathcal{L}(\vec{x},\tau)[m]e^{\gamma(t-\tau)}d\tau + e^{\gamma(t-T)}c_T(\vec{x}_T)\right\} \tag{4.10}$$

where $\gamma$ is the discount factor, and its inverse $1/\gamma$ defines an anticipatory timescale determining how far into the future agents will look while optimizing. Making use of the *dynamic programming principle* [9], as in section 3.3, $u(\vec{x},t)$ can be written as

$$\begin{aligned} u(\vec{x},t) &= \inf_{\vec{a}}\left[\mathcal{L}(\vec{x},t)[m]dt + e^{-\gamma dt}u(\vec{x}+d\vec{x},t+dt)\right] \\ &\overset{\text{Ito}}{=} \inf_{\vec{a}}\left\{\mathcal{L}(\vec{x},t)[m]dt + (1-\gamma dt)\left[u(\vec{x},t) + dt\left(\partial_t u + \vec{a}\cdot\vec{\nabla}u + \frac{\sigma^2}{2}\Delta u\right)\right]\right\} \end{aligned}$$

where in the last passage the Ito chain rule has been used to calculate the total time derivative of the value function. Then, by keeping only terms of order one in $dt$ we obtain

$$0 = \partial_t u - V[m] + \frac{\sigma^2}{2}\Delta u - \gamma u + \inf_{\vec{a}}\left\{\frac{\mu}{2}\vec{a}^2 + \vec{a}\cdot\vec{\nabla}u\right\}. \tag{4.11}$$

At this point, by minimizing the term in the curly brackets with respect to $\vec{a}$ we still find that the optimal velocity is given by $\vec{a}^* = -\vec{\nabla}u/\mu$. When we plug $\vec{a}^*$ in (4.11) we have

$$\begin{cases} \partial_t u = -\frac{\sigma^2}{2}\Delta u + \frac{1}{2\mu}(\vec{\nabla}u)^2 + \gamma u + V[m] \\ u(\vec{x},t=T) = c_T(\vec{x}) \end{cases}. \tag{HJB-d}$$

The (KFP) equation, on the other hand, is unchanged.

In subsection 3.3.1 we have introduced the ergodic state of MFG but for the model without discount factor. Now we make the rather natural hypothesis that, for large $T$, such a stationary state also exists when $\gamma \neq 0$, i.e. for a finite anticipation time $1/\gamma$. We therefore assume that for intermediate times, there exists a state of the discounted system where the observables are independent on time. If that is the case, (3.24) should still hold, and we can as before determine the time-dependent part of $u_e$ by considering what happens far from the cylinder where the density remains homogeneous, and the optimal strategy is simply to stand still. In this case (4.10) becomes

$$u(\vec{x},t) = -\int_t^T (gm_0)e^{-\gamma(\tau-t)}d\tau = \frac{gm_0}{\gamma}\left(e^{-\gamma(T-t)}-1\right) . \tag{4.12}$$

We observe that if we fix $T$ and let $\gamma \to 0$, the right-hand side of equation (4.12) becomes $-gm_0T + gm_0t$, recovering equation (4.4) and the $\gamma = 0$ case. On the other hand, if we fix $\gamma$ and let $T \to \infty$, we have that $u^e(t) \equiv 0$, and since $u^e(t)$ does not depend on the position, this must be true everywhere, meaning that when $\gamma \neq 0$

$$u^e(\vec{x},t) = u^e(\vec{x}) , \tag{4.13}$$

and therefore $\lambda = 0$. Finally, we can write (HJB-d) in its stationary form as

$$0 = \frac{\sigma^2}{2}\Delta u^e - \frac{1}{2\mu}(\vec{\nabla}u^e)^2 - \gamma u^e(x) - V[m^e]. \tag{4.14}$$

### 4.3.1 . Phase Space of the Partial Information Case

Before showing the simulation of the experimental configuration, we discuss the consequences on the phase space diagram of Figure 4.4 of the inclusion of the discount factor in the model. In fact, the inclusion of a non-zero discount factor $\gamma$, which has the dimension of the inverse of a time, implies that the MFG model is now characterized by three dimensionless quantities, $\tilde{R} \equiv R/\xi$, $\tilde{s} \equiv s/c_s$ and a third one that can be either $\tilde{\gamma}^{(1)} \equiv (\xi/c_s)\gamma$ or $\tilde{\gamma}^{(2)} \equiv (R/s)\gamma$ (Note $\tilde{\gamma}^{(2)} = (\tilde{R}/\tilde{s})\tilde{\gamma}^{(1)}$). The first option, $\tilde{\gamma}^{(1)}$, compares the timescale associated with anticipation to one of the crowd dynamics, while $\tilde{\gamma}^{(2)}$ measures it in terms of the timescale characterizing the cylinder. Figure 4.7 shows the numerical solution of the stationary equations of the discounted MFG model for four choices of $(\tilde{R},\tilde{s})$ and different values of $\gamma$. Note that in the $(\tilde{R} \gg 1, \tilde{s} \gg 1)$ and $(\tilde{R} \ll 1, \tilde{s} \ll 1)$ quadrants, we have assumed $\tilde{R} \sim \tilde{s}$, so that $\tilde{\gamma}^{(1)} \sim \tilde{\gamma}^{(2)}$, and both of them are therefore either large together or small together. However, in the quadrant $(\tilde{R} \gg 1, \tilde{s} \ll 1)$, we have $\tilde{\gamma}^{(2)} = (\tilde{R}/\tilde{s})\tilde{\gamma}^{(1)} \gg \gamma^{(1)}$, so we have distinguished the three possible cases $(\tilde{\gamma}^{(1)} \ll 1, \tilde{\gamma}^{(2)} \ll 1)$, $(\tilde{\gamma}^{(1)} \ll 1, \tilde{\gamma}^{(2)} \gg 1)$, and $(\tilde{\gamma}^{(1)} \gg 1, \tilde{\gamma}^{(2)} \gg 1)$; and in the same way in the quadrant $(\tilde{R} \ll 1, \tilde{s} \gg 1)$ where $\tilde{\gamma}^{(2)} \ll \gamma^{(1)}$ we distinguish the three cases $(\tilde{\gamma}^{(1)} \ll 1, \tilde{\gamma}^{(2)} \ll 1)$, $(\tilde{\gamma}^{(1)} \gg 1, \tilde{\gamma}^{(2)} \ll 1)$, and $(\tilde{\gamma}^{(1)} \gg 1, \tilde{\gamma}^{(2)} \gg 1)$. Let us consider for instance the III quadrant, where both

$\tilde{s}$ and $\tilde{R}$ are small. The fact that $\tilde{s}$ is small means the cylinder is perceived as nearly immobile by the crowd, which explains the rotational invariant shape of the solution. For small values of $\gamma$, the distance at which an immobile perturbation is felt by the crowd is, as mentioned above, given by the healing length $\xi$. As $\gamma$ increases, this length should be compared to $d_{c_s} = c_s/\gamma$, the length scale related to the finite nature of the anticipation horizon. Hence, from Figure 4.8 we see that the scale of the density perturbation around the obstacle is given by the smallest between the $d_{c_s}$ and $\xi$. In this case, a large $\gamma$ does not, however, modify the qualitative aspect of the density distribution, which remains vertically invariant. Figure 4.9 then focuses on the I quadrant, where both $\tilde{R}$ and $\tilde{s}$ are large. Because $\tilde{s}$ is large, the agents feel that the cylinder moves significantly more rapidly than the speed they can themselves maintain comfortably within the crowd. For small $\gamma$, they would therefore tend to anticipate the obstacle arrival by moving sideways quite early, which explains the low density corridor extending rather far in front of the cylinder in that case, typically at a distance of order $l_s = s\xi/c_s$. The density profile is in this case essentially symmetric, as for $\gamma = 0$ the system in the ergodic state is invariant under the symmetry $y \mapsto -y$. When $\gamma$ increases, $l_s$ should be compared with $d_s = s/\gamma$, which measures how far from the cylinder, agents can foresee its motion. As illustrated in Figure 4.9, we see that when $d_s < l_s$, the size of the perturbation in front of the cylinder is given by $d_s$. Contrarily to what happens in the third quadrant, however, this change of scale qualitatively alters the solution, with a density blob forming in front of the cylinder and, on the other hand, a density profile behind the cylinder which is much less affected. The variations of the density plots seen on quadrant II and IV are somewhat more complex since the four length scales $(\xi, l_s, d_{c_s}, d_s)$ are involved, but the mechanisms observed in Figure 4.8 and Figure 4.9 can be seen to be at work there too.

### 4.3.2 . MFG Simulation of the Partial Information Case

Now that we know how the model behaves when we introduce the discount $\lambda$, we use it to simulate the other two experimental configurations. In the experimental configuration where participants were asked to orient themselves randomly, we see, from the right column of Figure 4.10, that the main difference with the frontal case is in the decrease in the depletion in front of the obstacle, meaning that participants anticipate less. We can imagine that, when participants were placed randomly, only some of them could gather information about the obstacle visually, whereas the rest had to resort to all their other senses to decide how to react. This impacts the global anticipatory behavior and causes a later reaction to the obstacle arrival. The inclusion of the discount factor $\gamma$ in our MFG is enough to describe the change in the crowd's avoidance strategy. The left column of Figure 4.10 shows the nu-

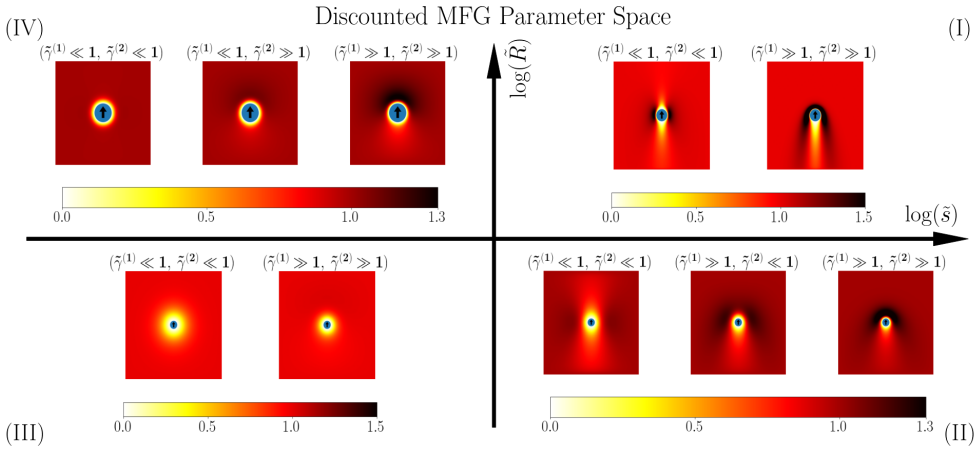


Figure 4.7: Exploration of the parameter space of the MFG model. Each sub-figure represents the discounted stationary MFG density obtained solving (3.27) and (4.14). The axes represent the dimensionless quantities $\tilde{R} \equiv R/\xi$ and $\tilde{s} \equiv s/c_s$. Each quadrant shows different values of $\tilde{\gamma}^{(1)} \equiv (\xi/c_s)\gamma$ (or $\tilde{\gamma}^{(2)} \equiv (R/s)\gamma$). Parameters of the sub-figures in each quadrant in format $(\tilde{s}, \tilde{R}; [\tilde{\gamma}^{(1)}])$ [with $\tilde{\gamma}^{(2)} = (\tilde{R}/\tilde{s})\tilde{\gamma}^{(1)}$]: quadrant I $(3, 3; [.25, 5])$, quadrant II $(3, 0.3; [0.5, 5, 40])$, quadrant III $(0.3, 0.3; [0.25, 5])$, quadrant IV $(0.3, 3; [0, 0.45, 1.8])$. Image taken from [16].

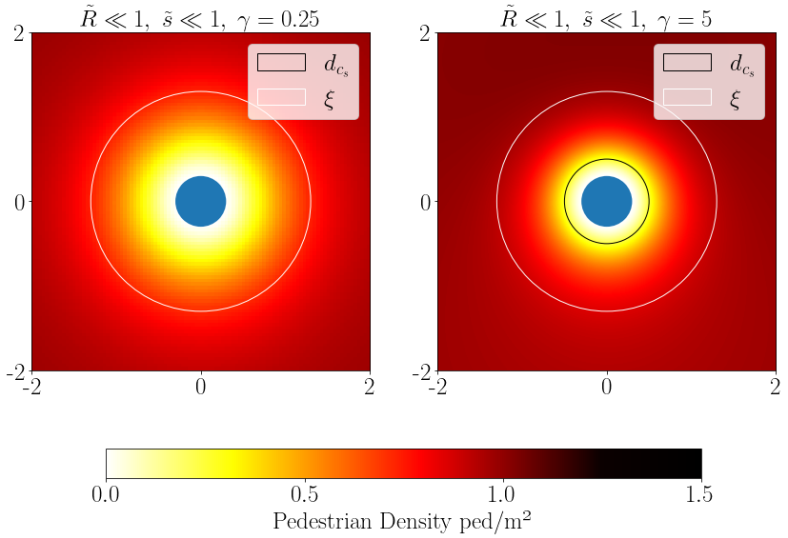


Figure 4.8: Focus on the quadrant III of Figure 4.7 with details about the size of the perturbation. The white circle has radius $R + \xi$ whereas the black circle has radius $R + d_{c_s}$, with $d_{c_s} \equiv c_s/\gamma$ (note that the left panel's black circle is not visible since $d_{c_s} = 4$). We observe how the smallest of the circles is the one governing the distance at which the perturbation due to the cylinder is felt. Image taken from [16].

merical solution of the MFG system for $\xi$ and $c_s$ as for the frontal case and with $\gamma = 0.5$. We can indeed observe that turning on the discount factor produces the desired effects, by reducing the crowd's displacement in front of the obstacle but still conserving the accumulation on the sides and the density depletion after its passage. Moreover, the simulated velocity field shows an increase in escaping dynamics in front of the cylinder and slight circulation around it, while still mantaining a strong lateral component.

Finally, when participants in the experiment had to give their back to the obstacle and were asked not to anticipate, the observed behavior changed decisively. As the right panel of Figure 4.11 shows, having lost the visual information, it was harder to estimate the obstacle's velocity and direction of motion, resulting in pedestrians being pushed along by the intruder, and behaving like granular material [12]. Behind the cylinder, on the other hand, no significant depletion is shown, and this, we believe, is due to the diffusivity of the crowd, given the pedestrians' intention to have as much space as possible. The left column of Figure 4.11 shows the MFG simulation for $\xi = 0.4$, $c_s = 0.2$ and $\gamma = 6$. Here we recover the accumulation in front of the obstacle and the smaller depletion behind it. By looking at the velocity plots, we clearly see that pedestrians in front of the cylinder are pushed by the intruder along the direction of its motion. Then, we also remark the agreement with the rotational

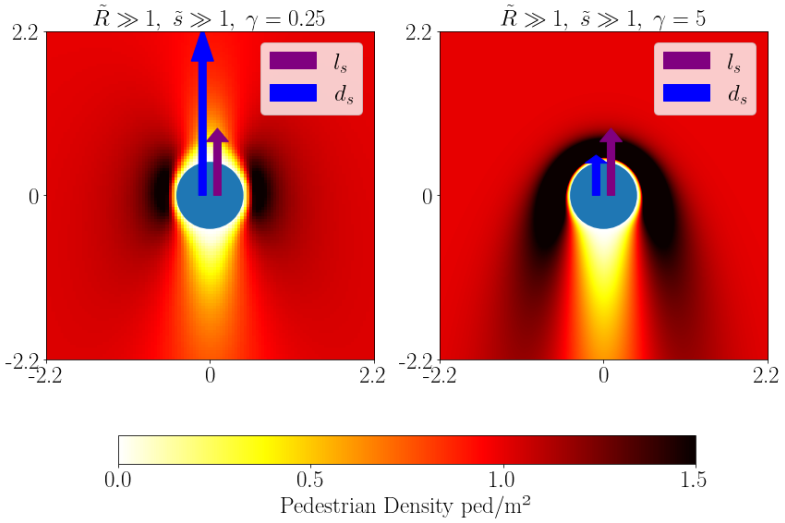


Figure 4.9: Focus on the quadrant I of Figure 4.7 with details about the size of the perturbation. The purple arrow's length is $R + l_s$, with $l_s \equiv s\xi/c_s$ the scale of the length at which agents would start moving to optimally avoid impact if $\gamma = 0$, whereas the blue arrow's length is $R + d_s$, where $d_s = s/\gamma$ represents how far the cylinder travels during time $1/\gamma$. It is apparent how a congestion in front of the cylinder appears when $d_s < l_s$ because the agents optimize only on a small portion of the cylinder's trajectory. Image taken from [16].

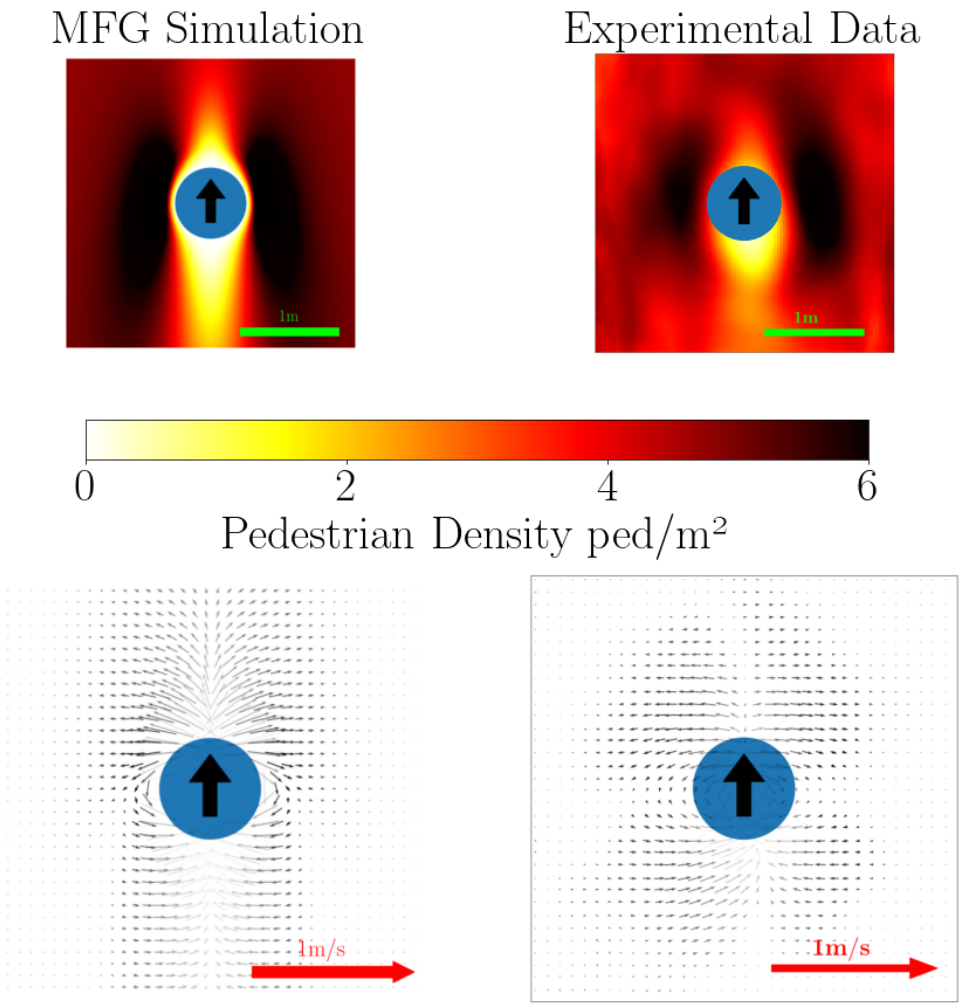


Figure 4.10: Qualitative comparison between density, first row, and velocity plots, second row, between the experiment, right column, and the ergodic state of the MFG model, with parameters $\xi = 0.2$, $c_s = 0.1$ and $\gamma = 0.5$, left column, for the case where pedestrians were oriented randomly. Image taken from [16].

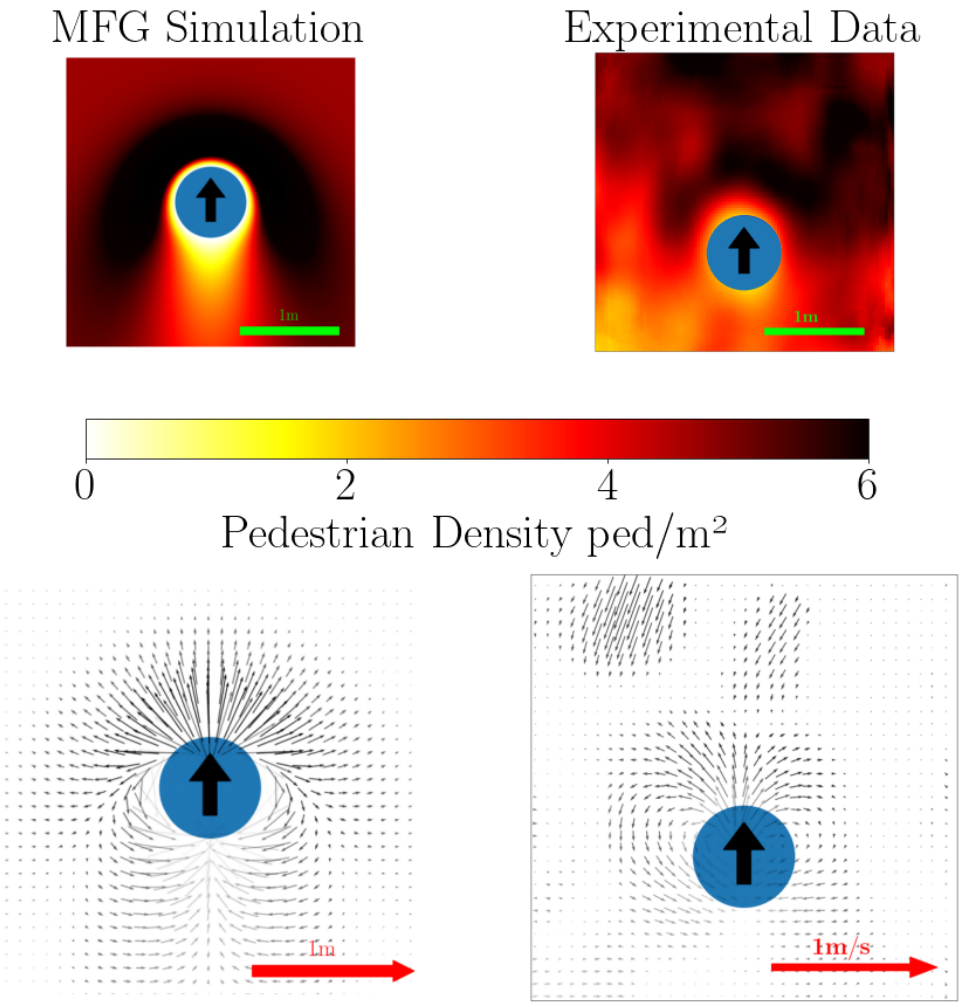


Figure 4.11: Qualitative comparison between density, first row, and velocity plots, second row, between the experiment, right column, and the ergodic state of the MFG model, with parameters $\xi = 0.4$, $c_s = 0.2$ and $\gamma = 6$, left column, for the case where pedestrians were giving their back to the incoming cylinder and were asked not to anticipate. Image taken from [16].

motion around the obstacle, analogously to what would happen for granular inert matter, under purely mechanical forces. We managed to recover the experimental behavior mainly using the discount factor, slightly modifying $\xi$ and $c_s$ to better fit the data, placing the solution at the boundary between quadrants I and II. This means that the discounting term correctly reproduces losses in anticipatory abilities.

## 4.4 . Solving the Equations

In the previous sections we have compared the results of the MFG simulations to the experimental data. As we said, to obtain them we have solved the model in the ergodic state. In fact, given that the experimental data were obtained when the cylinder was halfway of its path, we are not interested in exploring the transient regime. Solving for the stationary state allows us to directly access the information we need without solving the entire time-dependent process. This is, in fact, generally a longer process, in particular because of the backward-forward nature of the system. However, solving the ergodic state has its challenges as well. In fact, we already know that one of the critical aspects of this model is solving the equations under obstacles, where the value function is expected to be infinite. We know from section 3.3.2 that we can overcome this issue passing to the Schrödinger formulation. However, this same formulation when a discount factor is added, as we will see, brings to the table new logarithmic terms that do not allow for a straightforward implementation of the method we use for the undiscounted case. Nevertheless, we will show in section 4.4.3 how one can still find a way to directly solve for the discounted ergodic state. Before introducing this method, however, we need to understand how the solution behave near walls.

### 4.4.1 . Behavior near Walls

As we mentioned in 4.2.1, under the simulated cylinder, the solution for $u$ should be by definition infinite. In fact, if we look at the cost functional (4.10), we see that if $U_0 = -\infty$ then $u = \infty$ there. In this subsection we explain what kind of instability one faces when solving the HJB in its original formulation. This is true for both the time-dependent and the stationary problem, regardless of the presence of a discount factor. However, for simplicity, we will deal with the undiscounted ergodic equation. Moreover, since we want to understand what happens near walls, we restrict ourselves to the 1D equation and we assume that the wall is located at $x = 0$

$$0 = \frac{\sigma^2}{2} u_{xx} - \frac{1}{2\mu} u_x^2 - \gamma u - gm. \tag{4.15}$$

Now, since we do not want to be bothered with parameters and we are just interested in the behavior of the solution, we make the equation adimensional.

To do so, first we operate the transformation $u = u'\mu\sigma^2$, and have

$$0 = \frac{\mu\sigma^4}{2}u'_{xx} - \frac{\mu\sigma^4}{2}u'^2_x - \mu\sigma^2\gamma u' - gm. \tag{4.16}$$

Then we apply the change of variables $x = x'l$ and get

$$\begin{aligned} 0 &= \frac{\mu\sigma^4}{2l^2}u'_{x'x'} - \frac{\mu\sigma^4}{2l^2}u'^2_{x'} - \mu\sigma^2\gamma u' - gm \\ 0 &= u'_{x'x'} - u'^2_{x'} - \frac{2l^2\gamma}{\sigma^2}u' - \frac{2l^2 gm}{\mu\sigma^4} \end{aligned} \tag{4.17}$$

Which is now adimensional, without changing the location of the wall, which is still at $x' = 0$. From (4.17) we see that if we take $l \ll \sigma/\sqrt{2\gamma}$ we can neglect the $\gamma$ term and the density term. This means that for $x < l$ we can solve

$$u_{xx} - u_x^2 = 0, \tag{4.18}$$

This equation can be transformed into a simple heat equation via the Cole-Hopf transformation, but it can also be solved by applying the transformation $h(u) = u_x$, which means that $u_{xx} = h_u h$, that gives $h = \pm e^u$, and since we already know that $u$ grows to $+\infty$ near the obstacle, $h(u) = u_x$ must be negative, and thus we choose the minus sign, meaning that $h = -e^u$. At this point, we can write

$$x = -\int_{+\infty}^{u(x)} e^{-u}du = e^{-u(x)} \implies u(x) = -\log x \tag{4.19}$$

This tells us that near obstacles $u$ goes to $+\infty$ as fast as a negative logarithm. This is the reason we cannot solve the equations in their $(u, m)$ formulation. In fact, to approximate the solution near obstacles with a reasonable precision, we would need a space discretization more and more refined. In particular, since in HJB we have to compute the second derivative of $u$, and this behaves as a logarithm, if we consider the discretization of the logarithm's second derivative

$$\frac{d^2}{dx^2}(\log x) = -\frac{1}{x^2} \sim \frac{\log(x + \Delta x) + \log(x - \Delta x) - 2\log x}{\Delta x^2},$$

and expanding the logarithm in the numerator on the right we have that

$$-\frac{1}{x^2} \sim -\frac{1}{x^2} - \frac{\Delta x^2}{x^4},$$

therefore it must be that

$$\frac{1}{x^2} \gg \frac{\Delta x^2}{x^4} \implies \Delta x \ll \sqrt{2}x \tag{4.20}$$

which means that, if the wall is placed at $x = 0$, this approximation requires an ever decreasing $\Delta x$ the more we approach the wall, making it impossible to precisely approximate the HJB solution near obstacles and walls with the $(u, m)$ formulation.

### 4.4.2 . Solving the Complete Information Case

Luckily, as we already know, one workaround is found by transforming the equations through the Cole-Hopf change of variables $u = -\mu\sigma^2 \log \Phi$, $m = \Phi\Gamma$, which gives the ergodic system in the moving frame

$$\begin{cases} \frac{\mu\sigma^4}{2}\Delta\Phi - \vec{s}\cdot\vec{\nabla}\Phi + V[m]\Phi &= -\lambda\Phi, \\ \frac{\mu\sigma^4}{2}\Delta\Gamma + \vec{s}\cdot\vec{\nabla}\Gamma + V[m]\Gamma &= -\lambda\Gamma. \end{cases} \tag{So}$$

In this case, since $\Phi = \exp\{-u/(\mu\sigma^2)\}$, when $U_0 \to -\infty$, $\Phi \to 0$ and we have no more divergence near walls. At this point, we show that a simple iterative method is enough to solve (So) with the boundary conditions chosen in subsection 4.2.1, $\Phi_{asy} \equiv \Gamma_{asy} \equiv \sqrt{m_0}$. We will explain this method by focusing on the first equation of system (So), since it can be applied also on the other, simply changing the sign of the velocity term. The equation is

$$\frac{\mu\sigma^4}{2}\Delta\Phi - \vec{s}\cdot\vec{\nabla}\Phi + (gm + U_0(\vec{x}))\Phi = -\lambda\Phi, \tag{4.21}$$

We want to solve the equation in a box of side $L$, that we simulate as a grid of $N \times N$ points corresponding to the $(x, y)$ coordinates in discretized Euclidean space with equal spacing $dx = dy$. Then we define the matrix $\Phi \in \mathbb{R}^{N,N}$ whose entries are the discretized version of (4.21)

$$\begin{aligned} &\frac{\mu\sigma^4}{2dx^2}(\Phi_{i-1,j} + \Phi_{i+1,j} + \Phi_{i,j-1} + \Phi_{i,j+1} - 4\Phi_{i,j}) + \\ &- \frac{s}{dx}(\Phi_{i,j-1} - \Phi_{i,j+1}) + (gm_{i,j} + U_0U_{i,j})\Phi_{i,j} = -\lambda\Phi_{i,j} \end{aligned}$$

At this point, the trick is to make the term $\Phi_{i,j}$ explicit and obtain

$$\Phi_{i,j}^{k+1} = \frac{\frac{\mu\sigma^4}{2}(\Phi_{i-1,j}^k + \Phi_{i+1,j}^k + \Phi_{i,j-1}^k + \Phi_{i,j+1}^k) - s(\Phi_{i,j-1} - \Phi_{i,j+1})dx}{2\mu\sigma^4 - (\lambda + gm_{i,j} + U_0U_{i,j})dx^2}, \tag{4.22}$$

where $k$ is the iteration step, which gives a recursive rule that updates $\Phi_{i,j}$ until convergence using the values of each point's neighbor at the previous iteration. At convergence, $\Phi$ would solves (4.21). Now, the first step is choosing an initial guess for $\Phi_{i,j}$, and for $m$, which for convenience is chosen to be a constant function over the grid equal to the boundary values. Then, the second step is to use (4.22) to update each entry of the matrix $\Phi$, and this can be done simultaneously for all points in languages like Python, until a certain criterion of convergence is reached, and call $\Phi_{new}$ the results. The third step is to find $\Gamma_{new}$, by applying the same reasoning, simply by changing the sign of $s$, and the fourth step is to calculate $m_{new} = \Phi_{new}\Gamma_{new}$. Now, the loop restarts with step two, with $\Phi = \Phi_{new}$, $\Gamma = \Gamma_{new}$ and $m = m_{new}$. The algorithm stops when a certain criterion of convergence of $m_{new}$ is reached. As to why this algorithm works, let us take a look at its update rule (4.22).

There we see that what is solved is essentially a Laplace equation $\Delta\Phi = 0$, where $\Phi_{i,j}$ is taken as the average of its neighbors, but a perturbative term of order $dx^2$ is added to the denominator, and a gradient term of order $dx$ to the numerator. Moreover, we observe in particular that under walls or obstacles, $U_0$ is infinite (in practice a large number), therefore annihilating the entire fraction, correctly giving $\Phi = 0$. We will now proceed, showing how this changes when we introduce the discount term $\gamma$.

### 4.4.3 . Solving the Reduced Information Case

Unfortunately, when dealing with the ergodic equations of the discounted system, using the same Cole-Hopf transformation causes more problems than it solves. In fact, in this case the discounted ergodic equations are

$$\begin{cases} 0 &= -\frac{\mu\sigma^4}{2}\Delta\Phi - V[m_0]\Phi + \gamma\mu\sigma^2\Phi\log\Phi + \vec{s}\cdot\vec{\nabla}\Phi \\ 0 &= \frac{\mu\sigma^4}{2}\Delta\Gamma + V[m_0]\Gamma - \gamma\mu\sigma^2\Gamma\log m + \gamma\mu\sigma^2\Gamma\log\Gamma + \vec{s}\cdot\vec{\nabla}\Phi \end{cases} \tag{S1}$$

We immediately observe that the symmetry of (S0) is lost here, and various logarithmic terms appear. Let us take a closer look at why we do not like this. As before, we choose to focus on the first of the two equations of the system, whose discretized version reads

$$\begin{aligned} 0 = \frac{\mu\sigma^4}{2}&(\Phi_{i-1,j} + \Phi_{i+1,j} + \Phi_{i,j-1} + \Phi_{i,j+1} - 4\Phi_{i,j}) \\ &+ (gm_{i,j} + U_0U_{i,j})\Phi_{i,j}dx^2 - \gamma\mu\sigma^2\Phi_{i,j}\log\Phi_{i,j}dx^2 \\ &- s(\Phi_{i,j-1} - \Phi_{i,j+1})dx, \end{aligned}$$

If we try to explicit $\Phi_{i,j}$ we obtain

$$\Phi_{i,j} = \frac{\frac{\mu\sigma^4}{2}(\Phi_{i-1,j} + \Phi_{i+1,j} + \Phi_{i,j-1} + \Phi_{i,j+1}) - s(\Phi_{i,j-1} - \Phi_{i,j+1})dx}{2\mu\sigma^4 - (gm_{i,j} + U_0U_{i,j} - \gamma\mu\sigma^2\log\Phi_{i,j})dx^2} \tag{4.23}$$

One could immediately see here that a fundamental change occurs in the denominator, where a logarithmic term appears. What we observe empirically is that now the algorithm gets stuck and is unable to reach convergence. In fact, this is a consequence of the instability caused by the presence of the logarithmic term. Indeed, near walls, where $\Phi$ is supposed to vanish, the logarithm grows indefinitely, at some point becoming comparable with $U_0$, but with opposite sign, canceling out. There is no way to solve this, since to prevent the logarithm from diverging one should take an infinitely small $dx$. Fortunately, however, we have seen that up to a certain $l \ll \sigma/\sqrt{2\gamma}$ from the wall, the cylinder in this case, HJB reduces to equation (4.18), that after substituting Cole-Hopf gives $\Delta\Phi = 0$.

Therefore, what we propose is to solve the discounted problem by keeping the iterative approach, but to use it on both formulations $(\Phi, \Gamma)$ up to a

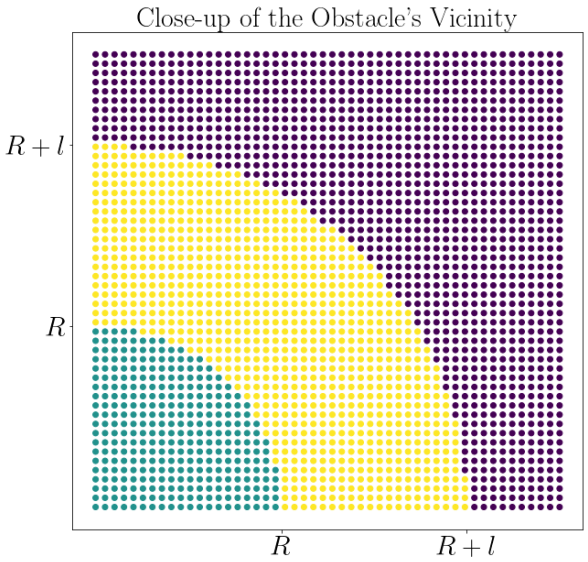


Figure 4.12: Sketch of the close-up of the grid $\mathcal{G}$ in the vicinity of the cylinder. The green points represents the cylinder. The yellow points are where we solve the MFG equations in the $(\Phi, \Gamma)$ formulation, whereas for the purple points we solve them in the $(u, m)$ one. Although in the picture the yellow area seems large with respect to the green one, in the real implementation, since $l$ is small with respect to the cylinder's radius, the yellow area would be much thinner.

distance $l \ll \sigma/\sqrt{2\gamma}$ from the cylinder, since it is the only way to cope with infinite potential, and $(u, m)$ elsewhere, to avoid dealing with the logarithmic terms. Our goal is to implement a numerical scheme that solves the discounted ergodic MFG using the $(\Phi, \Gamma)$ formulation under the cylinder and up to a distance $l \ll \sigma/\sqrt{2\gamma}$ from it, represented by the green and yellow points in Figure 4.12. Then, we solve the system in the $(u, m)$ formulation elsewhere, i.e. the purple points in Figure 4.12, and connect the two.

In practice, we simulate the space using two $N \times N$ matrices $X$ and $Y$ representing the $x$ and $y$ coordinates of $N \times N$ points inside a $L \times L$ square forming the grid $\mathcal{G}$. The only prescription is that we must choose the size of the grid step $\Delta x$ to be small enough to have enough points between the wall's edge and $l$. Moreover, since $l \ll \sigma/\sqrt{2\gamma}$, the higher $\gamma$ the smaller $\Delta x$ must be. Once the space-step is chosen, for all points of the grid up to a distance $l$ from the obstacle's edge, we use (4.22) to solve the equation in the $(\Phi, \Gamma)$ formulation. To better understand which points are updated with (4.22), let us define $\mathcal{V} = \{(x, y) \in \mathcal{G} | \, U_0(x, y) = +\infty\}$ as the set of points under the walls or eventual obstacles. Then, the set of points updated using rule (4.22) are those in the set $\mathcal{U} = \{(x, y) \in \mathcal{G} | \, d_{\mathcal{V}}(x, y) \leq l\}$, where $d_{\mathcal{V}}(x, y) = \inf\{\sqrt{(x-a)^2 + (y-b)^2} | \, \forall (a, b) \in \mathcal{V}\}$ is the distance of the point of coordinates $(x, y)$ from $\mathcal{V}$. In fact, $\mathcal{U}$ contains all points under the cylinder and all those at a distance at most $l$. For all other points, i.e. those contained in $\bar{\mathcal{U}} = \mathcal{G} - \mathcal{U}$, we solve the $(u, m)$ problem. To find the update rule, we need to discretize the discounted ergodic HJB equation (4.14) and the ergodic KFP equation (3.27). For reasons of simplicity, we deal with their form before the passage to the moving frame. Discretizing HJB equation (4.14) gives

$$\begin{aligned} 0 = &\frac{\sigma^2}{2}(u^k_{i-1,j} + u^k_{i+1,j} + u^k_{i,j-1} + u^k_{i,j+1} - 4u^k_{i,j}) + \\ &- \frac{1}{8\mu}((u^k_{i,j+1} - u^k_{i,j-1})^2 + (u^k_{i+1,j} - u^k_{i-1,j})^2) - \gamma u^k_{i,j} dx^2 - g m^k_{i,j} dx^2, \end{aligned}$$

from which we derive the rule

$$u^{k+1}_{i,j} = \frac{-\frac{\sigma^2}{2}(\Delta^k_{i,j}) + \frac{1}{8\mu}((u^k_{i,j+1} - u^k_{i,j-1})^2 + (u^k_{i+1,j} - u^k_{i-1,j})^2) + g m^k_{i,j} dx^2}{2\sigma^2 + \gamma dx^2}, \tag{4.24}$$

where

$$\Delta^k_{i,j} = u^k_{i-1,j} + u^k_{i+1,j} + u^k_{i,j-1} + u^k_{i,j+1}$$

Following an analogous reasoning one can obtain the update rule for the KFP equation (3.27). Finally, to compute derivatives at the boundary between $\bar{\mathcal{U}}$ and $\mathcal{U}$, we extend these two sets to overlap with their complement, correctly transforming the points to either the $(u, m)$ or $(\Phi, \Gamma)$ formulation, and then take the derivatives. Moreover, it can be

generalized to solve equations where other kinds of obstacles are simulated. In fact, in this section, we have shown how these equations behave near impassable obstacles and proposed a method to circumvent the challenge posed by the introduction of a discount factor under these circumstances.

# 5 - Related Projects

In the previous chapter I have completed the discussion of the core of my research during my PhD. However, during this time I have also explored other related topic which deviate from purely solving the MFG differential equation. In fact, in this chapter I present two research roads that I started exploring but that could not walk until the end. Nevertheless, although not being able to fulfill all the objectives of these projects, I managed to obtain some noteworthy results, which will be presented in the following. First, we will discuss about my ambition to blend together microscopic agent based modelling of pedestrian dynamics and MFG, by creating a model where force-based agents follow optimal trajectories obtained solving a MFG system. Then, I will discuss the results of my work in collaboration with the team of D. Kalise of Imperial College, in the context of the partnership between the Imperial College and the CNRS, which I am part of.

## 5.1 . Optimal Crowds

In chapter 2 I have introduced some simulation techniques for pedestrians dynamics, and divided them into microscopic and macroscopic. Then, we have seen in 4 that in situations like the experiment of the cylinder we described in 1.2, models based on short-term anticipation fail at properly reproducing empirically observed behavior. As mentioned in chapter 4, the reason lies into the the absence of a mechanism enabling the prediction of events far enough into the future. During my Ph.D. work, I have tried to use what I have learnt with Mean-Field Games to create an agent-based microscopic model where agents follow an optimal velocity obtained solving a MFG. In principle, this would keep the microscopic description of the motion, important when granularity effects play a key role in the dynamics, while giving the simulated pedestrians the ability to deal with obstacles with enough anticipation. This would be particularly useful around bottlenecks and doors, where the ability of pedestrians to orient themselves to find the right orientation of their body and the right velocity play a crucial role in their ability to pass through and continue their motion. My goal was also to build a model that others could download freely from my GitHub repository and integrate it with their suggestions. For this reason, I devoted a large part of the work in building a sound and user-friendly sandbox software, making it easy for the user to describe obstacles like walls,

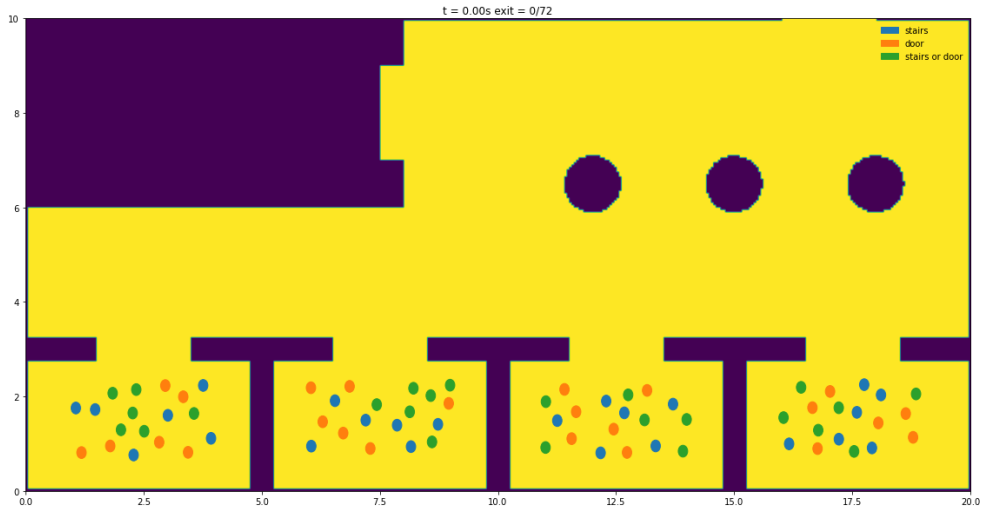


Figure 5.1: Initial configuration of a simulation representing a train station evacuation. Parts in violet represent impassable walls. In the lower part of the figure pedestrians are initialized inside the train cars, and the different colors represent their target, which can be the door in the wall in the top left part of the figure, representing an escalator, or the door in the top right part. The three cylinders represent columns in the train station. Video can be found here.

columns and doors, and to initialize the agents, eventually more than one group possibly with different targets.

**Creating the Simulation** The model I present here simulates the motion of an arbitrary number of pedestrians trying to evacuate a simulated environment reproducing possible real-life scenarios like train stations, concert-halls, stadiums etc. These spaces can be built and customised with obstacles like walls and cylinders, and with doors or escape points. In practice, we create a grid representing the environment, then we define a variable on this grid equal to a large negative values where there are walls and positive values where there are targets. Pedestrians in this model have the sole objective to reach a target, i.e. a door or an escape point, or multiple targets. These targets are chosen by the user during the initialization phase of the simulation, where the user describes where in the environment pedestrians will start their motion, how many of them and towards which objective. Figure 5.1 shows an example of an initial configuration of a simulation that represents the evacuation of a train station. In this case, pedestrians are initialized in the train cars, in the lower part of the figure. Each dot is a pedestrian in its initial position, and the color represents

the target, or the targets. The configuration is contained in a `.json` file and can be stored and shared separately from the code. Here we see that each pedestrian can aim either to the door, in the top right part of the figure (where the contour line is interrupted), or to the automatic stairs, represented by the hole in the wide rectangle in the top left part of the figure.

**Choosing the Desired Velocity** Once pedestrians are initialized, the model finds the trajectories the agents should follow to reach their targets, and agents will try to align their velocity to the desired one. This is where MFG enters into play. In fact, as we said the goal is to use MFG to give the agents to ability to anticipate the future, so that they can avoid obstacles and foresee congested areas and possibly avoid them. This means that one should, once the room is built and the pedestrians' initial positions initialized, solve the MFG equations and use the optimal control $\vec{a}^* = -\vec{\nabla} u/\mu$ to create a velocity floor field that for each point of the discretized space will give the optimal velocity. In principle, one could solve the stationary problem, as we previously did, obtaining desired velocities that do not depend on time, and that can be followed by the pedestrians until the room is empty. However, one can do this only if there are constant exiting and entering flows, which is not the situation we want to model here. For this reason, we choose to solve the time dependent problem instead. For each simulation the user decides a final time $T$, which is the terminal time of the cost functional (3.21), from which the HJB equation (in its Schrödinger formulation) is solved (backward). In this context, this final time can be interpreted as the total time the pedestrians are allowed to evacuate the premises. If this time $T$ is too small, agents do not have the time to fully evacuate the room, whereas when $T$ is chosen to be very large, i.e. in the $T \to \infty$ regime, pedestrians simply evacuate as fast as possible. Although more computationally intensive, at least solving the time dependent problem is in principle straightforward since it can be done with any Runge-Kutta scheme. Then, to find the solution of the MFG, one should solve the KFP, for $t \in [0, T]$, to find the new density, that one should then use to solve HJB again until convergence of the self consistency. However, I was only able to partly implement the full MFG system. In the following, I explain three main modes in which the simulation tool could work.

- **Without density:** in this case we take $g = 0$, meaning that we do not consider the mean-field interaction between pedestrians. The potential $V$ is therefore only composed by $U_0$, that gives the description of the environment. In this case, pedestrians will try

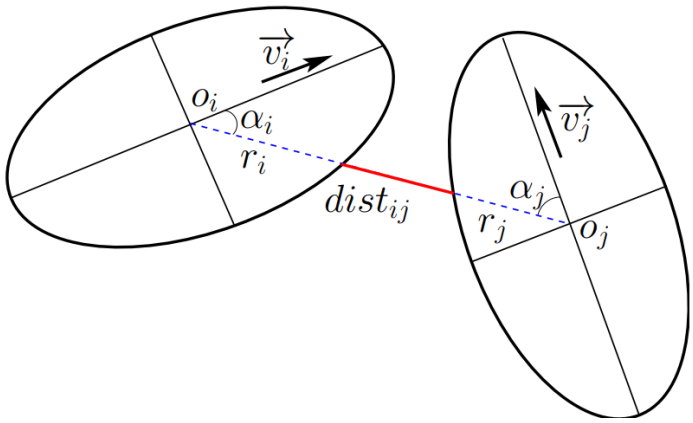


Figure 5.2: Elliptic exclusion zones representing two pedestrians. Image taken from [23].

to follow a trajectory that simply minimizes the time to the target, but that also contains the information about obstacles, giving them the best trajectory for avoiding them. This is simply an optimal control problem, it is not a MFG in any kind of form or aspect. In fact, the HJB is only solved once and its solution is used to obtain the velocity which is optimal again in the sense of the cost functional (3.21). This is the modality that I managed to implement fully and the most stable one.

- **With density periodically included:** in this mode the information about the density is included inside the HJB equation, but only at regular intervals. At first, the HJB is solved without density as in the previous case. Then, after every $n$ steps, a snapshot of the density is obtained by performing a Gaussian convolution of the positions of the simulated agents. This is then plugged into the HJB equation, which is solved again and a new optimal velocity is obtained. This new velocity will therefore include the information about the local density, and at least it principle,it should induce agents in highly congested areas to move away from there and possibly take an alternative route. I am still in the process of implementing this modality, since I am trying to find the right calibration the crowd's repulsion. Finally, it should be noted that this and the previous modes are analog to what already done by Hoogendoorn in [45, 46], although some details may vary.

- **Solving the MFG in Advance:** this is the mode I was aiming to fully implement. This mode would consist in, once the room is initialized, solving the time-dependent MFG, eventually including

a term for congestion. This should, in principle, give a optimal velocity field where the information about the density was already accounted for. The idea is that by solving the MFG one would find the trajectories that allow for the best occupation of the space already from the start of the simulation. This would constitute the ultimate blending between the MFG anticipation and optimization capability and the granular description of the agent-based model.We are still at the beginning of the conception of how to actually implement this mode, keeping it for future research.

**The Microscopic Rule** Once the room and the pedestrians are initialized, the microscopic simulation begins. At each time step, each agent's position and velocity are updated, using a force based model made of mainly two force terms

$$\vec{F} = \vec{F}_{des} + \vec{F}_{rep}. \tag{5.1}$$

The first term represents the strive of the agents to follow the desired velocity, which is the one obtained by solving the MFG in any of three ways we have listed before. Then, $\vec{F}_{rep}$ is a repulsion term, dealing with the interaction between agents and the walls and obstacles. To define it, I followed the footstep of Chraibi et al. [23]. In this work, the authors introduce what they call the Centrifugal Force Model (CFM). In this model the repulsion depends, other than on the distance, on the relative velocity as well. Moreover, it assumes that each pedestrian is described by an exclusion zone, that is an ellipse with center at the position of the pedestrian. The reason behind the choice of this shape is that it has been shown empirically that when humans walk the area they occupy is elongated in the direction of the motion, and, conversely, they do not take as much space on the sides as if they were circles. The dimensions of the ellipse changes with the velocity, with the major semiaxis being linearly dependent on the speed. Finally, the form of the intensity of the repulsion between pedestrians $i$ and $j$ is given by

$$F_{rep} = \min\left\{F_{max}, k_{vis}\exp\left\{\frac{R_{ij} - r_i - r_j}{\eta + k_{vel}}\right\}\right\} \tag{5.2}$$

- $R_{ij} = |\vec{R}_{ij}| = |\vec{R}_j - \vec{R}_i|$ is distance between the position of $i$ and the position of $j$. We also introduce $\vec{e}_{ij} = \vec{R}_{ij}/R_{ij}$
- $k_{vis} = \frac{1}{2}\frac{\vec{e}_{ij}\cdot\vec{v}_i + |\vec{e}_{ij}\cdot\vec{v}_i|}{\vec{v}_i}$ is a term simulating the fact that agents in the simulations only care about what they have in front of them, in a $180$ field-of-view.

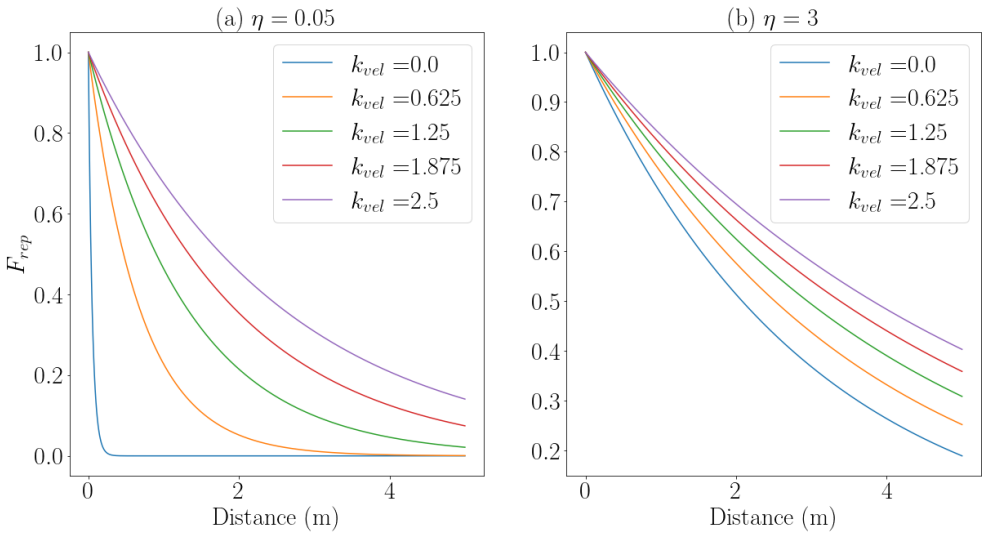


Figure 5.3: (a) - Repulsion profiles up to a cutoff of $5m$ for different values of $k_{vel}$ for a small value of $\eta$. (b) - Repulsion profiles up to a cutoff of $5m$ for different values of $k_{vel}$ for a large value of $\eta$. We observe that the larger the $\eta$, the less relevant the value of $k_{vel}$ becomes in determining the shape of the repulsion.

- $r_i$ and $r_j$ represent the distance from the center to the limit of the elliptical exclusion zone, respectively of $i$ and $j$, along the direction given by $\vec{e}_{ij}$. This can be seen in Figure 5.2, where the dashed blue segments represent $r_i$ and $r_j$ respectively.

- $k_{vel} = \frac{1}{2}(-\vec{e}_{ij} \cdot \vec{v}_{ij} + |\vec{e}_{ij} \cdot \vec{v}_{ij}|)$ describes the fact that the intensity of the repulsion increases towards those pedestrians whose velocity has a component pointing towards pedestrian $i$. In particular, this allows for pedestrians to be able to walk alongside without being repelled. This can be seen in both panels of Figure 5.3, where the repulsion profiles are plotted for different values of the relative velocities. Here we see how for small values of $k_{vel}$, the repulsion, especially for small $\eta$ rapidly drops.

- $\eta$ is a term that is necessary to avoid the divergence of the fraction when the two pedestrians are walking away from each other, meaning that $k_{vel} = 0$. In this, case, they keep feeling a certain repulsion whose intensity is given by $\eta$. Actually, $\eta$ also gives the importance of the relative velocity in the repulsion felt by the agents. In fact, for large values of $\eta$, the value of $k_{vel}$ has less and less impact on the repulsion intensity, as can be seen in Figure 5.3. A high value of $\eta$ stiffens the interactions, preventing overlapping,

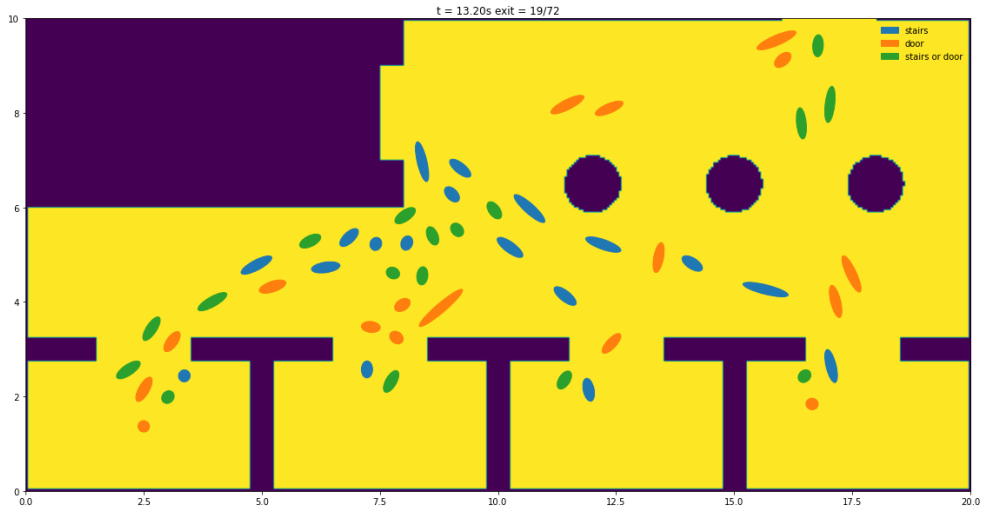


Figure 5.4: Snapshot of the train station simulation whose initialisation is shown in Figure 5.1. Video can be found here.

however it also causes oscillations. On the other hand, a lower value of $\eta$ decreases oscillations but leads to more overlapping. In [23], the authors show how to properly define both the average overlapping and the average oscillation, and show how $\eta$ can be chosen as the value that minimizes both quantities at the same time.

**Performance of the Model** In the following, we will show some snapshots of some simulations to showcase some of the most interesting features of the model. All the videos of the simulations discussed here and other which we do not mention but are noteworthy can be found here. It is not in the scope of this work to quantitatively prove the validity of the microscopical approach, since this analysis has already been performed in [23]. Here, we just want to show and discuss some of the most notable features this model produces.

- **Side by side walking** First, we consider a snapshot of the simulation of the train station whose initialization is showed in Figure 5.1. Figure 5.4 shows the state of the simulation at around $13s$. In this picture we observe how the relative velocity part of the repulsion plays a crucial role in allowing pedestrians to walk side by side. Moreover, and this can be seen even more clearly in the video, we observe that this model is capable of reproducing a realistic crossing behavior. For example, we observe a line of blue pedestrians being crossed by an orange one, who wants to go to

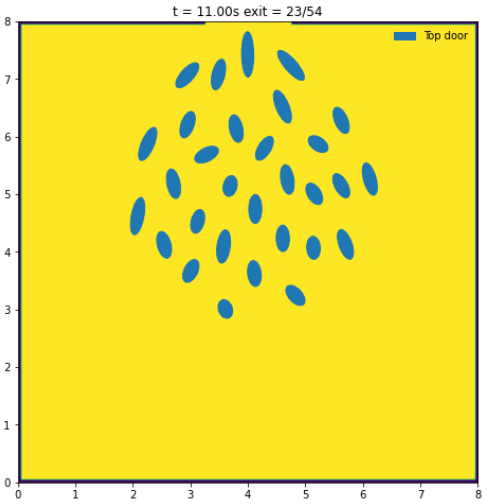


Figure 5.5: Snapshot of the evacuation of an empty room. Video can be found here.

the top door. In this case, we see how a blue pedestrian slows down and let an orange one pass.

- **Teardrop shape of evacuation** Another interesting test for this model is how it performs at simulating an evacuation of a single group of pedestrians from an empty room. This being a classical test for pedestrians, it is possible to find many experimental papers about it. In particular, my understanding is that evacuations can be calm, in which case a teardrop shaped queue forms in front of the door, where no one is crushed against the wall, or rushed, in which case a semicircle is produced, and people are pressed against the walls near the door. As Figure 5.5 shows, this models creates calm evacuations, with a teardrop shaped queue, and this is regardless of the choice of the parameters. In particular, I believe this is due to the fact that agents only react to what is in front of them. In fact, for a semicircle to be created, people must be pushed by those behind them and with a most central position trying to reach the exit. However in this case, agents feel no pressure coming from behind, which make them simply keep their distance from those in front, patiently waiting to exit the room.

- **Ability to find complex trajectories** The greatest advantage of obtaining the desired velocities by solving a HJB equation, is that the trajectories we obtain naturally include the information about the environment, providing, even when no information about the

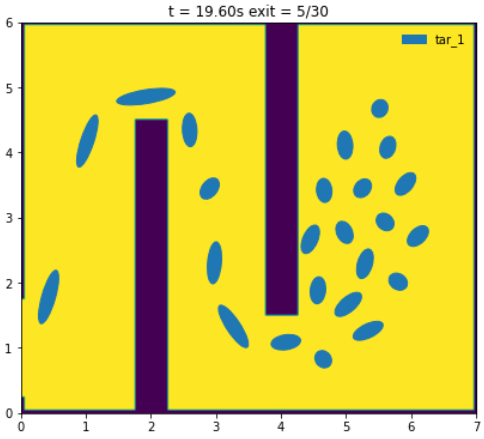


Figure 5.6: Snapshot of a simulation representing the evacuation of 54 pedestrians from a room where an N shape corridor is present. The advantage of finding the trajectories by solving HJB equation is that the information about the obstacle is naturally included in the solution. Video can be found here.

density is included, an obstacle avoidance strategy that usually produce realistic behavior, for example as shown in Figure , where pedestrians follow a narrow N shaped corridor with the exit at its end. Finding the trajectories through the corridor using HJB straightforwardly give the agents the good N shaped path, without the need of manually imposing them through eventually more complicated methods.

- **Aborting evacuation due to lack of time** Another interesting consequence of finding the desired velocities using the HJB is that if the total time of the simulation $T$, which is chosen by the user, is too small, all agents, or just some of them, may not even initiate the evacuation, or they may stop where they are. In fact, in the optimization problem solved by the HJB equation, if reaching the target in time means going too fast, then it could be more convenient, always in the sense of the cost functional (3.21), not to move at all and to accept the price of neglecting terminal conditions and attractive potential areas. This could be particularly useful for the simulation of the boarding of a train, where some of the furthest pedestrians anticipate that they do not have enough time left to board, and therefore simply give up and stand on the platform.

The creation of this agent-based model allowed me to experiment the implementation of the MFG trajectories in a microscopic force-based

model. In fact, as we said the ultimate goal of this project is to bring together the positive aspects of both worlds. In particular, solving a MFG describing the venue would allow to have an optimal occupation of the space and, therefore, an evacuation where accumulations at bottlenecks should be avoided at most. Then, it would be interesting to see if making the microscopic agents follow the MFG trajectories finally gives an evolution of the density similar to the MFG one. Clearly, a large effort should then be made to choose the right MFG matching the behavior of the microscopic model. In the process, one would possibly learn a lot about the relation between the microscopic interactions and their mean-field description. Alternatively, another interesting way to proceed would be to try to achieve the self-consistency by substituting the KFP equation with the evolution given by the microscopic model. In practice, one would solve HJB once, without information about the density, to obtain the "free trajectories". Then, the density of the agents evacuating the room following said trajectories would be computed at all time (for example using a Gaussian convolution, which is already implemented in the code), and this density would then be used to solve HJB again.

### 5.2 . Solving MFG using PINNs

Neural networks, a cornerstone of modern artificial intelligence, represent a class of algorithms inspired by the biological structure and function of the human brain. Conceptualized in the mid-20th century, the development of neural networks was propelled by the quest to mimic human cognitive processes through computational means. The seminal work by McCulloch and Pitts in 1943 [71] introduced the idea of a simplified brain model through their concept of a neural network composed of threshold logic units, which later evolved into what are now known as artificial neurons.

Despite their early promise, neural networks experienced periods of waning interest, known colloquially as the "AI winters," primarily due to limitations in computing power and data availability which were essential for training these models. The resurgence and explosion in the popularity of neural networks in recent decades can be attributed to several key advancements. The advent of powerful graphical processing units (GPUs) has drastically reduced the computational time for training complex models. Additionally, the digital age has facilitated the availability of large datasets, which are crucial for training accurate, robust neural network models. Moreover, breakthroughs in algorithmic design, particularly the development of backpropagation by

Rumelhart, Hinton, and Williams in the 1980s [81], have significantly enhanced the efficiency and feasibility of training deep neural networks.

Today, neural networks find applications across a diverse array of academic and professional sectors. Academically, they are pivotal in advancing research in fields such as neuroscience, where they help model brain functions and cognitive processes, and in theoretical computer science for solving complex computational problems. Professionally, neural networks underpin numerous applications in industries such as finance, for fraud detection and algorithmic trading; in healthcare, for disease diagnosis and personalized medicine; and in autonomous vehicle technology, where they contribute to the development of safe, efficient self-driving systems. Moreover, they play a critical role in the development of natural language processing tools, enhancing machine-human interaction. The broad applicability and robust performance of neural networks continue to drive their adoption in both academic research and practical, real-world applications, heralding a new era of innovation in numerous fields.

For an intuitive introduction to the actual implementation of these models, we refer to [38] for a rigorous mathematical explanation, whereas we recommend reading the work of Metha et al. [73] for a physicist-friendly introduction to the topic. In general, the simplest form of Neural Network are Feedforward Neural Networks, that will be described in details section 5.2.1. However, many variations of the Neural Network model have appeared in recent years. The most notable examples being Convolutional Neural Networks, that turned out to be very useful at image and sound recognition tasks [64], and Recurrent Neural Network [38], very useful in reproducing time series, with a generally high signal to noise ratio, and in language generation, a subject that recently reached the spotlight thanks to the appearance of Large Language Models, usually based on recurrent neural network.

Our goal, in collaboration with D. Kalise and S. Bicego of Imperial College, was to use a recently introduced kind of Neural Network, Physics Informed Neural Networks, a machine learning method inspired to the work of Sirignano et al. [84] and of Raissi et al. [80] and detailed in section 5.2.2, to find the solution of the differential equations of MFG, in particular in the ergodic regime. The broader reason behind this is to explore the possibility of creating a universal solver for differential equations. In particular, we were interested in exploring how well these models can solve equations regardless of their complexity. As we will see, in fact, using PINNs one should in principle be able to solve equations of arbitrary complexity. More specifically, our goal was to use the Deep Galerkin Method architecture designed in [84] to solve

the equations of MFG. However, although at the moment the solution of the full bi-dimensional backward forward system was not achieved yet, we will nevertheless show how we could solve a 1D equivalent. It should be noted that we are not the first to use Neural Networks to study a MFG system. In fact, one could also see the work of Laurière et al. [63], a review of the recent attempts at solving MFG models using Reinforcement Learning, and the work of Cohen et al. [24], where they porpose two methods using Neural Networks to solve a MFG master equation, proving the existence of Neural Networks that can learn the solution of the equation. In particular, they also show that this is independent of the choice of the initial distribution of the MFG density, a result which is particularly important for when the initial distribution is not known in advance.

#### 5.2.1 . A Short Introduction to NN

To briefly introduce the mathematical foundation of Neural Networks, we will follow the recipe of DeVore et al. [30]. In general, NN can be describe as a directed acyclic graph, composed of three sets of nodes $\mathcal{N} = \mathcal{I} \cup \mathcal{H} \cup \mathcal{O}$, called the input, hidden and output nodes, and of a set of edges $\mathcal{E}$. Then, to each node except for the input nodes, we associate a function $\sigma_\nu : \mathbb{R} \to \mathbb{R}$, $\forall \nu \in \mathcal{N}/\mathcal{I}$, called *activation function*, and a *bias*, $b_\nu \in \mathbb{R}$. Each node of the graph therefore becomes a computational unit, and in analogy with biology, in Machine Learning nodes are called also *neurons*. Then, to each edge $e \in \mathcal{E}$, we associate a *weight* $w_e \in \mathbb{R}$. Now, the way a Neural Networks work is by taking a value $x_\mathcal{I}$ as input, with dimensions the number of input nodes. Then, other nodes $\nu \in \mathcal{N}/\mathcal{I}$ receive values from nodes $\nu'$ they share an edge with $e = (\nu', \nu) \in \mathcal{E}$, and output

$$x_\nu = \sigma_\nu \left( \sum_{e=(\nu',\nu)\in\mathcal{E}} w_e x_{\nu'} + b_\nu \right) \tag{5.3}$$

This output is then passed to subsequent nodes following the sense of the directed graph until the output nodes $\nu \in \mathcal{O}$, which give the global output of the Neural Network. More precisely, given $x_\mathcal{I} \in \Omega \subseteq \mathbb{R}^d$, where $d = |\mathcal{I}|$, we define

$$\mathcal{S}_{\{w_e,b_\nu\}} : \begin{cases} \Omega \subseteq \mathbb{R}^d \to \mathbb{R}^{d'} \\ x_\mathcal{I} \mapsto x_\mathcal{O} \end{cases} \tag{5.4}$$

where $d' = |\mathcal{O}|$, a mapping between the input and the output values, that depends on $\{w_e, b_\nu\}$, $\forall e \in \mathcal{E}$ and $\forall \nu \in \mathcal{N}/\mathcal{I}$, which are called *trainable parameters* of the network. The definition we have just given is the

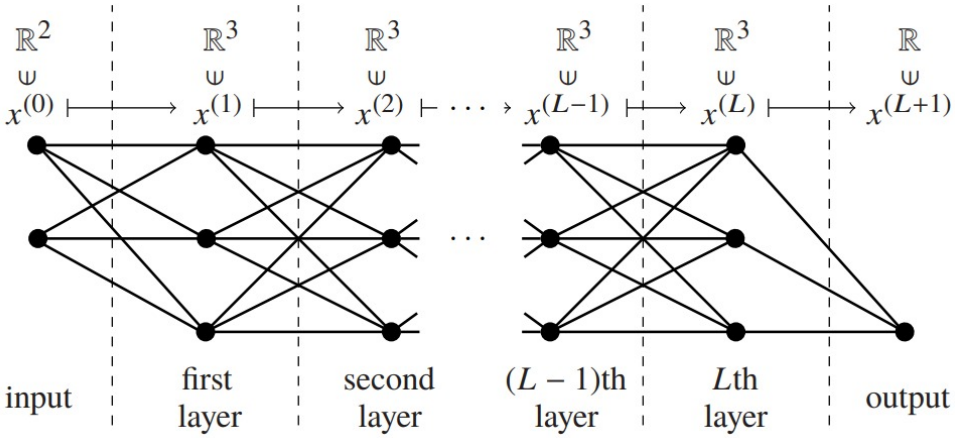


Figure 5.7: Schematic representation of a Neural Network based on a fully connected acyclic graph. Starting from the input layer, each layer's nodes are connected solely with all other nodes of the subsequent layer, until the output layer. Image taken from [30].

most general one can have for a Neural Network, and it allows us to conclude that these mathematical objects are just very complex maps of an input value to the output, and each NN is actually a family of functions parameterized by a large number of parameters.

The most successful type of Neural Network, is the one based on a *fully-connected graph*, where nodes apart from the input ones are organized in *layers*, and edges only exist between nodes of subsequent layers. Figure 5.7 shows a schematic representation of a fully connected graph. This kind of NN are also called *feed forward neural networks*, because the information goes from the input to the output nodes following the direction of the edges. All in all, therefore, we have established that NN are families of functions parameterized by their trainable parameters, that could be chosen to reproduce, in theory, any kind of given output. This makes NN an excellent choice to approximate empirical data or other functions. Indeed, it is known since the 1980s [29], that given any target function $f$ and $\varepsilon > 0$, it is possible to choose a set of trainable parameters, and an architecture, so that $\mathcal{S}_{\{w_e, b_\nu\}}$ can approximate $f$ over any given domain with tolerance of $\varepsilon$. However, what made it that NN did not emerge as the approximation method of choice until recently was the fact that finding the right set of trainable weights was deemed too hard to make this kind of model suitable for any practical application. It is only recently that, in fact, the computational power necessary to train these models with sufficiently large number of parameters became available to the public, which fostered

their use and sparkled their massive application in science and beyond.

In our case, however, we choose to focus on a specific application of NN, in particular the solution of differential equations emerging from physics related problems, which will be the subject of the next section.

#### 5.2.2 . Physics Informed Neural Networks - PINNs

As we said, Neural Networks are excellent approximation functions. Therefore, it should not surprise that attempts were made to used this objects to approximate solution of differential equations. This topic was first explored by Lagaris et al. [57] and Dissanayake et al. [31], in the 1990s, but it was not until recently that it gained new popularity thanks to the work of Raissi et al. [80]. In this paper, the authors use Neural Networks to solve some of the most famous equations in Physics. In general, let us consider any differential equation with unknown $u(\vec{x}, t)$ defined over $\Omega \subseteq \mathbb{R}^D \times [0, +\infty)$, this can be expressed as

$$f(u, \dot{u}, \ddot{u}, \dots, t; \vec{\omega}) = 0. \tag{5.5}$$

where $f$ is a real valued functional, and $\vec{\omega}$ represents the vector containing the parameters of the equation. Then, in [80] two situations are proposed. The first is, given equation (5.5) with fixed $\vec{\omega}$, and, eventually, a set of observations $O = \{u_i^o, x_i^o, t_i^o\}$, giving us the true value of the solution in certain points of the domain $\Omega$, we want to solve the differential equations, i.e. find the true value of $u$ for a set of uniformly sampled points $P = \{(x_i, t_i) \in \Omega \subseteq \mathbb{R}^D \times [0, +\infty)\}$. To do so, the authors in [80] propose to approximate the true solution by $u_\theta$, a Neural Network function like the one in equation (5.4), where $\theta$ is the set of the trainable parameters. Then, one would define the loss functions

$$\mathcal{L}_O(\theta) = \frac{1}{|O|} \sum_O |u_\theta(x_i^o, t_i^o) - u_i^o|^2, \tag{5.6}$$

$$\mathcal{L}_E(\theta) = \frac{1}{|P|} \sum_P |f(u_\theta(x_i), \dot{u}_\theta(x_i), \ddot{u}_\theta(x_i), \dots, t_i; \vec{\omega})|^2. \tag{5.7}$$

and the goal is therefore to train the Network, i.e. find the trainable parameters that minimize the global loss function

$$\mathcal{L}(\theta) = \mathcal{L}_O(\theta) + \mathcal{L}_E(\theta). \tag{5.8}$$

It should be observed that the operator describing the differential equation $f$, could be, in theory, of any complexity, and possibly non linear. In fact, thanks to the advances in the field of automatic differentiation [8], routines available in programming languages such as Python are able to calculate the derivative of the approximating function $u_\theta$, with

respect to the input coordinates and model parameters. therefore, it is possible to define any kind of differential operator.

The second scenario discussed in [80], is the one where a large dataset of empirical measurements $\{u_i^o, x_i^o, t_i^o\}_{i \in N \subseteq \mathbb{N}}$ is available, and the physical law, i.e. the differential equation defined by the operator

$$f(u_\theta(x_i), \dot{u}_\theta(x_i), \ddot{u}_\theta(x_i), \ldots, t_i; \vec{\omega}),$$

the phenomenon originates from is known, but the parameters $\vec{\omega}$ are unknown. In this case, by using a loss function like $\mathcal{L}_O(\theta)$, one is able to find both the function best reproducing the measurements and the parameters of the equation originating them.

#### 5.2.3 . Solving MFG with PINNs

In our case however, the data at our disposal is too noisy and, although the MFG accurately reproduce the experimental features, we are not in the position to claim to have found a general physical law of pedestrians motion, with the same confidence one has about the Schrödinger equation for Quantum Mechanics. Therefore, we cannot use the experimental data in the same way as explained above. However, nothing prevents us from trying to create a Neural Network and to train it to solve the differential equations of the MFG model. Indeed, this is what we have been trying to do, together with Ph.D. student Sara Bicego and Dr. Dante Kalise of the Imperial College of London, during the last three years.

In particular, we were interested in leveraging PINNs to create a universal solver for MFG equations, which would be extremely useful to explore different formulations of the MFG model. In fact, in all relevant literature on the subject, little assumptions are made on the form of the loss $\mathcal{L}_E(\theta)$, and the approach has been proven working for linear, elliptic, parabolic or hyperbolic, and non-linear differential equations. In particular, this would give us freedom to modify the MFG without worrying about how much more complicated the model would become, for example like when we added the discount factor to the model in section 4.3. In that case, the appearance of the logarithmic term meant that we could no longer use our finite different scheme without modifying it profoundly.

To explore how such a solver could be defined, we followed the work of Sirignano and Spiliopoulos [84]. In this work, the authors define a model where, in addition to minimizing the loss related to the equation's operator, they also add terms related to the initial and boundary conditions. In fact, when using PINNs, we can include the information about initial conditions $u(x, 0) = u_0(x)$, for time-dependent prob-

lems, and eventually also boundary values $u(x,t) = u_b(x)$, $x \in \partial\Omega$, simply by adding the corresponding terms in the lost function. The initial condition term would read

$$\mathcal{L}_{IC}(\theta) = \frac{1}{|P|} \sum_{P} |u_\theta(x_i, t=0) - u_0(x_i)|^2 \tag{5.9}$$

whereas for the boundary condition we have

$$\mathcal{L}_{BC}(\theta) = \frac{1}{|\partial P|} \sum_{\partial P} |u_\theta(x_i, t_i) - u_b(x_i)|^2 \tag{5.10}$$

where $\partial P = \{(x_i, t_i) \in \partial\Omega \times [0, +\infty)\}$. Our effort consisted in adapting the tools introduced in [84] and [80] to our MFG problem at hand. In fact, as said we do not use any experimental points to guide towards the discovery of the solution, and the problem we want to solve is time-independent, since we only care solving the stationary state of the MFG. Therefore, the only loss terms adapted to the solution of our problem are the one relative to the boundary conditions $\Phi = \Gamma = \sqrt{m_0}$, as we saw in section 4.2.1, and to the solution of the equation.

So, to sum it up, our goal was to use Machine Learning, and in particular PINNs, as intended by the spirit of the papers [80, 84], to solve the stationary discounted MFG coupled system differential equations (S1). We have not accomplished this goal and, in the following, I will talk about what results we were able to obtain and explain what are the major issues preventing us from completely solving the problem. The results are listed in order of complexity and of level of achievement.

To have a gradual approach to the problem, and thus to eventual complications, we started by solving only the equation for $\Phi$, in one dimension, for $\gamma = 0$ and $g = 0$. In this case, the equation becomes

$$\frac{\mu\sigma^4}{2}\partial_{xx}\Phi + U_0\Phi = 0, \tag{5.11}$$

where $U_0$ represents an obstacle between $-1$ and $1$. We want to solve this equation in the interval $[-5, 5]$, with boundary conditions given by $\Phi(-5) = \Phi(5) = 1$. In this case we already know how the solution should look like. In fact, we expect $\Phi$ to be equal to $0$ for all points under the obstacle. Then the solution is a straight line on both sides of it, between its base at $-1$ and $1$ and the boundary of the interval, where the solution is equal to $1$, as per the boundary condition. This equation can be easily solved with a finite difference method similar to the one already used in section 4.4, but now we want to use a Neural Network and see if we recover the good results. We define a NN composed of $4$ feed-forward hidden layers, composed of 100 nodes each.

| | |
|---|---|
| Rectified Linear Unit (ReLU) | $f(x) = \max(x, 0),\ \forall x \in \mathbb{R}$ |
| Exponential Linear Unit (ELU) | $f(x) = x\, \forall x \leq 0$, $f(x) = e^x - 1$ otherwise. |
| Scaled Exponential Linear Unit (SELU) | $f(x) = x\, \forall x \leq 0$, $f(x) = \lambda\alpha(e^x - 1)$ otherwise $\lambda = 1.050711...$ and $\alpha = 1.673263...$ |
| Sigmoid | $f(x) = (1 + e^{-x})^{-1}$ |

Table 5.1: Definition of the activation functions used in our PINNs model.

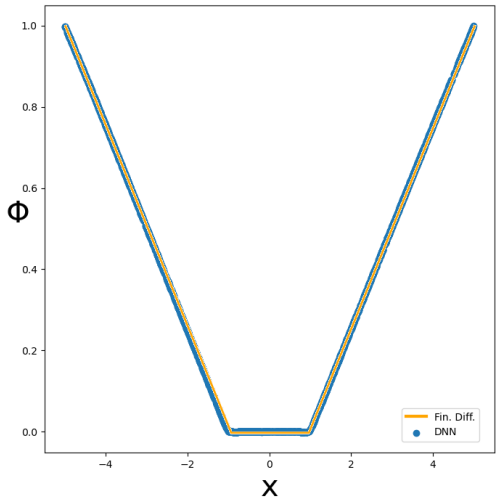


Figure 5.8: Solution of equation (5.11) using both a finite difference scheme (solid line behind the dots), and a Neural Network (blue dots). We can see how the NN correctly recovers the finite difference solution.

For each layer we choose *ReLU* activation function (see table 5.1) and use the *Adam* method [51] to perform the learning. To reproduce the interval we uniformly sample $2000$ points between $-5$ and $5$, and the terms composing the loss will be the one relative to the PDE $\mathcal{L}_E$, and the one for the boundary conditions $\mathcal{L}_{BC}$. As Figure 5.8 shows, the NN is able to correctly recover the finite difference solution, with a cumulative loss of $2.5 \times 10^{-2}$, after $10000$ training steps. This does not surprise us, given the simplicity of the problem.

Now that we proved that this model is capable of solving the simple equation (5.8), we complicate the problem, always in one dimension, without discount but with now $g < 0$. In this case the equation for $\Phi$ becomes

$$\frac{\mu\sigma^4}{2}\partial_{xx}\Phi + (U_0 + gm + \lambda m_0)\Phi = 0, \tag{5.12}$$

where $\lambda = -gm_0$ and $m = \Phi^2$, since we know that in the ergodic state

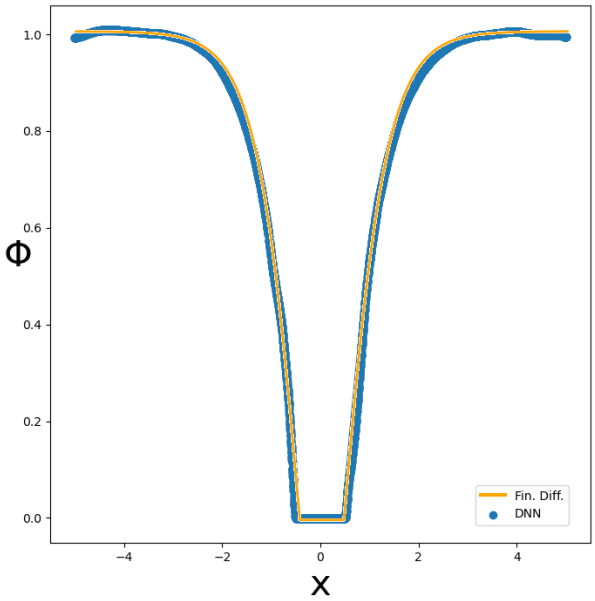


Figure 5.9: Solution of equation (5.12) using both a finite difference scheme (solid line behind the dots), and a Neural Network (blue dots). We can see how the NN correctly approximates the finite difference solution.

$\Phi = \Gamma$. The space interval and the boundary conditions are the same as before. In this case, we have found that the configuration that seems working best is with 9 hidden layer, alternating *ReLU*, *ELU* and *SELU* (see table 5.1), activation functions, of 300 nodes each. The idea behind this configuration is to have enough complexity to let the training decide what kind of layers to use to reproduce the various features of the solution. As we did before, we train the NN using *Adam* optimizer, and the loss function is defined by the PDE and the boundary term, plus, contrarily to what we had before, a term forcing the solution to be equal to $0$ under the obstacle. In fact, one of the most interesting features of solving the equations with NN is that we can include into the loss function any information we have on the solution, ad this should help the training discover the solution of the PDE more easily. As Figure 5.9 shows, the Neural Network configuration we have chosen is capable to approximate fairly well the finite different curve, obtained with the usual technique of section 4.4. However, we can clearly see how the curve wiggles in some areas, especially near the boundary. Moreover, since we have used a large value of $U_0$ to simulate the obstacle the value of the loss function is high and around $10e2$. However, what we have observed is that the loss does not seem to go any lower than that order of magnitude, even when we let the training go on for longer. The

loss stabilizes after around 10k steps and remains at that level regardless of the choice of the learning rate or the implementation of a learning schedule. Other relevant literature in the field, such as [10] suggest that this problem can be addressed by changing the optimizer. In this work, the authors show that a modified version of the Levenberg-Marquardt algorithm drastically outperforms Adam especially in solving non linear differential equations. We leave the exploration of this topic in relation to MFG for future research.

At this point, we felt confident enough to pass to the two dimensional problem, and to add the moving cylinder to the model, therefore adding the velocity term to the MFG equations. However, we were only able to recover something meaningful for the $\gamma = 0$ case, therefore the equations of system (S0). In this case, we used a NN with 5 hidden layers, 100 each, 4 of them with *sigmoid* activation function (see table 5.1) and the last one with *ReLU* activation. The loss function used in this case is comprised of a term penalizing the PDE operator and one term for the boundary condition. Figure 5.10 shows the best results we were able to obtain, with a loss of the order of $10^{-2}$. Here we see the density plot obtained solving the MFG equations with the same parameters of section 4.2.1, but with average density $2.5 ped/m^2$. As we can see, the algorithm seems to find something that resembles the finite difference solution, with the low density corridors in front and behind the obstacle (located at $(0, 0)$ but not shown in the picture to better show the solution details around it), and a higher density at the sides. However, it is evident that the level of accuracy of the details is far from what we obtain with the finite difference scheme. Moreover, the computational time needed to train the NN is several orders of magnitude larger than the time needed to obtain a much crispier result with the finite difference method. All in all, although we admit that we are not Machine Learning engineers and we have not taken the time to methodically explore a wide number of configurations of the NN, what we have observed suggests that this kind of method to solve differential equations, although very promising on paper, is still at its infancy and we leave future researchers discover how to tune it to make it a viable alternative in situations where finite difference schemes cannot be used.

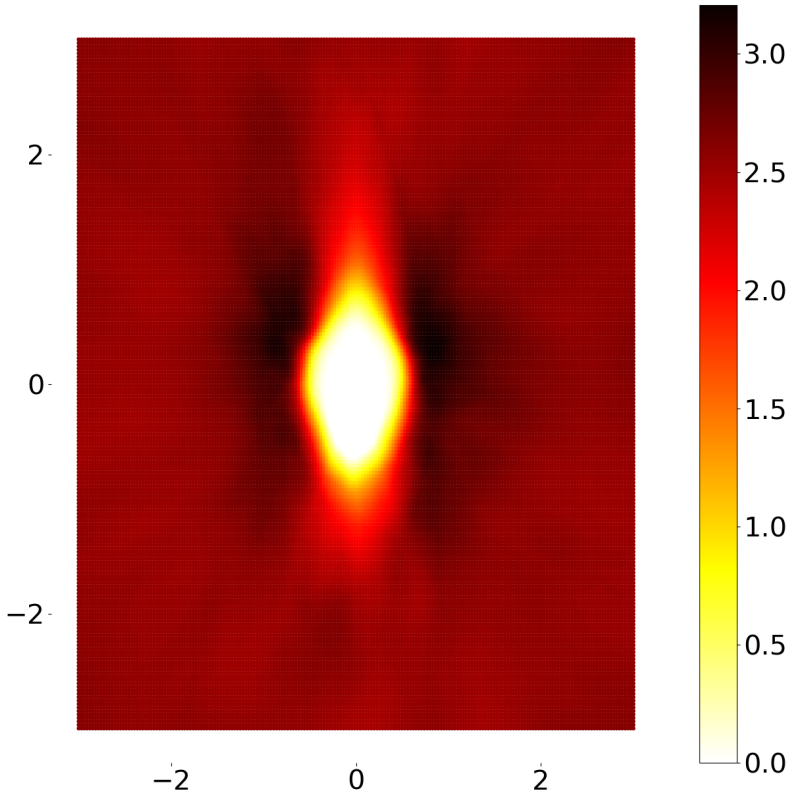


Figure 5.10: Solution of the MFG equations (S0) using a Neural Network with the same parameters used in section 4.2.1 for the frontal case, but with average density of $2.5 ped/m^2$.

# Conclusion

Pedestrian dynamics is a fundamental field of study for urban planning, architecture, transportation engineering, and crowd management. Throughout this thesis, we have explored the pedestrians' behavior through experimental observations and simulations, with a particular focus on long-term anticipation in pedestrian movements. This research has highlighted the limitations of existing models and used a model based on the theory of Mean-Field Games (MFG), capable of more accurately capturing these behaviors. The experimental setup, involving controlled crowds and a moving cylindrical obstacle, revealed that pedestrians exhibit anticipatory behaviors that deviate significantly from those observed in granular materials. This finding underscores the necessity of models that account for the cognitive and anticipatory aspects of human behavior, which are often oversimplified or overlooked in traditional pedestrian dynamics models.

The critical analysis of two widely used pedestrian dynamics models—Helbing's social force model and the ANDA model—demonstrated their inability to fully capture the anticipatory nature of pedestrian movement. These models were found to be too myopic, incapable of correctly describing the long term anticipation necessary to reproduce the experimental behavior. To address these shortcomings, we proposed a model based on Mean-Field Games. MFG models, which merge optimal control and game theory, offer a robust framework for describing interactions among a large number of agents through their average density. This approach simplifies the mathematical treatment of the problem while capturing the essential features of anticipation and decision-making in pedestrian behavior. By incorporating a discount factor that modulates the weight given to future events during the optimization process, our MFG model successfully predicted the experimental anticipation patterns.

Most importantly, the good agreement between the experimental data and the MFG simulation suggest something crucial. In fact, with our work we do not want to convince that humans walk while solving a complex system of differential equations, nor that they always have a complete information about the future. However, we want to convey the message that in some simple a familiar enough cases, humans can coordinate and spontaneously find a Nash equilibrium strategy. This is otherwise not always the case. In fact, Nash equilibria are not always immediately recognized. Moreover, as we have seen with the prisoner's dilemma, they may not even be the best collective choice.

However, as we have seen, once the individuals start playing the NE, no one has any interest in deviating from this trajectory, and this usually ensures the stability of the system. For example, in the case of the avoidance of the cylinder, pedestrians as a group spontaneously coordinated and behaved following the NE, granting a stable and efficient process.

With respect to all the contributions to the field of pedestrian dynamics, our MFG model highlights some important aspects of pedestrians motion that may have been overlooked, or that have been poorly implemented in the past. In particular, our model showed that macroscopic models, although falling short of accurately describing the granularity of crowds, can accurately describe some aspects of the operational dynamics of pedestrians. In particular, to the best of our knowledge, this is the first time that a MFG model is directly tested against the empirical data, which adds the validity of our findings. Moreover, our model, although mathematically quite complex, has simple hypotheses and few assumptions, with a very similar structure to the model introduced by Lasry and Lions. Interestingly, already with this simple form of the model we were able to reproduce the experimental configuration where pedestrians were facing the obstacle, simply finding the right regime of parameters. Besides, we have seen that thanks to the addition of a single parameter, the discount factor, we were also able to simulate the other two experimental configurations. This proves that the discount factor is indeed enough to modulate the agents' knowledge about the future. It is clear, however, that using a MFG model to simulate pedestrians motion is not always realistic. For example, it would be hard to justify that a person evacuating a multi-storey building perfectly knows everything that happens in the building. Nevertheless, as our work shows, there still are situations that are simple and familiar enough where MFG can achieve a better result than other simulation techniques. Finally, thanks to the passage to the Schrödinger formulation, we are able to provide a complete analysis of the parameter space of MFG, analyzing their role and their impact on the observed behavior. To the best of our knowledge, ours constitutes the first attempt at such an extensive analysis.

In addition to the theoretical advancements, this thesis presented two corollary projects that extend the application of MFG in practical scenarios. The first project involved developing a simulation software named *Optimal Crowds*, which integrates MFG with agent-based microscopic models. This hybrid approach allows for detailed individual interactions in scenarios such as evacuations, where traditional density-based models fall short. This project can be seen as a natural contin-

uation of my main work. In fact, with our MFG model we were able to generate a strategy that we proved to be very similar to the one used by real pedestrians in the experiment. Therefore, it would be interesting to use this knowledge to create a microscopic model where agents deal with obstacles similarly to what happens in real life.

The second project explored the use of Physics Informed Neural Networks (PINNs) to solve MFG equations. This innovative approach leverages the power of neural networks to find solutions to complex equations, paving the way for more efficient and scalable simulations. This project was certainly ambitious in its attempt to find a universal solver for differential equations. However, being able to reach this goal at least partially would certainly ease the understanding of many physical phenomena, even beyond pedestrian dynamics. For this reason, we hope that future discoveries in how these machine learning models work will allow for the creation of reliable and effective solvers.

The implications of this research are far-reaching. By incorporating long-term anticipation into pedestrian dynamics models, we provide a more accurate and realistic representation of pedestrian behavior. This has significant implications for the design and management of urban environments. With better predictive models, urban planners and engineers can create safer, more efficient, and more inclusive public spaces. These models can help identify potential congestion points, optimize layouts to enhance flow, and implement effective crowd management strategies to prevent incidents such as overcrowding and stampedes. Recognizing the anticipatory nature of pedestrians can lead to more humane and responsive designs, accommodating the diverse needs of all city dwellers, including those with disabilities or mobility challenges. In conclusion, this thesis represents a significant step forward in the field of pedestrian dynamics. By challenging existing models and proposing a novel approach based on Mean-Field Games, we have laid the groundwork for more accurate and practical simulations of pedestrian behavior. As cities continue to grow and evolve, the importance of understanding and managing pedestrian dynamics will only increase, making this research both timely and essential.

# Bibliography


[1] Y. Achdou, F. J. Buera, J.-M. Lasry, Lions P.-L., and B. Moll. Partial differential equation models in macroeconomics. *Phil. Trans. R. Soc.*, 372, 2014.

[2] Y. Achdou, P-N. Giraud, J.-M. Lasry, and P.-L. Lions. A long-term mathematical model for mining industries. *Appl. Math. Optim.*, 74:579–618, 2016.

[3] Yves Achdou, Martino Bardi, and Marco Cirant. Mean field games models of segregation. *Math. Models Methods Appl. Sci*, 27(01):75–113, 2017.

[4] Yves Achdou, Manh-Khang Dao, Olivier Ley, and Nicoletta Tchou. A class of infinite horizon mean field games on networks. *arXiv preprint arXiv:1805.11290*, 2018.

[5] Saeed Sadeghi Arjmand and Guilherme Mazanti. Multipopulation minimal-time mean field games. *SIAM Journal on Control and Optimization*, 60(4):1942–1969, 2022.

[6] Saeed Sadeghi Arjmand and Guilherme Mazanti. Nonsmooth mean field games with state constraints. *ESAIM: Control, Optimisation and Calculus of Variations*, 28:74, 2022.

[7] Dario Bauso, Hamidou Tembine, and Tamer Basar. Opinion dynamics in social networks through mean-field games. *SIAM Journal on Control and Optimization*, 54(6):3225–3257, 2016.

[8] Atilim Gunes Baydin, Barak A Pearlmutter, Alexey Andreyevich Radul, and Jeffrey Mark Siskind. Automatic differentiation in machine learning: a survey. *Journal of machine learning research*, 18(153):1–43, 2018.

[9] R. Bellman, R.E. Bellman, and Rand Corporation. *Dynamic Programming*. Princeton University Press, 1957.

[10] Andrea Bonfanti, Giuseppe Bruno, and Cristina Cipriani. The challenges of the nonlinear regime for physics-informed neural networks. *arXiv preprint arXiv:2402.03864*, 2024.

[11] T. Bonnemain, T. Gobron, and D. Ullmo. Lax connection and conserved quantities of quadratic mean field games. *J. Math. Phys.*, 62(8):083302, 2021.

[12] Thibault Bonnemain, Matteo Butano, Théophile Bonnet, Iñaki Echeverría-Huarte, Antoine Seguin, Alexandre Nicolas, Cécile Appert-Rolland, and Denis Ullmo. Pedestrians in static crowds are not grains, but game players. *Phys. Rev. E*, 107, 2023.

[13] Louis Bremaud, Olivier Giraud, and Denis Ullmo. Epidemic models on homogeneous networks: some analytical results. *arXiv preprint arXiv:2312.11321*, 2023.

[14] Louis Bremaud and Denis Ullmo. Social structure description of epidemic propagation with a mean-field game paradigm. *Physical Review E*, 106(6):L062301, 2022.

[15] Martin Burger, Marco Di Francesco, Peter Markowich, and Marie-Therese Wolfram. Mean field games with nonlinear mobilities in pedestrian dynamics. *arXiv preprint arXiv:1304.5201*, 2013.

[16] Matteo Butano, Cécile Appert-Rolland, and Denis Ullmo. Discounted mean-field game model of a dense static crowd with variable information crossed by an intruder. *SciPost Physics*, 16(4):104, 2024.

[17] Matteo Butano, Cécile Appert-Rolland, and Denis Ullmo. Mean-field games modeling of anticipation in dense crowds. *arXiv preprint arXiv:2403.01168*, 2024.

[18] Matteo Butano, Thibault Bonnemain, Cécile Appert-Rolland, Alexandre Nicolas, and Denis Ullmo. Modeling of obstacle avoidance by a dense crowd as a mean-field game. *arXiv preprint arXiv:2403.00603*, 2024.

[19] R Candelier and Olivier Dauchot. Creep motion of an intruder within a granular glass close to jamming. *Physical review letters*, 103(12):128001, 2009.

[20] P. Cardaliaguet and Lehalle C.-A. Mean field game of controls and an application to trade crowding, 2017.

[21] P. Cardaliaguet, J.-M. Lasry, P.-L. Lions, and A. Porretta. Long time average of mean field games with a nonlocal coupling. *SIAM J. Control Optim*, 51(5):3558–3591, 2013.

[22] René Carmona, François Delarue, and Aimé Lachapelle. Control of mckean–vlasov dynamics versus mean field games. *Math. Financ. Econ.*, 7(2):131–166, 2013.

[23] Mohcine Chraibi, Armin Seyfried, and Andreas Schadschneider. Generalized centrifugal-force model for pedestrian dynamics. *Physical Review E*, 82(4):046111, 2010.

[24] Asaf Cohen, Mathieu Laurière, and Ethan Zell. Deep backward and galerkin methods for the finite state master equation. *arXiv preprint arXiv:2403.04975*, 2024.

[25] Areski Cousin, Stéphane Crépey, Olivier Guéant, David Hobson, Monique Jeanblanc, Jean-Michel Lasry, Jean-Paul Laurent, Pierre-Louis Lions, and Peter Tankov. *Paris-Princeton lectures on mathematical finance 2010*. Springer, 2010.

[26] Emiliano Cristiani, Arianna De Santo, and Marta Menci. A generalized mean-field game model for the dynamics of pedestrians with limited predictive abilities. *arXiv preprint arXiv:2108.00086*, 2021.

[27] Emiliano Cristiani, Fabio S Priuli, and Andrea Tosin. Modeling rationality to control self-organization of crowds: an environmental approach. *SIAM Journal on Applied Mathematics*, 75(2):605–629, 2015.

[28] Sean Curtis. *Pedestrian velocity obstacles: Pedestrian simulation through reasoning in velocity space*. PhD thesis, The University of North Carolina at Chapel Hill, 2013.

[29] George Cybenko. Approximation by superpositions of a sigmoidal function. *Mathematics of control, signals and systems*, 2(4):303–314, 1989.

[30] Ronald DeVore, Boris Hanin, and Guergana Petrova. Neural network approximation. *Acta Numerica*, 30:327–444, 2021.

[31] MWMG Dissanayake and Nhan Phan-Thien. Neural-network-based approximations for solving partial differential equations. *communications in Numerical Methods in Engineering*, 10(3):195–201, 1994.

[32] Christian Dogbé. Modeling crowd dynamics by the mean-field limit approach. *Mathematical and Computer Modelling*, 52(9-10):1506–1520, 2010.

[33] Iñaki Echeverría-Huarte and Alexandre Nicolas. Body and mind: Decoding the dynamics of pedestrians and the effect of smartphone distraction by coupling mechanical and decisional processes. *Transportation research part C: emerging technologies*, 157:104365, 2023.

[34] John J Fruin. Pedestrian planning and design. Technical report, 1971.

[35] C.W. Gardiner. *Handbook of stochastic methods for physics, chemistry, and the natural sciences*. Springer-Verlag, 1985.

[36] D. A. Gomes and J. Saúde. Mean field games models – a brief survey. *J. Dyn. Games Appl.*, 4(2):110–154, 2014.

[37] Diogo Gomes, Laurent Lafleche, and Levon Nurbekyan. A mean-field game economic growth model. In *2016 American Control Conference (ACC)*, pages 4693–4698. IEEE, 2016.

[38] Ian Goodfellow, Yoshua Bengio, and Aaron Courville. *Deep learning*. MIT press, 2016.

[39] Olivier Guéant. A reference case for mean field games models. *Journal de mathématiques pures et appliquées*, 92(3):276–294, 2009.

[40] O. Guéant. Mean field games equations with quadratic hamiltonian: a specific approach. *Math. Models Methods Appl. Sci.*, 22, 2012.

[41] Dirk Helbing. Similarities between granular and traffic flow. In *Physics of Dry Granular Media*, pages 547–552. Springer, 1998.

[42] Dirk Helbing, Illés Farkas, and Tamas Vicsek. Simulating dynamical features of escape panic. *Nature*, 407(6803):487–490, 2000.

[43] Dirk Helbing, Anders Johansson, and Habib Zein Al-Abideen. Dynamics of crowd disasters: An empirical study. *Physical review E*, 75(4):046109, 2007.

[44] Dirk Helbing and Peter Molnar. Social force model for pedestrian dynamics. *Phys. Rev. E*, 51(5):4282, 1995.

[45] Serge Hoogendoorn and Piet HL Bovy. Simulation of pedestrian flows by optimal control and differential games. *Optimal control applications and methods*, 24(3):153–172, 2003.

[46] Serge P Hoogendoorn and Piet HL Bovy. Pedestrian route-choice and activity scheduling theory and models. *Transp. Res. B: Methodol.*, 38(2):169–190, 2004.

[47] M. Huang, R. P. Malhamé, and P. E. Caines. Large population stochastic dynamic games: closed-loop McKean–Vlasov systems and the nash certainty equivalence principle. *Commun. Inf. Syst.*, 6(3):221–252, 2006.

[48] Roger L Hughes. A continuum theory for the flow of pedestrians. *Transportation Research Part B: Methodological*, 36(6):507–535, 2002.

[49] Ioannis Karamouzas, Brian Skinner, and Stephen J Guy. Universal power law governing pedestrian interactions. *Phys. Rev. Lett.*, 113(23):238701, 2014.

[50] Ioannis Karamouzas, Nick Sohre, Rahul Narain, and Stephen J Guy. Implicit crowds: Optimization integrator for robust crowd simulation. *ACM Transactions on Graphics (TOG)*, 36(4):1–13, 2017.

[51] Diederik P Kingma and Jimmy Ba. Adam: A method for stochastic optimization. *arXiv preprint arXiv:1412.6980*, 2014.

[52] Arman C. Kizilkale and Roland P. Malhamé. Load shaping via grid wide coordination of heating-cooling electric loads: A mean field games based approach.

[53] Arman C Kizilkale, Rabih Salhab, and Roland P Malhamé. An integral control formulation of mean field game based large scale coordination of loads in smart grids. *Automatica*, 100:312–322, 2019.

[54] A. Lachapelle and M.-T. Wolfram. On a mean field game approach modeling congestion and aversion in pedestrian crowds. *Transp. Res. B: Methodol.*, 45(10):1572–1589, 2011.

[55] Aimé Lachapelle, Jean-Michel Lasry, Charles-Albert Lehalle, and Pierre-Louis Lions. Efficiency of the price formation process in presence of high frequency participants: a mean field game analysis. *Mathematics and Financial Economics*, 10:223–262, 2016.

[56] Aimé Lachapelle. *Quelques problèmes de transport et de contrôle en économie: aspects théoriques et numériques*. PhD thesis, Université Paris Dauphine - Paris IX, 2010.

[57] Isaac E Lagaris, Aristidis Likas, and Dimitrios I Fotiadis. Artificial neural networks for solving ordinary and partial differential equations. *IEEE transactions on neural networks*, 9(5):987–1000, 1998.

[58] Laetitia Laguzet and Gabriel Turinici. Individual vaccination as nash equilibrium in a sir model with application to the 2009–2010 influenza a (h1n1) epidemic in france. *Bulletin of mathematical biology*, 77:1955–1984, 2015.

[59] Taras I. Lakoba, D. J. Kaup, and Neal M. Finkelstein. Modifications of the Helbing-Molnár-Farkas-Vicsek social force model for pedestrian evolution. *Simulation*, 81:339–352, 2005.

[60] J.-M. Lasry and P.-L. Lions. Jeux à champ moyen. i – le cas stationnaire. *C. R. Acad. Sci. Paris*, 343(9):619–625, 2006.

[61] J.-M. Lasry and P.-L. Lions. Jeux à champ moyen. ii – horizon fini et contrôle optimal. *C. R. Acad. Sci. Paris*, 343(10):679–684, 2006.

[62] J.-M. Lasry and P.-L. Lions. Mean field games. *Japanese Journal of Mathematics*, 2(1):229–260, 2007.

[63] Mathieu Laurière, Sarah Perrin, Matthieu Geist, and Olivier Pietquin. Learning mean field games: A survey. *arXiv preprint arXiv:2205.12944*, 2022.

[64] Yann LeCun, Yoshua Bengio, et al. Convolutional networks for images, speech, and time series. *The handbook of brain theory and neural networks*, 3361(10):1995, 1995.

[65] Kurt Lewin. *Field Theory in Social Science*. Harper & Brothers, New York, 1951.

[66] Michael James Lighthill and G Be Whitham. On kinematic waves i. flood movement in long rivers. *Proceedings of the Royal Society of London. Series A. Mathematical and Physical Sciences*, 229(1178):281–316, 1955.

[67] Michael James Lighthill and Gerald Beresford Whitham. On kinematic waves ii. a theory of traffic flow on long crowded roads. *Proceedings of the royal society of london. series a. mathematical and physical sciences*, 229(1178):317–345, 1955.

[68] Lindsay W Ludlow and Peter G Weyand. Energy expenditure during level human walking: seeking a simple and accurate predictive solution. *Journal of Applied Physiology*, 120(5):481–494, 2016.

[69] Bertrand Maury, Aude Roudneff-Chupin, Filippo Santambrogio, and Juliette Venel. Handling congestion in crowd motion modeling. *Networks and Heterogeneous Media*, 6:485–519, 2011.

[70] John Maynard Smith. Evolution and the theory of games. *American scientist*, 64(1):41–45, 1976.

[71] Warren S McCulloch and Walter Pitts. A logical calculus of the ideas immanent in nervous activity. *The bulletin of mathematical biophysics*, 5:115–133, 1943.

[72] Laurentius Antonius Meerhoff, Julien Bruneau, Alexandre Vu, A-H Olivier, and Julien Pettré. Guided by gaze: Prioritization strategy when navigating through a virtual crowd can be assessed through gaze activity. *Acta psychologica*, 190:248–257, 2018.

[73] Pankaj Mehta, Marin Bukov, Ching-Hao Wang, Alexandre GR Day, Clint Richardson, Charles K Fisher, and David J Schwab. A high-bias, low-variance introduction to machine learning for physicists. *Physics reports*, 810:1–124, 2019.

[74] Mehdi Moussaïd, Dirk Helbing, and Guy Theraulaz. How simple rules determine pedestrian behavior and crowd disasters. *Proceedings of the National Academy of Sciences*, 108(17):6884–6888, 2011.

[75] A. Nicolas, M. Kuperman, S. Ibañez, S. Bouzat, and C. Appert-Rolland. Mechanical response of dense pedestrian crowds to the crossing of intruders. *Sci. Rep.*, 9(105), 2019.

[76] Daniel R Parisi, Marcelo Gilman, and Herman Moldovan. A modification of the social force model can reproduce experimental data of pedestrian flows in normal conditions. *Physica A: Statistical Mechanics and its Applications*, 388(17):3600–3608, 2009.

[77] José M Pastor, Angel Garcimartín, Paula A Gago, Juan P Peralta, César Martín-Gómez, Luis M Ferrer, Diego Maza, Daniel R Parisi, Luis A Pugnaloni, and Iker Zuriguel. Experimental proof of faster-is-slower in systems of frictional particles flowing through constrictions. *Physical Review E*, 92(6):062817, 2015.

[78] Etienne Pinsard. *Modélisation du mouvement de foules denses : phénoménologie et couplage de modèles*. PhD thesis, Université Paris-Saclay, 2022.

[79] William Poundstone. *Prisoner's dilemma*. Anchor, 2011.

[80] Maziar Raissi, Paris Perdikaris, and George E Karniadakis. Physics-informed neural networks: A deep learning framework for solving forward and inverse problems involving nonlinear partial differential equations. *Journal of Computational physics*, 378:686–707, 2019.

[81] David E Rumelhart, Geoffrey E Hinton, and Ronald J Williams. Learning representations by back-propagating errors. *nature*, 323(6088):533–536, 1986.

[82] Antoine Seguin. *De la pénétration en milieu granulaire*. PhD thesis, Université Paris-Sud, 2010.

[83] Masahiro Shiomi, Francesco Zanlungo, Kotaro Hayashi, and Takayuki Kanda. Towards a socially acceptable collision avoidance for a mobile robot navigating among pedestrians using a pedestrian model. *International Journal of Social Robotics*, 6(3):443–455, 2014.

[84] Justin Sirignano and Konstantinos Spiliopoulos. Dgm: A deep learning algorithm for solving partial differential equations. *Journal of computational physics*, 375:1339–1364, 2018.

[85] Leonardo Stella, Fabio Bagagiolo, Dario Bauso, and Giacomo Como. Opinion dynamics and stubbornness through mean-field games. In *52nd IEEE Conference on Decision and Control*, pages 2519–2524. IEEE, 2013.

[86] Igor Swiecicki, Thierry Gobron, and Denis Ullmo. Schrödinger approach to mean field games. *Physical review letters*, 116(12):128701, 2016.

[87] Denis Ullmo, Igor Swiecicki, and Thierry Gobron. Quadratic mean field games. *Phys. Rep.*, 799:1–35, 2019.

[88] Jur Van Den Berg, Sachin Patil, Jason Sewall, Dinesh Manocha, and Ming Lin. Interactive navigation of multiple agents in crowded environments. In *Proceedings of the 2008 symposium on Interactive 3D graphics and games*, pages 139–147, 2008.

[89] Iker Zuriguel, Daniel Ricardo Parisi, Raúl Cruz Hidalgo, Celia Lozano, Alvaro Janda, Paula Alejandra Gago, Juan Pablo Peralta, Luis Miguel Ferrer, Luis Ariel Pugnaloni, Eric Clément, et al. Clogging transition of many-particle systems flowing through bottlenecks. *Scientific reports*, 4(1):7324, 2014.

# Published Papers

In the following, I attach the two journal papers I have published during my doctorate and whose content is summarized in chapter 4.

1. The first paper [12] was published in 2023 in the journal *Physical Reviews E* and is titled *"Pedestrians in static crowds are not grains, but game players"*.

2. The second paper [16] was published in 2024 in the journal *SciPost Physics* and is titled *"Discounted Mean Field Game model of a dense static crowd with variable information crossed by an intruder"*.

# Pedestrians in static crowds are not grains, but game players

Thibault Bonnemain[1,2*], Matteo Butano[3], Théophile Bonnet[4,3,¤], Iñaki Echeverría-Huarte[5], Antoine Seguin[6], Alexandre Nicolas[7], Cécile Appert-Rolland[4], and Denis Ullmo[3]

**1** *Department of Mathematics, Physics and Electrical Engineering, Northumbria University, Newcastle upon Tyne, United Kingdom*

**2** *Department of Mathematics, King's College, London, United Kingdom*

**3** *Université Paris-Saclay, CNRS, LPTMS, 91405, Orsay, France*

**4** *Université Paris-Saclay, CNRS, IJCLab, 91405, Orsay, France*

**5** *Laboratorio de Medios Granulares, Departamento de Física y Matemática Aplicada, Univ. Navarra, 31080, Pamplona, Spain*

**6** *Université Paris-Saclay, CNRS, FAST, 91405, Orsay, France*

**7** *Institut Lumière Matière, CNRS & Université Claude Bernard Lyon 1, 69622, Villeurbanne, France*

¤*Current address: Université Paris-Saclay, CEA, Service d'Etudes des Réacteurs et de Mathématiques Appliquées, 91191, Gif-sur-Yvette, France and*

* *Corresponding author: thibault.bonnemain@kcl.ac.uk*

The local navigation of pedestrians is assumed to involve no anticipation beyond the most imminent collisions, in most models. These typically fail to reproduce some key features experimentally evidenced in dense crowds crossed by an intruder, namely transverse displacements towards regions of higher density, due to the anticipation of the intruder's crossing. We introduce a minimal model based on mean-field games, emulating agents planning out a global strategy that minimizes their overall discomfort. By solving the problem in the permanent regime thanks to an elegant analogy with the nonlinear Schrödinger's equation, we are able to identify the two main variables governing the model's behavior and to exhaustively investigate its phase diagram. We find that, compared to some prominent microscopic approaches, the model is remarkably successful in replicating the experimental observations associated with the intruder experiment. Besides, the model can capture other daily-life situations such as partial metro boarding.

## I. INTRODUCTION

Although crowd disasters (such as the huge stampedes that grieved the Hajj in 1990, 2006 and 2015 [1]) are more eye-catching to the public, the dynamics of pedestrian crowds are also of great relevance in less dire circumstances. They are central when it comes to designing and dimensioning busy public facilities, from large transport hubs to entertainment venues, and optimizing the flows of people. Modelling pedestrian motion in these settings is a multi-scale endeavour, which requires determining where people are heading for (*strategic* level), what route they will take (*tactical* level), and finally how they will move along that route in response to interactions with other people (*operational* level) [2]. The *strategic* and *tactical* levels typically involve some planning in order to make a choice among a discrete or continuous set of options, such as targeted activities, destinations [2], paths (possibly knowing their expected level of congestion) [3], or, in the context of evacuations, egress alternatives [3, 4]. These choices are often handled as processes of maximisation (minimisation) of a utility (cost), which may depend on lower-level information such as pedestrian density or streaming velocity [5, 6].

The *operational* level deals with much shorter time scales and is generally believed to involve no planning ahead. Anticipatory effects are thus merely neglected in so-called *reactive* models, especially at high densities, possibly with the lingering idea that mechanical forces then prevail. For example, the popular social force model of Helbing and Molnar [7], still at the heart of several commercial software products, combines contact forces and pseudo-forces ("social" forces) which, in the original implementation, are only functions of the agents' current positions (and possibly orientations). Some degree of anticipation has since been introduced into these models to better describe collision avoidance, e.g., by making the pseudo-forces depend on future positions rather than current ones [8, 9]. In a dual approach, the most imminent collisions can be avoided by scanning the whole velocity space [10–12] or a subset of it [13] in search of the optimal velocity. All these dynamic models, at best premised on a constant-velocity hypothesis, owe their high computational tractability to their relative shortsightedness. Note that, to mitigate these limitations, in particular in the case of denser crowds, anticipated collisions beyond the most imminent one [14] or, at a more coarse-grained scale, local density inhomogeneities [5] can be taken into account.

In this paper, we argue that, even at the *operational* level, crowds in some daily-life circumstances display signs of anticipation that may elude the foregoing shortsighted models; this will be exemplified by the recently studied response of a dense static crowd when crossed by an 'intruder' [15, 16]. We purport to show that a minimal game theoretical approach, made tractable thanks to an elegant analogy between its mean-field formulation [17–19] and Schrödinger equation [20, 21], can replicate the empirical observations for this example case, provided that it accounts for the anticipation of future costs. To our knowledge this is the first experimental validation of Mean Field Games (MFG) as a relevant framework

to study pedestrian dynamics. Beyond that particular example, the approach efficiently captures certain behaviours of crowds at the interface between the *operational* and *tactical* levels that are crucial to consider in attempts to improve the security of dense crowds.

## II. CROSSING A STATIC CROWD

Crossing a static crowd is a common experience in busy premises, from standing concerts and festivals to railway stations. Recently, small-scale controlled experiments [15, 22] shed light on trends that robustly emerged in the response of a crowd crossed by a cylindrical intruder, as displayed in Fig. 1 (right column). The induced response consists of a fairly symmetric density field around the intruder, displaying depleted zones both upstream and downstream from the intruder, as well as higher-density regions on the sides. Consistently the crowd's displacements are mostly transverse: pedestrians tend to simply step aside. A similar behavior - though more noisy - was observed when the intruder was a single pedestrian. Incidentally, a qualitatively similar response was filmed at much larger scale in a dense crowd of protesters in Hong-Kong, which split open to let an ambulance through [23].

As penetration by an intruder is a benchmark test for granular matter, it is instructive to compare the response of the two systems. Actually the above crowd features strongly depart from the mechanical response observed in experiments [24, 25] or simulations [26] of penetration into a granular mono-layer below jamming, where grains are pushed forward by the intruder [see Fig. 1 (left column) and Movie S1] and accumulate downstream, instead of moving crosswise. More worryingly, these "mechanical" features are also observed (see Fig. 1 in [27]) in simulations of pedestrian dynamics performed with the social-force model [7], which rests on tangential and normal forces at contact and radial repulsive forces for longer-ranged interactions.

Introducing collision anticipation in the pedestrian model helps reproduce the opening of an agent-free 'tunnel' ahead of the intruder, as illustrated with a 'time to (first) collision' model (second column of Fig. 1 and Movie S2) directly inspired from [12], details of which can be found in Appendix B. However, even though the displacements need not align with the contact forces in this agent-based model, the displacement pattern diverges from the experimental observations, with streamwise (walk-away) moves that prevail over transverse (step-aside) ones. Indeed, such models rely on 'short-sighted' agents, who do not see past the most imminent collision expected from constant-velocity extrapolation.

Results will naturally vary with the specific collision-avoidance model and the selected parameters. Yet, the failure of diverse state-of-the-art models to reproduce prominent experimental features suggests that an ingredient is missing in these approaches based on short-time (first-collision) anticipation.

## III. A GAME THEORETICAL APPROACH TO ACCOUNT FOR LOW-LEVEL PLANNING

To bring in the missing piece, we start by noticing that the observed behaviours are actually most intuitive: Pedestrians anticipate that it will cost them less effort to step-aside and then resume their positions, even if it entails enduring high densities temporarily, than to endlessly run away from an intruder that will not deviate from its course. But accounting for this requires a change of paradigm compared to the foregoing approaches. Game theory is an adequate framework to handle conflicting impulses of interacting agents endowed with planning capacities: agents are now able to optimize their strategy taking into account the choices (or strategies) of others. So far, its use in pedestrian dynamics has mostly been restricted to evacuation tactics in discrete models [4, 28, 29]. Unfortunately, the problem becomes intractable when the number of interacting agents grows.

To overcome this quandary, we turn to MFG, introduced by Lasry and Lions [17, 18] as well as Huang et al. [19] in the wake of the mean-field approximations of statistical mechanics, and since used in a variety of fields, ranging from finance [30–32] to economics [33–35], epidemiology [36–38], sociology [36, 39, 40], or engineering [41–43]. While applications of MFG to crowd dynamics have already been proposed [3, 44–48], our goal here is to demonstrate the practical relevance of this approach at the *operational* level, using an elementary MFG belonging to one of the first class of models introduced by Lasry and Lions [17], and which can be thoroughly analysed thanks to its connection with the nonlinear Schrödinger equation.

In the mean field approximation, the "$N$-player" game is replaced by a generalized Nash equilibrium [49] where indiscriminate microscopic agents play against a macroscopic state of the system (a density field) formed by the infinitely many remaining agents. Consider a large set of pedestrians, the agents of our game, characterised by their spatial position (state variable) $\mathbf{X}^i \equiv (x^i, y^i) \in \mathbb{R}^2$, which we assume follows Langevin dynamics

$$d\mathbf{X}_t^i = \mathbf{a}_t^i dt + \sigma d\mathbf{W}_t^i \tag{1}$$

where the drift velocity (*control* variable) $\mathbf{a}_t^i$ reflects the agent's strategy. In (1), $\sigma$ is a constant and components of $\mathbf{W}^i$ are independent white noises of variance one accounting for unpredictable events. Agents are supposed identical, apart from their initial positions $\mathbf{X}^i(t=0)$ and realisations of $\mathbf{W}^i$.

Each agent strives to adapt their velocity $\mathbf{a}_t^i$ in order to minimise a cost functional we assume to take the simple form

$$c[\mathbf{a}^i](t, \mathbf{x}_t^i) = \left\langle \int_t^T \left[ \frac{\mu \mathbf{a}^2}{2} - \left( g m^{\mathrm{e}}(t, \mathbf{x}) + U_0(\mathbf{x} - \mathbf{v}t) \right) \right] d\tau \right\rangle \tag{2}$$

where $\langle \cdot \rangle$ denotes averaging over all realizations of the noise for trajectories starting at $\mathbf{x}_t^i$ at time $t$. In this

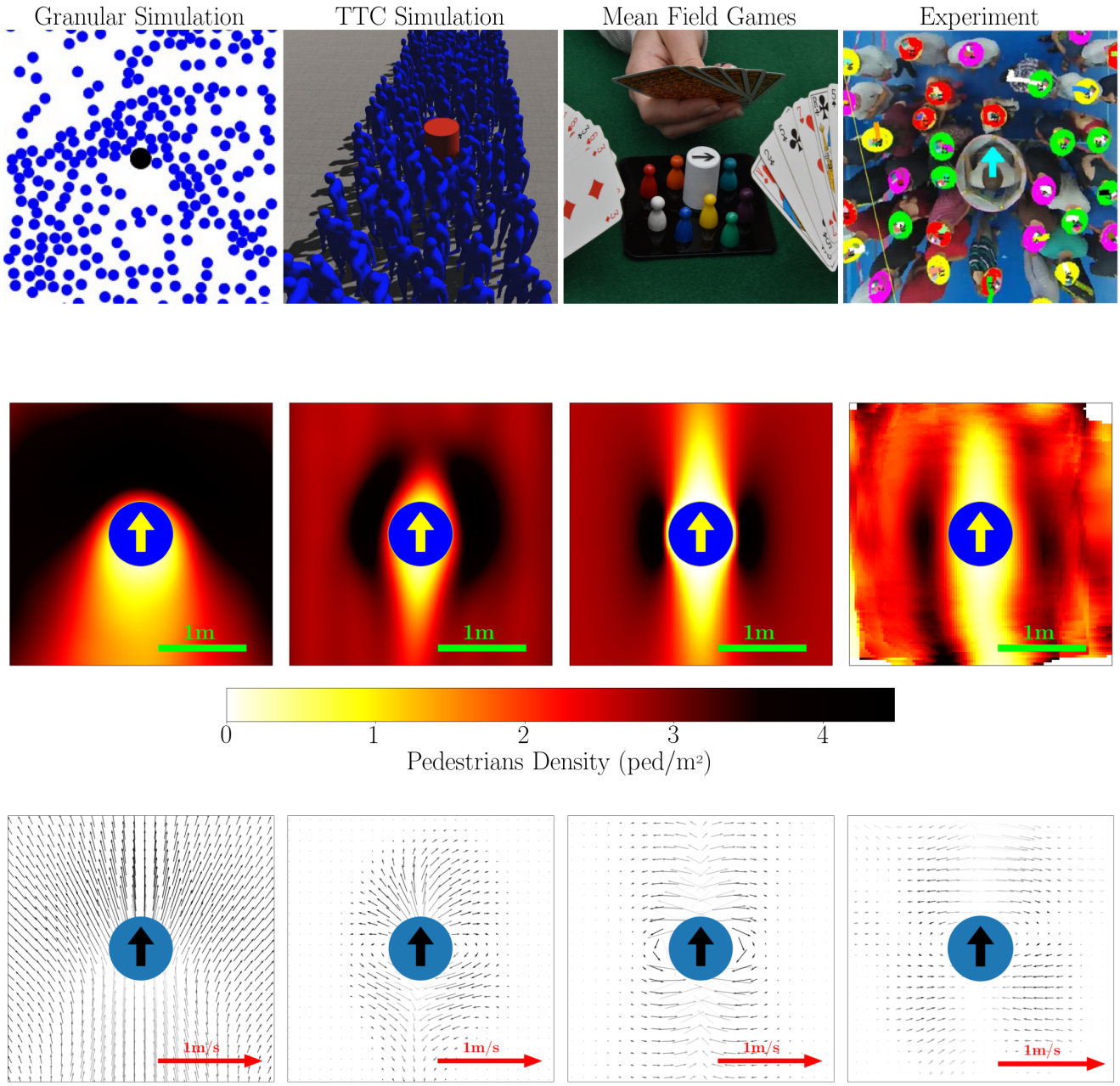


Figure 1: Data (middle row) and velocity (bottom row) fields induced in a static crowd by a cylindrical intruder that crosses it; the transparency of the velocity arrows is linearly related to the local density. (Column 1) Simulations of a mono-layer of vibrated disks. (Column 2) Simulations of an agent-based model wherein agents may anticipate the most imminent collision. All fields have been averaged over many realisations. (Column 3) Results of the mean-field game introduced in this paper. (Column 4) Controlled experiments of [15]. Note the relatively symmetrical density dip in front and behind the intruder, as well as the transverse moves. (Columns 1-3) The crowd's density and intruder's size have been adjusted to match the experimental data (average density of 2.5 ped/m$^2$). Details of simulations and videos showcasing time evolution can be found in Appendix.

expression, the term $\mu\mathbf{a}^2/2$, akin to a kinetic energy, represents the efforts required by the agent to enact their strategy (how much/how fast they have to move in this case), while the interactions with the other agents via the empirical density $m^{\mathrm{e}}(t,\mathbf{x}) = \sum_i \delta(\mathbf{x} - \mathbf{X}^i(t))/N$ are controlled by a parameter $g < 0$. Finally, the space occupied by the intruding cylinder, which moves at a velocity $\mathbf{v} = (0, v)$, is characterised by a 'potential'

$U_0(\mathbf{x}) = V_0\Theta(\|\mathbf{x}\|-R)$ that tends to $V_0 \to -\infty$ inside the radius $R$ of the cylinder and is zero elsewhere. Agents need to balance those three terms *over the whole duration* $T$ *of the game*, which enables them to make costly, but temporary moves if they lower the overall cost. For example, depending on the parameters, stepping aside into a high density region (a cost-inefficient strategy *a priori*) to let the intruder through may prove overall more efficient than running away from it; the first strategy implies paying a high cost upfront, but nothing afterwards, while the second implies paying a comparatively low cost that however extends over the whole duration of the game, resulting in a potentially worse pay-off.

In the presence of many agents, the density self-averages to $m(t,\mathbf{x}) = \langle m^{\mathrm{e}}(t,\mathbf{x})\rangle_{\underline{\text{noise}}}$ and the optimization problem (2) does not feature explicit coupling between agents anymore. It can then be solved by introducing the value function $u(t,\mathbf{x}) = \min_{a(\cdot)} c[\mathbf{a}](t,\mathbf{x})$, which obeys a Hamilton-Jacobi-Bellman [HJB] equation [18, 50], with optimal control $\mathbf{a}^*(t,\mathbf{x}) = -\nabla u(t,\mathbf{x})/\mu$. Consistency imposes that $m(t,\mathbf{x})$ is solution of the Fokker-Planck [FP] equation associated with (1), given the drift velocity $\mathbf{a}(t,\mathbf{x}) = \mathbf{a}^*(t,\mathbf{x})$. As such, MFG can be reduced to a system of two coupled partial differential equations [17, 18, 20, 21].

$$\begin{cases} \partial_t u(t,\mathbf{x}) = \dfrac{1}{2\mu}\left[\nabla u(t,\mathbf{x})\right]^2 - \dfrac{\sigma^2}{2}\Delta u(t,\mathbf{x}) + g m(t,\mathbf{x}) + U_0(\mathbf{x}-\mathbf{v}t) & \text{[HJB]} \\ \partial_t m(t,\mathbf{x}) = \dfrac{1}{\mu}\nabla\cdot\left[m(t,\mathbf{x})\nabla u(t,\mathbf{x})\right] + \dfrac{\sigma^2}{2}\Delta m(t,\mathbf{x}) & \text{[FP]} \end{cases} \tag{3}$$

The atypical "forward-backward" structure of Eqs. (3), highlighted by the opposite signs of Laplacian terms in the two equations, accounts for anticipation. The boundary conditions epitomise this structure: based on (2), the value function has terminal condition $u(t=T,\mathbf{x}) = 0$, while the density of agents evolves from a uniform initial distribution $m(t=0,\mathbf{x}) = m_0$. In previous work, we have evinced a formal, but insightful mapping of these MFG equations onto a nonlinear Schrödinger equation (NLS) [20, 21, 51], well studied in fields ranging from nonlinear optics [52, 53] to Bose-Einstein condensation [54, 55] and fluid dynamics [56, 57].

We perform a change of variables $(u(t,\mathbf{x}), m(t,\mathbf{x})) \mapsto (\Phi(t,\mathbf{x}), \Gamma(t,\mathbf{x}))$ through $u(t,\mathbf{x}) = -\mu\sigma^2 \log\Phi(t,\mathbf{x})$, $m(t,\mathbf{x}) = \Gamma(t,\mathbf{x})\Phi(t,\mathbf{x})$ [21]. The first relation is the usual Cole-Hopf transform [58]; the second corresponds to an "Hermitization" of Eqs. (3). In terms of the new variables $(\Phi,\Gamma)$, the MFG equations read

$$\begin{cases} -\mu\sigma^2\partial_t\Phi = \dfrac{\mu\sigma^4}{2}\Delta\Phi + (U_0 + g\Gamma\Phi)\Phi \\ +\mu\sigma^2\partial_t\Gamma = \dfrac{\mu\sigma^4}{2}\Delta\Gamma + (U_0 + g\Gamma\Phi)\Gamma \end{cases}. \tag{4}$$

Besides the missing imaginary factor associated with time derivation, these equations have exactly the structure of NLS describing the evolution of a quantum state $\Psi(t,\mathbf{x})$ of a Bose-Einstein condensate, with formal correspondence $\Psi \to \Gamma$, $\Psi^* \to \Phi$ and $\rho \equiv ||\Psi||^2 \to m \equiv \Phi\Gamma$. This system, however, retains the forward-backward structure of MFG evidenced by mixed initial and final boundary conditions $\Phi(T,\mathbf{x}) = 1$, $\Gamma(0,\mathbf{x})\,\Phi(0,\mathbf{x}) = m_0(\mathbf{x})$. Several methods have been developed to deal with NLS and most can be leveraged to tackle the MFG problem [21, 59].

Self-consistent solutions of Eqs. (4) are obtained by iteration: (i) Assume $m(t,\mathbf{x}) = m_{\mathrm{in}}(t,\mathbf{x})$; (ii) Solve the equation for $\Phi$ backward in time with terminal condition $\Phi(T,\mathbf{x}) = 1$; (iii) Solve the equation for $\Gamma$ forward in time with initial condition $\Gamma(0,\mathbf{x}) = m_0(\mathbf{x})/\Phi(0,\mathbf{x})$; (iv) iterate with $\Phi(t,\mathbf{x})\Gamma(t,\mathbf{x}) = m_{\mathrm{out}} \mapsto m_{\mathrm{in}}$ until $m_{\mathrm{out}}$ is sufficiently close to $m_{\mathrm{in}}(t,\mathbf{x})$. A video illustrating the evolution of the agents' density for a particular set of parameters, along with additional details about the numerical scheme, can be found in Appendix C.

Focusing on the *permanent* regime [60], for which we have experimental data [15], rather than on the transients associated with the intruder's entry or exit, further simplifies the resolution. In this regime, defined by time-independent density and velocity fields in the intruder's frame, the auxiliary functions $\Phi$ and $\Gamma$ are not constant in time, but they assume the trivial dynamics $\Phi(t,\mathbf{x}) = \exp\left[\lambda t/\mu\sigma^2\right]\Phi_{\mathrm{er}}(\mathbf{x})$ and $\Gamma(t,\mathbf{x}) = \exp\left[-\lambda t/\mu\sigma^2\right]\Gamma_{\mathrm{er}}(\mathbf{x})$ where, in the intruder's frame

$$\begin{cases} \dfrac{\mu\sigma^4}{2}\Delta\Phi_{\mathrm{er}} - \mu\sigma^2\mathbf{v}\cdot\vec{\nabla}\Phi_{\mathrm{er}} + [U_0(\mathbf{x}) + g m_{\mathrm{er}}]\Phi_{\mathrm{er}} = -\lambda\Phi_{\mathrm{er}} \\ \dfrac{\mu\sigma^4}{2}\Delta\Gamma_{\mathrm{er}} + \mu\sigma^2\mathbf{v}\cdot\vec{\nabla}\Gamma_{\mathrm{er}} + [U_0(\mathbf{x}) + g m_{\mathrm{er}}]\Gamma_{\mathrm{er}} = -\lambda\Gamma_{\mathrm{er}} \end{cases} \tag{5}$$

(with $m_{\mathrm{er}} = \Phi_{\mathrm{er}}\Gamma_{\mathrm{er}}$ independent of time). Far from the intruder $U_0(\mathbf{x}) = 0$, $m \simeq m_0$ and pedestrians have constant velocity $-\mathbf{v}$ in the intruder's frame. This imposes the asymptotic solutions $\Phi_{\mathrm{er}}(\mathbf{x}) = \Gamma_{\mathrm{er}}(\mathbf{x}) = \sqrt{m_0}$, from which $\lambda = -g m_0$.

## IV. RESULTS

The stationary Eqs. (5) have two remarkable features: (i) They give direct access to the permanent regime, and

are straightforward to implement numerically since time dependence has disappeared (results with reasonable resolution can be obtained in a few minutes on a mid-range laptop). (ii) As in [61], rescaling Eqs. (5) shows that solutions are entirely specified by only two dimensionless parameters.

Indeed, the intruder is characterised by its radius $R$ and its velocity $v$. Similarly, pedestrians are characterized by a length scale $\xi = \sqrt{|\mu\sigma^4/2gm_0|}$, the distance over which the crowd density tends to recover its bulk value from a perturbation, a.k.a *healing length*, and a velocity scale $c_s = \sqrt{|gm_0/2\mu|}$, the typical speed at which pedestrians tend to move [1]. Up to a scaling factor, solutions of Eqs. (5) can be expressed as a function of the two ratios $\xi/R$ and $c_s/v$ instead of depending on the full set of parameters $(R, v, \mu, \sigma, m_0, g)$, which facilitates the exploration of the parameter space, makes modeling more robust, and highlights the uttermost importance of anticipation. It should be noted that in MFG the individual anticipation time, usually defined explicitly in classical agent-based models, is encoded in the choice of $\xi$ and $c_s$ but it is not readily available as a function of the two. In fact, MFG leads to a strategy of motion where the anticipation time is optimal, without prescribing it.

Figure 2 presents typical density and velocity fields simulated in the permanent regime, for each quadrant of the reduced parameter space. Intuitively, one understands that $c_s$ governs the cost of motion for the agents while $\xi$ gives the extent of the perturbation caused by the presence of the intruder. The main difference between large and small $c_s/v$ is the change in rotational symmetry, which reflects a fundamental change in strategy. For large values of $c_s/v$ pedestrians do not mind moving, and they rather try to avoid congested areas for as long as possible, thus creating circulation around the intruder, as shown in the velocity plots. On the other hand, for small values of $c_s/v$, moving fast costs more; therefore, in order to avoid the intruder, pedestrians have to move earlier, and accept to temporarily side-step into a more crowded area, thereby stretching the density along the vertical direction.

Experimental observations [15] are best reproduced for small $c_s/v$ and small $\xi/R$ ($c_s = 0.11$ and $\xi = 0.15$), as shown in the third column of Fig. 1. Considering the minimalism of our MFG model, the obtained agreement is especially satisfying. In particular it demonstrates that even basic MFG models can naturally capture prominent features of the response of static crowds which may be out of reach of more short-sighted pedestrian dynamics models.

[1] Note that $\mu\xi c_s = \mu\sigma^2$ has the dimension of an action and plays the role of $\hbar$ in the original nonlinear Schrödinger equation.

## V. ALTERNATIVE CONFIGURATION: BOARDING OF A TRAIN

Although our model reproduces remarkably well the experiments of [15] in view of its minimalism, we realise that a single test might not be sufficient to justify our claim that MFG theory is a good candidate for modeling pedestrian dynamics. We argue that MFG are also applicable to a broader array of crowd-related problems at the operational level, beyond crossing scenarios. In this section we illustrate this assertion by exploring the daily-life situation of people waiting to board a coach in an underground station. This is a common configuration at the frontier between the operational and tactical level, which should give a strong edge to MFG over alternative models, owing to the important role played by anticipation.

This situation can be readily simulated by suitably modifying the external potential $U_0(\mathbf{x})$ and the geometry of the system, as shown on Fig. 3; $U_0(\mathbf{x})$ here is a box-like infinite potential representing the walls of the coach (black bands). On top of that we introduced a terminal cost $c_T(\mathbf{x})$ [21, 59] that is lower aboard the metro than on the platform

$$c_T(\mathbf{x}) = c_{\text{platform}} + [c_{\text{coach}} - c_{\text{platform}}]\Theta\left(x_{\text{wall}} - x\right) \ , \quad (6)$$

where $c_{\text{coach}} < c_{\text{platform}}$, $\Theta$ is the Heaviside function and $x_{\text{wall}}$ is the $x$-coordinate (horizontal) where the walls of the coach start. This terminal cost $c_T(\mathbf{x})$ does not modify the MFG equations (3) but serves as terminal condition for the value function $u(\mathbf{x}, t = T) = c_T(\mathbf{x})$ (and accordingly for $\Phi$). We then numerically solve the nonlinear Schrödinger type system using the algorithm described succinctly in Section III and in more details in Appendix C. Results of our simulations can be seen in Movie S4, of which Fig. 3 (right) is a snapshot.

There are sadly no experimental evidence to support this at the moment, but we manage to reproduce the boarding process in a qualitatively realistic way, despite the simplicity of our model. We even naturally capture the decision made by some agents to stay on the platform rather than board the overcrowded metro. We believe this last point to be particularly interesting since this "passive" behaviour emerges naturally from our (anticipatory) game theoretical model, which would be more difficult to implement in traditional approaches of crowd dynamics.

## VI. DISCUSSION

To conclude, our results have been obtained with a simple, generic MFG model which depends linearly on density via $gm(t, \mathbf{x})$. The NLS representation provides important insight, efficient numerical schemes and powerful analytical tools. Most notably it draws a bridge between pedestrian dynamics and optics, fluid dynamics or Bose-Einstein condensation. Naturally our minimal model can

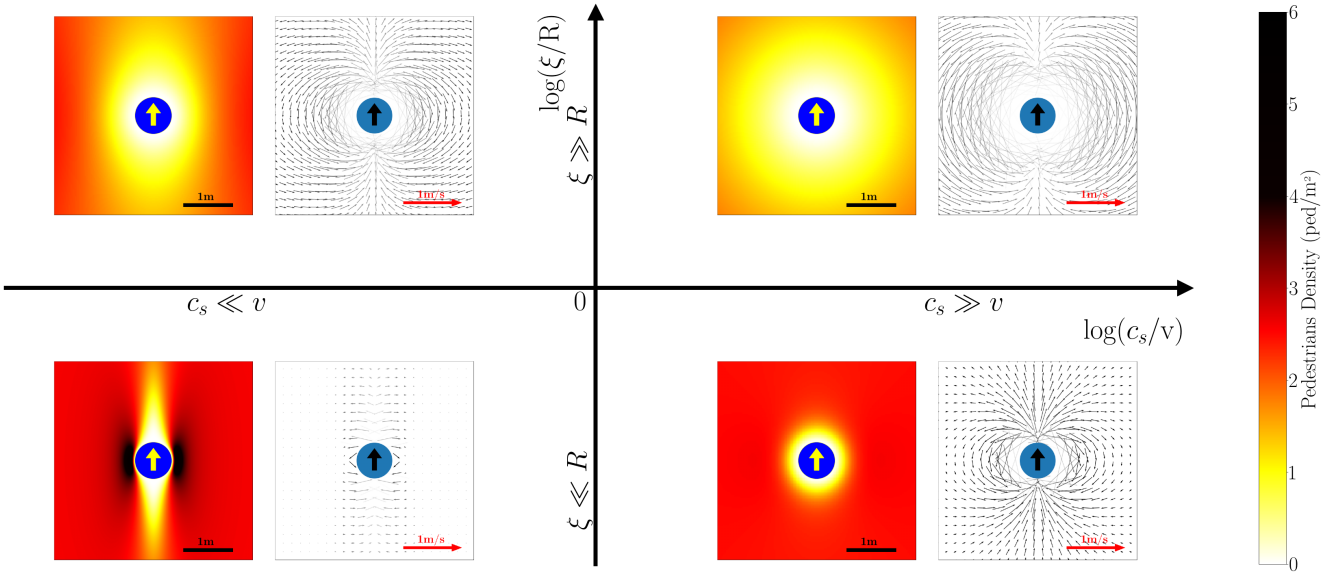


Figure 2: Typical density and velocity fields induced by the crossing intruder in the permanent regime, as predicted by the MFG model in different regions of the parameter space. Parameters taken in the small $c_s/v$ and small $\xi/R$ quadrant display good visual agreement with the experimental data.

be refined: the MFG formalism is flexible enough to incorporate further elements and make it truer to life, including time-discounting effects [62, 63] and congestion [44, 64, 65]. Higher quantitative accuracy will be within reach of these more sophisticated approaches, possibly at the expense of less transparent outcomes. For sure, MFG will struggle to capture a variety of problems of crowd dynamics at the operational level, notably those for which the granularity of the crowd is central. However, the afore-studied experiments strikingly illustrate that *even the simplest* of MFG model is able to capture qualitative features that generally elude existing agent-based models, even if they include short-time anticipation.

We also believe MFG can apply in various other configurations. In particular, we show in Section V an MFG simulation of train-boarding at peak hours that qualitatively reproduces some nontrivial features associated with this situation (Movie S4) [66]. All this bolsters the claim that *optimization* and *anticipation* stand among the essential ingredients for the description of crowd dynamics at the *operational* level, and justifies to claim entry for MFG based approaches into the toolkit of practitioners of the field.

## ACKNOWLEDGMENTS

We acknowledge financial support for the internship of Theophile Bonnet by the "Investissements d'Avenir" of LabEx PALM (ANR-10-LABX-0039-PALM), as part of the PERCEFOULE project, and funding from the Hubert Curien Partnership France-Malaysia Hibiscus (PHC-Hibiscus) programme [203.PKOMP.6782005].

## Appendix A: Granular simulations

This first appendix provides details on the numerical method used to produce the granular matter simulation, displayed in the first column of the Fig. 1 of the main text (also see Movie S1). The numerical method is adapted from [67].

To simulate the displacement of an intruder in a two-dimensional granular medium, we resort to molecular dynamics. The diameter of the grains is $d = 0.37$ m and they all have the same mass. All interactions between two grains $i$ and $j$ in the simulation are modelled with a dissipative Hertz law of the form $F_{ij} = k\zeta^{3/2} - \lambda\frac{d\zeta}{dt}$ where $\zeta$ is the interpenetration of the grains, $k$ is the stiffness of the contact and $\lambda$ is a damping coefficient. The stiffness $k$ is related to the Young's modulus $E = 1$ GPa of the grains by $k = E\sqrt{d/2}$. The coefficient of viscous damping $\lambda$ simulates a restitution coefficient $e = 0.5$. One can notice that the grains are frictionless. The time step is small enough to ensure numerical convergence. The details of these calculations were reported in [67]. The diameter of the intruder is $D = 2d = 0.74$ m and its mechanical properties are identical to those of the grains. The tank containing the granular material is of length $L_x = 25d$ in the $x$-direction and $L_y = 200d$ in the $y$-direction.

To prepare the initial state, the intruder is initially fixed in the tank. The $y$ position of the intruder in the $y$-direction corresponds to the vertical distance from the bottom wall of the tank to the center of the intruder such that $y = 2.5D$ is the initial vertical position of the intruder. The $x$ position of the intruder in the $x$-direction

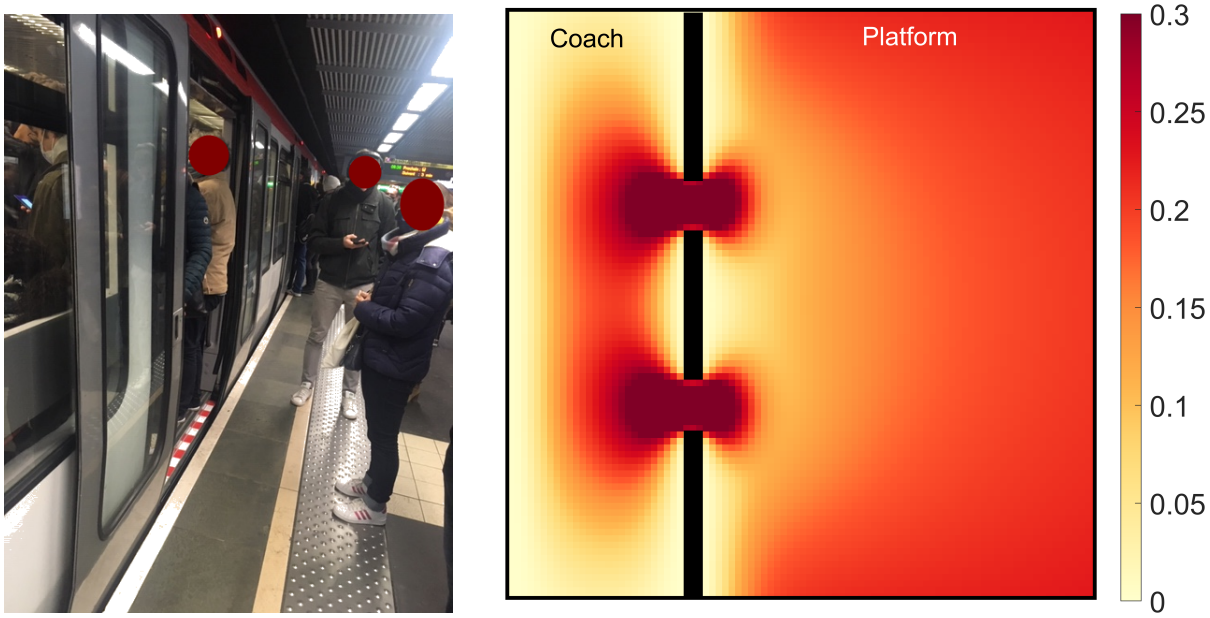


Figure 3: Boarding a crowded metro coach at rush hour. Left: Morning rush hour of November 18, 2021, on the platform of Metro A in Lyon, France. The doors are about to close and the gap between boarding passengers and those who preferred to wait for the next metro is clearly visible. Right: Snapshot from a MFG simulation at $t = 0.9T$. Players start uniformly distributed on the platform and would like to get on the coach before the doors close, at $t = T$. Just before that moment, the players closest to the doors choose to rush towards the coach and cram themselves in it despite the high density. Others prefer to stay on the platform (see Movie S4 for the whole process). Simulations have been performed in a box of dimensions 15x15 over a time $T = 10$, with an initial density on the platform $m_0 = 0.2$. Parameters are chosen to have healing length $\xi = 1.1$, and speed of sound $c_s = 0.45$, while $c_{\text{coach}} = 0$ and $c_{\text{platform}} = 6.21$.

corresponds to the equal distance from the left wall and right wall of the tank to the center of the intruder such that $x = L_x/2$ is the initial horizontal position of the intruder. Once the intruder is placed, we fill the remaining space by randomly drawing $x$ and $y$ positions for each grain. The number of grains to insert depends on the chosen objective density. We ensure that there is no spatial overlap between the grains. Once the initial configuration has been prepared, we move the intruder at constant velocity $v = 0.6$ m.s$^{-1}$ along the $y$ direction. The intruder runs a distance equivalent almost to $80D$ in the $y$-direction to avoid getting too close to the top wall of the tank. The displacement of the intruder in this granular material naturally leaves a wake behind it since there is no pressure scale that comes to fill it up [26, 68, 69]. In order to create a process that fills this wake, we introduce a small Gaussian noise in the displacement of the grains during the simulation. This noise acts as diffusion for the displacement which will then have the possibility of filling the wake.

The run of the intruder through the granular medium allows to get the positions of the grains over time. Considering these data after passing through the spatial transient regime (of the order of one $D$), we reach a stationary regime in average for the grain flow around the intruder. For each simulation, we can calculate the density field and the velocity field around the intruder. In order to smooth the results, they have been averaged over 10 runs of intruder displacement.

## Appendix B: Agent-based model for pedestrian dynamics based on an anticipated time to collision

The second appendix provides details on the numerical methods used to produce the agent based simulations, displayed in the second column of Fig. 1 of the main text (also see Movie S2).

### 1. Principle

The Social Force Model (SFM), initially propounded by Helbing and Molnar [7], arguably remains the continuous model that is most widely used commercially to simulate pedestrian dynamics. In this model, agents essentially obey Newtonian dynamics, with a sum of binary pseudo-forces (social forces) mimicking their attractive and repulsive interactions with neighbouring agents, which are mostly based on their relative positions.

However, it has been shown that substituting these positional variables with a time-to-collision (TTC) variable,

reflecting the time at which each agent expects the most imminent collision with other agents, better renders the spatial organisation of pedestrians in diverse empirical settings [9]. The agent-based model used in the main text to represent a crowd of agents displaying some degree of anticipation is based on the same approach, but incorporates a number of changes aimed at correcting some issues as identified in Karamouzas et al.'s seminal paper [9].

First, to enhance numerical stability, instead of solving a Newtonian equation with a TTC-based force, we opt for a numerical scheme in which the velocities selected at each time step result from the minimisation of a total energy (including the TTC contribution), following [12]. Nonetheless, contrary to [12], each agent minimises their own energy, rather than solving for the set of agents' velocities that minimises the global energy of the assembly; these individual choices better reflect the decisional process at play in a crowd of autonomous agents (and not robots), in line with the concept of utility used in Economics rather than the global energy used in Physics [70]. Besides, only the most imminent collision is taken into account to compute the TTC energy. Finally, to avoid grazing trajectories and smooth the agents' response [71], each agent is modelled as a disk whose radius is uncertain, i.e., estimated between $R$ and $(1+\epsilon)\,R$. In addition to avoiding discontinuities in the collision avoidance response, this uncertainty accounts for the existence of an immaterial private sphere around each agent, which others are reluctant to cross.

All in all, the total energy $E[\boldsymbol{v'_p}]$ minimised by each agent with respect to their velocity $\boldsymbol{v'_p}$ comprises the following contributions:

- a driving term $E^{\text{target}} = FF(\boldsymbol{r}+\tau_\phi \boldsymbol{v'_p})$ with a static floor field FF giving the shortest-path distance to a target or a set of targets, computed with the Dijkstra algorithm. Here, $\tau_\phi$ is a reaction time and $\boldsymbol{r}+\tau_\phi \boldsymbol{v'_p}$ is the position at which the agent expects to be after this reaction time, should they choose velocity $\boldsymbol{v'_p}$,

- a term constraining the agent's speed, $E^{\text{speed}} = \alpha v'_p(\boldsymbol{v'_p} - \boldsymbol{v_p}^{\text{pref}})^2$, where $v'_p = ||\boldsymbol{v'_p}||$. Note that $v'_p = 0$ is a minimum of this term, which means that not moving is a suitable option for static agents, as it should be,

- a term penalising sudden changes in velocity (direction), compared to the current velocity $\boldsymbol{v_p}^t$, $E^{\text{inertia}} = \beta \left|\boldsymbol{v'_p} - \boldsymbol{v_p}^t\right|^2 dt^{-2}$,

- an interpedestrian repulsion term, $E^{\text{core-repulsion}} = \eta\left(\frac{1}{d} - \frac{1}{d^*}\right)$, with $d$ the actual distance between pedestrians and $d^*$ a threshold distance beyond which this term is no longer zero. Here, $\epsilon$ takes into account the uncertainty that each pedestrian has when estimating the radii of their neighbours,

- the TTC energy $E_i^{\text{TTC}} = \max_j E^{TTC}(\tau_{ij})$, where $\tau_{ij}$ is the anticipated time to collision between agent $i$ and agent $j$ under the assumption that the current velocities are maintained and $E^{TTC}$ is the TTC energy expression given by [9] which we characterise with the parameter $\gamma$. This is actually the most important term in our model. Should it be turned off, particles would stop anticipating the upcoming intrusion.

The minimisation over $\boldsymbol{v_p}$ is performed with the Nelder-Mead algorithm for each agent and the updating scheme is made via:

$$\boldsymbol{v_p}^{t+1} = \text{argmin}_{\boldsymbol{v'_p}} \left(E[\boldsymbol{v'_p}]\right)$$

$$\boldsymbol{x}^{t+1} = \boldsymbol{x}^t + \boldsymbol{v_p}^{t+1} \cdot \Delta t$$

with a time step $\Delta t = 0.1\,s$ (lower values of $\Delta t$ were also used to test the convergence of the implemented framework with no significant changes).

### 2. Simulation layout

To simulate the crossing of a static crowd by an intruder, the model is specified as follows:

The floor-field energy $E^{\text{target}}$ is specific to each agent, with a target that matches their initial position. The interaction with the intruder (and other particles) will make them move away from this position, but they will strive to come back to it once it has passed. The speed term in the energy is computed with a preferential speed $v_p^{\text{pref}}$ coinciding with experimental measurements for the avoidance response.

Regarding the geometry, an intruder of diameter $D = 0.74\,\text{m}$ has to cross a region of 20 m length x 4 m width along its median part. The intruder moves uniformly and linearly along the y-axis at a prescribed speed $v = 0.5\,\text{m}\cdot\text{s}^{-1}$. Inside this zone, 200 particles (thus obtaining a global density of $2.5\,\text{ped/m}^2$) of diameter $d = D/2$ are randomly distributed.

The results presented in the main text correspond to moments when the intruder is at least 3 m from the boundaries (entrance and exit of the corridor). This was done in an attempt to minimise boundary effects in the measurements and achieve an approximately stationary state.

For the sake of completeness, we include here an exhaustive exploration of parameter space determined by the values of $\boldsymbol{\alpha}$, $\boldsymbol{\beta}$ and $\boldsymbol{\gamma}$. Indeed, figures 4, 5 and 6 show the density and velocity plots for the TTC model for four different choices of these parameters. For each figure, the rightmost columns shows the results for the values used in the Letter, whereas the other three columns show the variation of one of the three parameters, leaving the other two untouched. By observing these figure, we

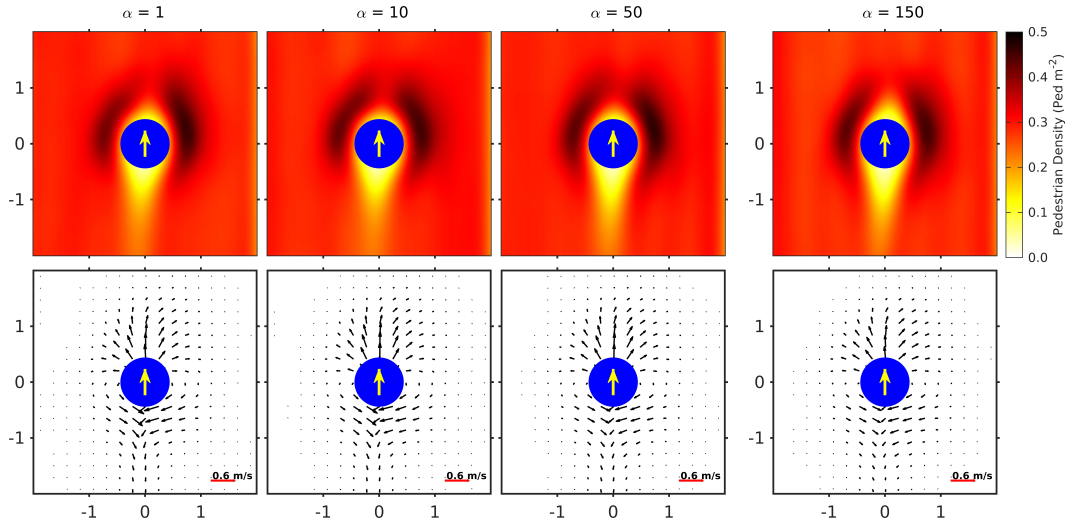


Figure 4: Variation of the agent speed term for the TTC model, while keeping the other parameters equal to those of the picture displayed in the letter.

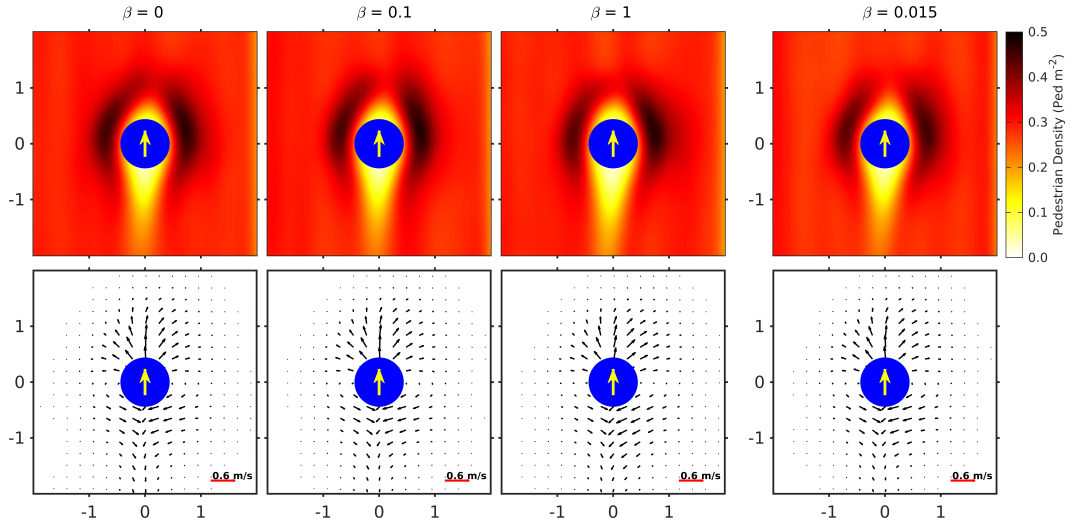


Figure 5: Variation of the inertial term for the TTC model, while keeping the other parameters equal to those of the picture displayed in the letter.

can conclude that the fundamental parameter of the TTC model is indeed the time to collision amplitude term $\gamma$, indeed the only one capable to produce significant variations of the solution. The other two parameters, while introducing some changes in the velocity plots, do not have a real impact on the main features we look for, such as the horizontal displacement and the lateral accumulation of the agents.

## Appendix C: Mean-Field Game simulations

This third and last section describes the numerical schemes used to produce Mean-Field Game simulations. Results of a time independent simulation are displayed on the third column of the Figure 1 of the main text, whereas time-dependent one are used to simulate metroboarding. Naturally we expect both schemes to be consistent in the appropriate regime as evidenced by Movie S3.

### 1. Time Independent MFG

The equation we want to solve numerically is the first of system (5), which we recall,

$$\frac{\mu\sigma^4}{2}\Delta\Phi - \mu\sigma^2 v\partial_y\Phi + (gm + U_0(\vec{x}))\Phi = -\lambda\Phi, \quad \text{(C1)}$$

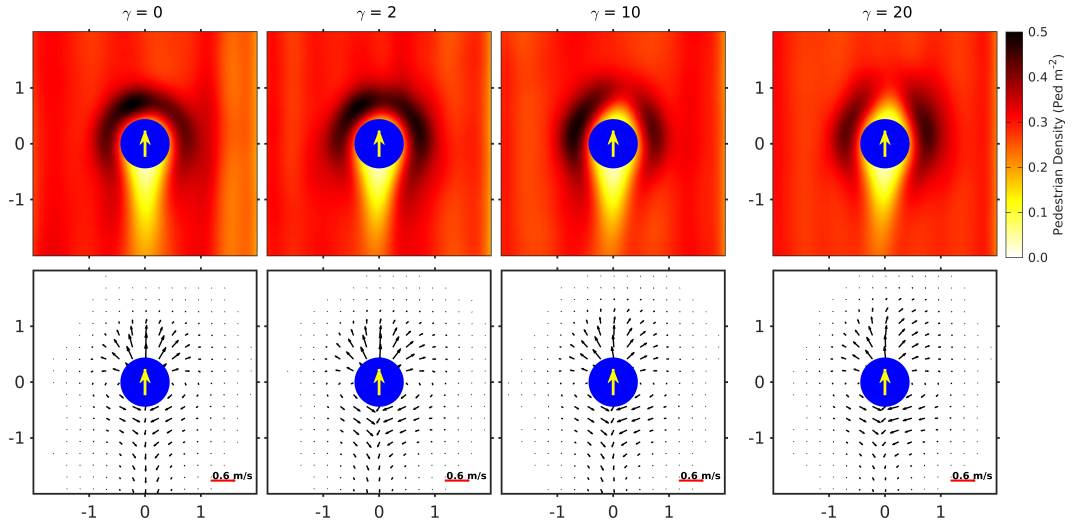


Figure 6: Variation of the time to collision amplitude term for the TTC model, while keeping the other parameters equal to those of the picture displayed in the letter.

where $\lambda = -gm_0$. We want to solve the equation in a box of side $L$. We define the matrices $\Phi \in \mathbb{R}^{N,N}$ and $\Gamma \in \mathbb{R}^{N,N}$ that we have to evaluate on a grid of $N \times N$ points corresponding to the $(x, y)$ coordinates in Euclidean space. In order to do this, we first write the discrete form of equation (C1)

$$\frac{\mu\sigma^4}{2dx^2}(\Phi_{i-1,j} + \Phi_{i+1,j} + \Phi_{i,j-1} + \Phi_{i,j+1} - 4\Phi_{i,j}) - \mu\sigma^2 v\frac{\Phi_{i,j+1} - \Phi_{i,j-1}}{2dy} + (gm_{i,j} + V_0V_{i,j})\Phi_{i,j} = -\lambda\Phi_{i,j} \quad ,$$

where we choose $dx = dy$. Then we make the term $\Phi_{i,j}$ explicit and obtain

$$\Phi^{k+1}_{i,j} = \frac{\frac{\mu\sigma^4}{2}(\Phi^k_{i-1,j} + \Phi^k_{i+1,j} + \Phi^k_{i,j-1} + \Phi^k_{i,j+1}) - \frac{\mu\sigma^2}{2}vdx(\Phi^k_{i,j+1} - \Phi^k_{i,j-1})}{2\mu\sigma^4 - \lambda dx^2 - (gm_{i,j} + V_0V_{i,j})dx^2}.$$

This is the recursive rule that updates $\Phi_{i,j}$ until convergence. For a generic geometry, the same rule with opposite sign of $v$ would be used to find $\Gamma_{i,j}$. Here we take advantage of the symmetry $\Phi \to \Gamma$ and $(x, y) \to (x, -y)$ to directly obtain $\Gamma$. Starting from an initial guess for $\Phi$, $\Gamma$ and $m$, we fix boundary conditions given by the asymptotic solution $\Phi_{\text{er}}(\mathbf{x}) = \sqrt{m_0}$, then iterate the formula to find $\Phi$ and $\Gamma$, and, recalling that $\Phi\Gamma = m$, also the density. We repeat this operation until convergence of $m$.

### 2. Time-Dependent MFG

Time-dependent simulations were realized using a C++ algorithm, using the Schrödinger representation of MFG equations to lean on the symmetry between the fields $\Phi$ and $\Gamma$ and on well-proven numerical methods such as Crank-Nicolson [72, 73] implicit scheme which provide added stability compared to Euler method. Details of the discretisation, along with a stability analysis of the method, can be found in Appendix A of [74].

The forward-backward conditions, along with the nonlinear coupling between the fields, make direct resolution of MFG equations difficult. A simple, though not perfectly controlled, way to bypass those difficulties is to solve the system iteratively:

- Assume a plausible form of the density $m^0$ (e.g. a constant equal to the average density).
- Compute, using the Crank-Nicolson scheme, a first solution $\Phi^1$ of the backward equation

$$-\mu\sigma^2\partial_t\Phi^1 = \frac{\mu\sigma^4}{2}\Delta\Phi^1 + (U_0 + gm^0)\Phi^1 \ , \qquad \text{(C2)}$$

with given terminal condition $\Phi(T, \mathbf{x})$.

- Compute $\Gamma^1$, solution of the forward equation

$$\mu\sigma^2\partial_t\Gamma^1 = \frac{\mu\sigma^4}{2}\Delta\Gamma^1 + (U_0 + gm^0)\Gamma^1 \,, \qquad \text{(C3)}$$

  with initial condition $m^0(\mathbf{x}, t=0)/\Phi^1(\mathbf{x}, t=0)$.

- Update the initial guess $m^0 \to m^1 = \Phi^1\Gamma^1$ and repeat the process until $m^n$ is sufficiently close to $m^{n-1}$. In practice we check for

$$\max_{\mathbf{x},t} |m^n(\mathbf{x}, t) - m^{n-1}(\mathbf{x}, t)| < \epsilon \,. \qquad \text{(C4)}$$

  (We will use $\epsilon = 0.001$, which we expect to be sufficiently small given the average density $m_0 = 2.5$, in accordance with the experiments of [15].)

This method is easy to implement and fairly efficient but in some particular circumstances convergence may not occur. This may be alleviated by updating the guess differently

$$m^{i+1} = \alpha m^i + (1-\alpha)\Phi^{i+1}\Gamma^{i+1} \,, \qquad \text{(C5)}$$

$\alpha$ being a suitable number between 0 and 1.

The complete dynamics of the time-dependent MFG can be found in Movie S3. All MFG simulations are realized with parameters $\xi = 0.15$ and $c_s = 0.11$. In the time-dependent simulations, the intruder (of diameter $D = 0.74$ and velocity $v = 0.5$) crosses vertically a static crowd in a box of dimensions 6x11 (with periodic boundary conditions) over a time $T = 27.5$ long enough to reach the ergodic state. The time independent simulation is performed in a box of side $L = 40$, large enough so that differences between the boundary conditions of the two approaches are negligible. As proof of the soundness of both approaches, the comparison between the time-dependent simulation at $t \simeq T/2$ and the time independent results shows excellent agreement.


[1] D. Helbing, A. Johansson, and H. Z. Al-Abideen, "Dynamics of crowd disasters: An empirical study," *Physical review E*, vol. 75, no. 4, p. 046109, 2007.

[2] S. P. Hoogendoorn and P. H. Bovy, "Pedestrian route-choice and activity scheduling theory and models," *Transportation Research Part B: Methodological*, vol. 38, no. 2, pp. 169–190, 2004.

[3] Y.-Q. Jiang, W. Zhang, and S.-G. Zhou, "Comparison study of the reactive and predictive dynamic models for pedestrian flow," *Physica A: Statistical Mechanics and its Applications*, vol. 441, pp. 51–61, 2016.

[4] B. L. Mesmer and C. L. Bloebaum, "Incorporation of decision, game, and bayesian game theory in an emergency evacuation exit decision model," *Fire Safety Journal*, vol. 67, pp. 121–134, 2014.

[5] A. Best, S. Narang, S. Curtis, and D. Manocha, "Densesense: Interactive crowd simulation using density-dependent filters," in *Proceedings of the ACM SIGGRAPH/Eurographics Symposium on Computer Animation*, pp. 97–102, 2014.

[6] A. van Goethem, N. Jaklin, A. C. IV, and R. Geraerts, "On streams and incentives - a synthesis of individual and collective crowd motion," in *Proceedings of the 28th International Conference on Computer Animation and Social Agents (CASA)*, 2015.

[7] D. Helbing and P. Molnar, "Social force model for pedestrian dynamics," *Physical review E*, vol. 51, no. 5, p. 4282, 1995.

[8] F. Zanlungo, T. Ikeda, and T. Kanda, "Social force model with explicit collision prediction," *EPL (Europhysics Letters)*, vol. 93, no. 6, p. 68005, 2011.

[9] I. Karamouzas, B. Skinner, and S. J. Guy, "Universal power law governing pedestrian interactions," *Physical review letters*, vol. 113, no. 23, p. 238701, 2014.

[10] J. van den Berg, M. C. Lin, and D. Manocha, "Reciprocal velocity obstacles for real-time multi-agent navigation," in *Proceedings of the 2008 IEEE International Conference on Robotics and Automation*, pp. 1928–1935, 2008.

[11] S. Paris, J. Pettré, and S. Donikian, "Pedestrian reactive navigation for crowd simulation: a predictive approach," in *Computer Graphics Forum*, vol. 26, pp. 665–674, Wiley Online Library, 2007.

[12] I. Karamouzas, N. Sohre, R. Narain, and S. J. Guy, "Implicit crowds: Optimization integrator for robust crowd simulation," *ACM Transactions on Graphics (TOG)*, vol. 36, no. 4, pp. 1–13, 2017.

[13] M. Moussaïd, D. Helbing, and G. Theraulaz, "How simple rules determine pedestrian behavior and crowd disasters," *Proceedings of the National Academy of Sciences*, vol. 108, no. 17, pp. 6884–6888, 2011.

[14] J. Bruneau and J. Pettré, "EACS: Effective Avoidance Combination Strategy," *Computer Graphics Forum (CGF)*, vol. 36, no. 8, pp. 108–122, 2017.

[15] A. Nicolas, M. Kuperman, S. Ibañez, S. Bouzat, and C. Appert-Rolland, "Mechanical response of dense pedestrian crowds to the crossing of intruders," *Scientific reports*, vol. 9, no. 1, p. 105, 2019.

[16] B. Kleinmeier, G. Köster, and J. Drury, "Agent-based simulation of collective cooperation: from experiment to model," *Journal of the Royal Society Interface*, vol. 17, no. 171, p. 20200396, 2020.

[17] J.-M. Lasry and P.-L. Lions, "Jeux à champ moyen. I – le cas stationnaire," *Comptes Rendus Mathematique*, vol. 343, pp. 619–625, Nov. 2006.

[18] J.-M. Lasry and P.-L. Lions, "Jeux à champ moyen. II – horizon fini et contrôle optimal," *Comptes Rendus Mathematique*, vol. 343, pp. 679–684, Nov. 2006.

[19] M. Huang, R. P. Malhamé, P. E. Caines, and others, "Large population stochastic dynamic games: closed-loop McKean-vlasov systems and the nash certainty equivalence principle," *Communications in Information & Systems*, vol. 6, no. 3, pp. 221–252, 2006.

[20] O. Guéant, "Mean field games equations with quadratic hamiltonian: a specific approach," *Math. Models Methods Appl. Sci.*, vol. 22, p. 1250022, 2012.

[21] D. Ullmo, I. Swiecicki, and T. Gobron, "Quadratic mean

field games," *Physics Reports*, vol. 799, pp. 1–35, 2019.
[22] C. Appert-Rolland, J. Pettré, A.-H. Olivier, W. Warren, A. Duigou-Majumdar, E. Pinsard, and A. Nicolas, "Experimental study of collective pedestrian dynamics," *Collective Dynamics*, vol. 5, pp. 1–8, 2020.
[23] https://twitter.com/AmichaiStein1/status/1140374111258140673, 2019.
[24] A. Seguin, Y. Bertho, P. Gondret, and J. Crassous, "Dense granular flow around a penetrating object: Experiment and hydrodynamic model," *Physical review letters*, vol. 107, no. 4, p. 048001, 2011.
[25] A. Seguin, Y. Bertho, F. Martinez, J. Crassous, and P. Gondret, "Experimental velocity fields and forces for a cylinder penetrating into a granular medium," *Physical Review E*, vol. 87, no. 1, p. 012201, 2013.
[26] A. Seguin, A. Lefebvre-Lepot, S. Faure, and P. Gondret, "Clustering and flow around a sphere moving into a grain cloud," *The European Physical Journal E*, vol. 39, no. 6, pp. 1–7, 2016.
[27] M. D. Raj and V. Kumaran, "Moving efficiently through a crowd: A nature-inspired traffic rule," *Physical Review E*, vol. 104, no. 5, p. 054609, 2021.
[28] S. Heliövaara, H. Ehtamo, D. Helbing, and T. Korhonen, "Patient and impatient pedestrians in a spatial game for egress congestion," *Physical Review E*, vol. 87, no. 1, p. 012802, 2013.
[29] S. Bouzat and M. Kuperman, "Game theory in models of pedestrian room evacuation," *Physical Review E*, vol. 89, no. 3, p. 032806, 2014.
[30] A. Lachapelle, J. Salomon, and G. Turinici, "A monotonic algorithm for a mean field games model in economics," *Les Cahiers de la Chaire (Finance & Développement Durable)*, vol. 16, 2009.
[31] P. Cardaliaguet and C.-A. Lehalle, "Mean field game of controls and an application to trade crowding," *Math Finan Econ*, vol. 12, pp. 335–363, 2017.
[32] R. Carmona, F. Delarue, and A. Lachapelle, "Control of McKean–vlasov dynamics versus mean field games," *Mathematics and Financial Economics*, vol. 7, no. 2, pp. 131–166, 2013.
[33] Y. Achdou, P.-N. Giraud, J.-M. Lasry, and P.-L. Lions, "A long-term mathematical model for mining industries," *Appl. Math. Optim.*, vol. 74, p. 579–618, 2016.
[34] O. Guéant, J.-M. Lasry, and P.-L. Lions, "Mean field games and applications," in *Paris-Princeton Lectures on Mathematical Finance 2010*, Springer, 2011.
[35] Y. Achdou, F. J. Buera, J.-M. Lasry, P.-L. Lions, and B. Moll, "Partial differential equation models in macroeconomics," *Phil. Trans. R. Soc.*, vol. A 2014, pp. 372,, 2014.
[36] L. Laguzet and G. Turinici, "Individual vaccination as nash equilibrium in a sir model with application to the 2009-2010 influenza a (h1n1) epidemic in france," *Bull Math Biol*, vol. 77, pp. 1955–1984, 2015.
[37] R. Djidjou-Demasse, Y. Michalakis, M. Choisy, M. T. Sofonea, and S. Alizon, "Optimal covid-19 epidemic control until vaccine deployment," *medRxiv*, 2020.
[38] R. Elie, E. Hubert, and G. Turinici, "Contact rate epidemic control of covid-19: an equilibrium view," *Mathematical Modelling of Natural Phenomena*, vol. 15, p. 35, 2020.
[39] A. Lachapelle and M.-T. Wolfram, "On a mean field game approach modeling congestion and aversion in pedestrian crowds," *Transportation Research Part B: Methodological*, vol. 45, pp. 1572–1589, Dec. 2011.
[40] Y. Achdou, M. Bardi, and M. Cirant, "Mean field games models of segregation," *Mathematical Models and Methods in Applied Sciences*, vol. 27, no. 01, pp. 75–113, 2017.
[41] A. C. Kizilkale and R. P. Malhamé, "Load shaping via grid wide coordination of heating-cooling electric loads: A mean field games based approach." submitted paper to IEEE Transactions on Automatic Control., 2016.
[42] A. C. Kizilkale, R. Salhab, and R. P. Malhamé, "An integral control formulation of mean field game based large scale coordination of loads in smart grids," *Automatica*, vol. 100, pp. 312–322, 2019.
[43] F. Mériaux, V. S. Varma, and S. Lasaulce, "Mean field energy games in wireless networks," *CoRR*, vol. abs/1301.6793, 2013.
[44] O. Guéant, "Existence and uniqueness result for mean field games with congestion effect on graphs," *Applied Mathematics & Optimization*, vol. 72, p. 291–303, 2015.
[45] A. Lachapelle and M.-T. Wolfram, "On a mean field game approach modeling congestion and aversion in pedestrian crowds," *Transportation research part B: methodological*, vol. 45, no. 10, pp. 1572–1589, 2011.
[46] Y.-Q. Jiang, R.-Y. Guo, F.-B. Tian, and S.-G. Zhou, "Macroscopic modeling of pedestrian flow based on a second-order predictive dynamic model," *Applied Mathematical Modelling*, vol. 40, no. 23-24, pp. 9806–9820, 2016.
[47] B. Djehiche, A. Tcheukam, and H. Tembine, "A mean-field game of evacuation in multilevel building," *IEEE Transactions on Automatic Control*, vol. 62, no. 10, pp. 5154–5169, 2017.
[48] N. Nasser, A. El Ouadrhiri, M. El Kamili, A. Ali, and M. Anan, "Crowd management services in Hajj: a mean-field game theory approach," *2019 IEEE Wireless Communications and Networking Conference (WCNC)*, pp. 1–7, 2019.
[49] D. M. Kreps, "Nash equilibrium," in *Game Theory*, pp. 167–177, Springer, 1989.
[50] R. Bellman, *Dynamic Programming*. Rand Corporation research study, Princeton University Press, 1957.
[51] T. Bonnemain, T. Gobron, and D. Ullmo, "Universal behavior in non-stationary mean field games," *Physics Letters A*, vol. 384, no. 25, p. 126608, 2020.
[52] D. J. Kaup, "Perturbation theory for solitons in optical fibers," *Physical Review A*, vol. 42, pp. 5689–5694, Nov 1990.
[53] F. Copie, S. Randoux, and P. Suret "The Physics of the one-dimensional nonlinear Schrödinger equation in fiber optics: rogue waves, modulation instability and self-focusing phenomena," *Reviews in Physics*, vol. 5, pp. 100037, 2020.
[54] L. Pitaevskii and S. Stringari, *Bose-Einstein condensation and superfluidity*, vol. 164. Oxford University Press, 2016.
[55] R. Koch, J.S. Caux, and A. Bastianello, "Generalized hydrodynamics of the attractive non-linear Schrödinger equation," *Journal of Physics A: Mathematical and Theoretical*, vol. 55, no. 13, pp. 134001, 2022.
[56] C. Kharif, E. Pelinovsky, and A. Slunyaev, *Rogue Waves in the Ocean*. Advances in Geophysical and Environmental Mechanics and Mathematics, Springer Berlin Heidelberg, 2008.
[57] G. A. El, E. G. Khamis, and A. Tovbis, "Dam break problem for the focusing nonlinear Schrödinger equation

and the generation of rogue waves," *Nonlinearity*, vol. 29, no. 9, pp. 2798, 2016.

[58] E. Hopf, "The partial differential equation $u_t + uu_x = \mu xx$," *Communications on Pure and Applied Mathematics*, vol. 3, no. 3, pp. 201–230, 1950.

[59] T. Bonnemain, T. Gobron, and D. Ullmo, "Schrödinger approach to Mean Field Games with negative coordination," *SciPost Phys.*, vol. 9, p. 59, 2020.

[60] P. Cardaliaguet, J. Lasry, P. Lions, and A. Porretta, "Long time average of mean field games with a nonlocal coupling," *SIAM Journal on Control and Optimization*, vol. 51, no. 5, pp. 3558–3591, 2013.

[61] T. Bonnemain, T. Gobron, and D. Ullmo, "Lax connection and conserved quantities of quadratic mean field games," *Journal of Mathematical Physics*, vol. 62, no. 8, p. 083302, 2021.

[62] S. Frederick, G. Loewenstein, and T. O'donoghue, "Time discounting and time preference: A critical review," *Journal of economic literature*, vol. 40, no. 2, pp. 351–401, 2002.

[63] D. A. Gomes, L. Nurbekyan, and E. Pimentel, "Economic models and mean-field games theory," *Publicaoes Matematicas, IMPA, Rio, Brazil*, 2015.

[64] C. Dogbé, "Modeling crowd dynamics by the mean-field limit approach," *Mathematical and Computer Modelling*, vol. 52, pp. 1506–1520, Nov. 2010.

[65] Y. Achdou and A. Porretta, "Mean field games with congestion," *Annales de l'Institut Henri Poincaré C, Analyse non linéaire*, vol. 35, no. 2, pp. 443 – 480, 2018.

[66] See the associated movies deposited on the Open Science Foundation website under https://osf.io/hytbd/?view_only=a5c81b95c08e4604b8d3845c16e22b57, 2022.

[67] A. Seguin, Y. Bertho, P. Gondret, J. Crassous, *EPL (Europhysics Letters)* **88**, 44002 (2009).

[68] R. Candelier, O. Dauchot, *Physical Review E* **81**, 011304 (2010).

[69] E. Kolb, P. Cixous, N. Gaudouen, T. Darnige, *Physical Review E* **87**, 032207 (2013).

[70] S. Grauwin, E. Bertin, R. Lemoy, P. Jensen, *Proceedings of the National Academy of Sciences* **106**, 20622 (2009).

[71] Z. Forootaninia, I. Karamouzas, R. Narain, *Robotics: Science and Systems* (2017), vol. 7.

[72] D. Harder, The crank-nicolson method and insulated boundaries (2012).

[73] Y.Y. Choy, W.N. Tan, K.G. Tay, and C.T. Ong, "Crank-nicolson implicit method for the nonlinear schrodinger equation with variable coefficient", *AIP Conference Proceedings*, vol. 1605, p. 76-82, 2014.

[74] T. Bonnemain "Quadratic mean field games with negative coordination." Diss. Université Cergy Pontoise, 2020.

SciPost Phys. 16, 104 (2024)

# Discounted Mean-Field Game model of a dense static crowd with variable information crossed by an intruder

Matteo Butano[1,2⋆], Cécile Appert-Rolland[2] and Denis Ullmo[1]

**1** Université Paris-Saclay, CNRS, LPTMS, 91405, Orsay, France
**2** Université Paris-Saclay, CNRS, IJCLab, 91405, Orsay, France

⋆ matteo.butano@universite-paris-saclay.fr

## Abstract

**It was demonstrated in [1] that the anticipation pattern displayed by a dense crowd crossed by an intruder can be successfully described by a minimal Mean-Field Games model. However, experiments show that changes in the pedestrian knowledge significantly modify the dynamics of the crowd. Here, we show that the addition of a single parameter, the discount factor $\gamma$, which gives a lower weight to events distant in time, is sufficient to observe the whole variety of behaviors observed in the experiments. We present a comparison between the discounted MFG and the experimental data, also providing new analytic results and insight about how the introduction of $\gamma$ modifies the model.**



Received 20-02-2023
Accepted 25-03-2024
Published 12-04-2024
doi:10.21468/SciPostPhys.16.4.104

## Contents

## 1 Introduction

As discussed by Hoogendorn et al. [2], pedestrian motion is a multi-scale endeavour that needs to be described at different levels, and one typically distinguishes the strategic level (what are the goals of the travel and the general timing), the tactical level (which route to take) and the operational level (how to move on that route). If the strategic and tactical levels naturally assume some form of long term optimisation, it is on the other hand quite generally expected that the operational level, especially for dense crowds, could be described by dynamical models involving physical and social forces [3], and possibly a short term (up to the next collision) anticipation [4–6]. However, the comparison of experimental data from a control experiment involving a static dense crowd [7] with various simulation models showed that [1], in such cases, it appears necessary to include long term anticipation in order to reproduce the observed experimental features. This could be achieved with a very simple Mean-Field Game model.

Mean-Field Games, introduced by Lasry and Lions [8, 9] as well as Huang et al. [10] is a mathematical formalism in which both anticipation and competitive optimization between the agents, here pedestrians, are accounted for at the mean field level. The fact that it may provide a good description of human behaviour is a priori non trivial for at least two reasons. The first one is that the agents clearly cannot compute the predictions of the Mean-Field Games model, the second is that they usually do not have the perfect information assumed in the model.

The answer to this first concern is, as in many game theoretical context, that we expect the behaviour of the agents to be learnt rather than computed. In the same way that we do not need to use the laws of dynamics to know where a ball thrown in the air will land, there are in daily life many circumstances which are familiar enough that we can, by instinct, predict the behavior of the crowd and act accordingly. It is clearly in these circumstances that we can expect a Mean-Field-Game description to apply, and this was the case in the experimental context of [7]. The second of these concerns, which will be the main focus of this paper, was actually addressed experimentally in [7]. The experimental setup studied there consisted in the crossing of a dense static crowd by a cylindrical intruder. However, the experiments have been performed in three configurations: with pedestrian facing the obstacle, being randomly oriented, or giving their back to it. Moreover, in the latter case pedestrians were asked not to anticipate, while no such instruction was given in the first two cases. Clearly, if, in this simple context, we can consider that in the first configuration, participants have perfect information about the incoming cylinder, this is not the case for the other two, and indeed, as seen on Fig. 1, the observed density maps, obtained by an average over repeated realizations of the experiment, clearly differ significantly in the three cases.

In [1], we focused only on the case where pedestrians were facing the obstacle (for an average density of $2.5 ped/m^2$, slightly lower than the one shown in Fig. 1(a), but displaying the same features). Observing Figure 1(a), we see that in the frontal configuration, individuals move in advance, temporarily accepting a higher local density in order to get rid of the obstacle sooner, showing evidence of a trade-off dynamics. The crowd's density increases on the sides and depletes in front of and behind the cylinder, with pedestrians moving outward

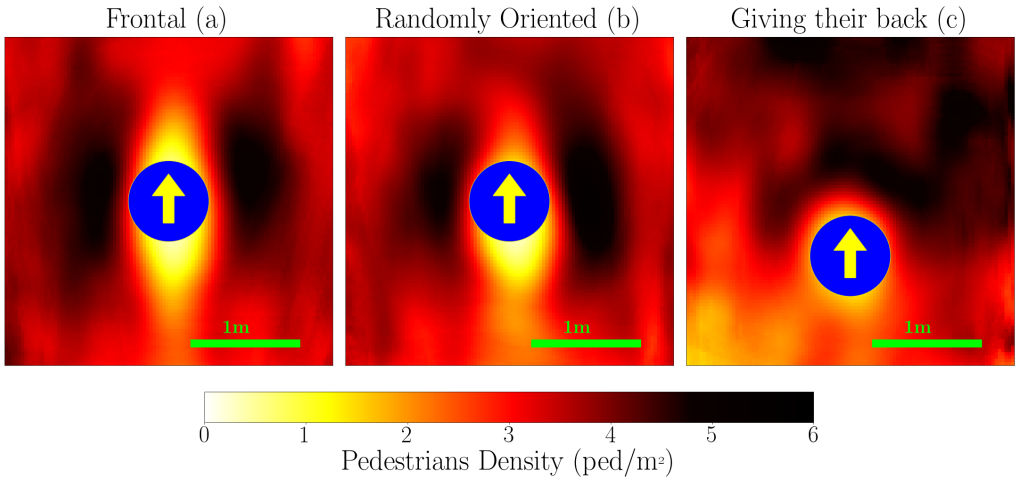


Figure 1: Experimental results of the passage of a cylindrical intruder (blue disc) through a static dense crowd for an average density of $\sim 3.5 ped/m^2$ for three different configurations. In (a) pedestrians were all facing the obstacle, in (b) they were randomly oriented and in (c) participants were asked to give their back to it and not to anticipate. Data from [7].

to avoid its arrival and inward to regain a less congested position, always perpendicularly to the obstacle's motion. This clearly is an anticipatory dynamics. Indeed even pedestrians far from the cylinder know that it will arrive and, depending on its speed, they will start moving accordingly. However, when individuals are placed randomly, as in the second panel of Figure 1, we notice a shorter corridor of anticipation in front of the obstacles, but with similar accumulation patterns on its sides. When pedestrians in the experiment were asked not to anticipate and to give their back to the incoming intruder, effectively looking away from it, as the third panels of Figure 1 shows, we observe that the accumulation of the individuals moves from the sides to the front of the obstacle, similarly to what happens in analog configurations with granular matter [1].

The main goal of this paper is to demonstrate that at least in the experimental setup corresponding to Fig.1, this lack of information can be taken into account simply by introducing a *discount factor*, i.e. a term discounting the cost of actions in a future further than a certain cutoff, to the model already used in [1] to simulate the frontal case. Such discount factors are, for example, usually introduced in optimization problem spanning a long time period (typically in economic context) to express the unwillingness of agents to wait too long for a reward. Here however we use it as a way to simulate the shortsightedness of pedestrians. We shall in section 2 introduce the corresponding Mean-Field-Game model and give some discussion about its generic behavior. Then, section 4 will feature the comparison with the three experimental cases discussed above. We will first come back on the case where pedestrians were facing the obstacle, providing more details about the results presented in [1]. Then, the other experimental setups will be considered, and we will show how the introduction of the discount factor helps in modeling these configurations.

## 2 The mean-field games model

Mean-Field Games (MFG) constitutes a relatively new field of research. Its foundations are in the works of J.-M. Lasry and P.-L. Lions [8, 9], and of M. Huang, R. P. Malhamé and P. E. Caines [10]. During the years, many works have been focused on the mathematical properties

of MFG [11–15]. Although there are applications of MFG to pedestrian dynamics [16], to the best of our knowledge comparisons of crowds simulated with MFG to experimental data [1] are rare. A general and mathematically rigorous discussion of the foundations of MFG being found in the book [14], and a physicist-friendly version being exposed in [17], here we will limit ourselves to essentials.

### 2.1 The discounted equations

In the specific settings of our MFG model, each agent's *state variable* $\vec{X}(t) \in \mathbb{R}^2$, representing their position, evolves following the *Langevin equation*

$$\dot{\vec{X}} = \vec{a}(t) + \sigma\vec{\xi}(t), \tag{1}$$

where $\vec{\xi}(t)$ is a two dimensional Gaussian white noise of variance one, and $\vec{a}$ is the drift velocity, the *control parameter* that represents the strategy players choose by minimizing the discounted cost functional defined, in this case, as

$$c[\vec{a}](\vec{x},t) = \mathbb{E}\left\{\int_t^T \mathcal{L}(\vec{x},\tau)[m]e^{\gamma(t-\tau)}d\tau + e^{\gamma(t-T)}c_T(\vec{x}_T)\right\}, \tag{2}$$

where $c_T$ is a *terminal cost*, that could be used to represent a target for pedestrians, as for instance an exit, but which here is simply taken as $c_T = 0$. In this equation, $\gamma$ is the discount factor, and its inverse $1/\gamma$ defines an anticipatory time scale determining how far into the future agents will look while optimizing. Finally

$$\mathcal{L}(\vec{x},\tau)[m] = \frac{\mu}{2}(\vec{a}(\tau))^2 - V[m](\vec{x},\tau), \tag{3}$$

can be seen as the term describing the agents' preferences. In fact, the squared velocity tells that going too fast is detrimental, and that the best would be to stand still, but the presence of the external world, represented by the potential term

$$V[m](\vec{x},t) = gm(\vec{x},t) + U_0(\vec{x},t), \tag{4}$$

describing the interaction with the others and with the environment, cause agents to actually move. The main assumptions of MFG are that all agents are equal and the interaction with others is of mean-field type, determined only through the average density

$$m(\vec{x},t) = \mathbb{E}\left[\frac{1}{N}\sum_{i=1}^{N}\delta(\vec{x}-\vec{X}_i(t))\right].$$

For $g < 0$, the first term in the right hand side of Eqs. (4), $gm(\vec{x},t)$, expresses the agents' desire to stay away from densely packed areas. On the other hand, the term $U_0(\vec{x},t)$ describes the interaction with the environment, and in the case of the crossing cylinder reads

$$U_0(\vec{x},t) = \begin{cases} +\infty, & \|\vec{x}-\vec{s}t\| < R, \\ 0, & \text{otherwise}, \end{cases} \tag{5}$$

where $\vec{s}$ is the velocity and $R$ the radius of the cylinder. A quantity of interest of the MFG is then the *value function*

$$u(\vec{x},t) = \inf_{\vec{a}} c[\vec{a}](\vec{x},t), \tag{6}$$

that, as shown in appendix A, can be obtained solving the *Hamilton-Jacobi-Bellman* equation

$$\begin{cases} \partial_t u = -\frac{\sigma^2}{2}\Delta u + \frac{1}{2\mu}(\vec{\nabla}u)^2 + \gamma u + V[m], \\ u(\vec{x}, t = T) = c_T(\vec{x}). \end{cases} \tag{HJB}$$

This is a backward equation, that is solved starting from the terminal condition expressed by the terminal cost $c_T(\vec{x})$. The optimal choice of the control parameter is $\vec{a}^* = -\vec{\nabla}u/\mu$. Given the stochastic evolution of each player's state variable, the corresponding average density evolves following the Kolmogorov-Fokker-Plank equation

$$\begin{cases} \partial_t m = \frac{\sigma^2}{2}\Delta m + \frac{1}{\mu}\vec{\nabla}\cdot(m\vec{\nabla}u), \\ m(\vec{x}, t = 0) = m_0(\vec{x}), \end{cases} \tag{KFP}$$

a forward equation solved starting from an initial density profile.

As discussed extensively in [1, 17], in the $\gamma = 0$ limit the sytem of equations (HJB)-(KFP) can be cast in a form analog to the non-linear Schrödinger equation through the combination of a Cole-Hopf transformation and of an hermitization of the KFP equation. We show in appendix B how this formulation evolves for a general $\gamma$.

## 2.2 The ergodic state

### 2.2.1 Without discount factor

When $\gamma = 0$, i.e. when the anticipation time $1/\gamma$ is not bounded, we know from [18], that under certain hypothesis, among which a large optimisation time $T$ and the time independence of the potential $V$, and for times far from the beginning and the end, an ergodic or stationary state exists. Such state is characterised by the fact that its observable quantities, i.e. the optimal velocity field and the density field, do not depend on time anymore. In particular, for the velocity this means that

$$\partial_t \vec{a}^*_e(\vec{x}, t) = -\frac{1}{\mu}\partial_t \vec{\nabla} u^e(\vec{x}, t) = 0 \qquad \Longrightarrow \qquad u^e(\vec{x}, t) = u^e(\vec{x}) + u^e(t), \tag{7}$$

where the superscript $e$ refers to the ergodic state. Moreover, again from [18] we also know that for $\gamma = 0$, $\vec{u}(t)_e = -\lambda t$, where $\lambda$ is a parameter to be estimated. In the settings of our experiment, in the frontal case, so that we can use $\gamma = 0$, we can determine the value of $\lambda$ by looking at what happens far enough from the cylinder for the density to be unaffected by its presence. In fact, away from the obstacle we expect $m_e(\vec{x}, t) \simeq m_0$, $\forall t \in [0, T]$ and the optimal strategy is just to stay at rest, meaning $\vec{a}^* = 0$. Therefore, using definition (2) with $\gamma = 0$ we have

$$u(\vec{x}, t) = -\int_t^T (g m_0) d\tau = \underbrace{-g m_0 T}_{u^e(\vec{x})} + \underbrace{g m_0}_{-\lambda} t, \tag{8}$$

and thus $\lambda = -g m_0$.

### 2.2.2 With discount factor

Here we make the rather natural hypothesis that, for large $T$, such a stationary state exists also when $\gamma \neq 0$, i.e. for a finite anticipation time $1/\gamma$. We therefore assume that for intermediate times, there exists a state of the discounted system whose observables are independent on

time. If that is the case, (7) should still hold, and we can as before determine the time dependent part of $u_e$ by considering what happens far from the cylinder where the density remains homogeneous and the optimal strategy is simply to stand still. In this case (2) becomes

$$u(\vec{x},t) = -\int_t^T (gm_0)e^{-\gamma(\tau-t)}d\tau = \frac{gm_0}{\gamma}\left(e^{-\gamma(T-t)}-1\right). \tag{9}$$

We observe that if we fix $T$ and let $\gamma \to 0$, the right hand side of Eq. (9) becomes $-gm_0T+gm_0t$, recovering Eq. (8) and the $\gamma = 0$ case. On the other hand, if we fix $\gamma$ and let $T \to \infty$, we have that $u^e(t) \equiv 0$, and since $u^e(t)$ does not depend on the position, this must be true everywhere, meaning that when $\gamma \neq 0$

$$u^e(\vec{x},t) = u^e(\vec{x}), \tag{10}$$

and we can write both (HJB) and (KFP) in their stationary form as

$$0 = \frac{\sigma^2}{2}\Delta u^e - \frac{1}{2\mu}(\vec{\nabla}u^e)^2 - \gamma u^e(x) - V[m^e], \tag{11}$$

$$0 = \frac{\sigma^2}{2}\Delta m^e + \frac{1}{\mu}\nabla\cdot(m^e\nabla u^e). \tag{12}$$

### 2.3 Passing to the moving frame

When we introduced the ergodic state in subsection 2.2 we stressed the necessity of the absence of any explicit time dependence in the cost functional (2) for Eqs. (11)-(12) to be possible, which conflicts with the fact that we simulate the presence of the intruder by using a cylindrical potential whose position evolves with time. We thus change the reference frame in which we describe the experimental setting by passing from the point of view of the laboratory to the point of view of the cylinder, and define

$$\hat{u}(\vec{x}-\vec{s}t,t) = u(\vec{x},t), \quad \hat{m}(\vec{x}-\vec{s}t,t) = m(\vec{x},t).$$

In the framework of the cylinder the potential becomes $\hat{V}[\hat{m}] = g\hat{m} + \hat{U}_0(\vec{x})$, not depending explicitly on time anymore, and with

$$\hat{U}_0(\vec{x}) = \begin{cases} +\infty, & x < R, \\ 0, & \text{otherwise}, \end{cases} \tag{13}$$

where $R$ is the radius of the cylinder. For all other quantities we observe that, in general,

$$\partial_t f(\vec{x},t) = \frac{\mathrm{d}}{\mathrm{d}t}f(\vec{x},t) = \frac{\mathrm{d}}{\mathrm{d}t}\hat{f}(\vec{x}-\vec{s}t,t) = \partial_t\hat{f} - \vec{s}\cdot\vec{\nabla}\hat{f}, \tag{14}$$

where the total derivative is taken in the lab's reference frame. Using (14) in (HJB) and (KFP) gives us the time dependent version of the MFG equation in $\hat{u}$ and $\hat{m}$ variables in the moving frame

$$\partial_t\hat{u} - \vec{s}\cdot\vec{\nabla}\hat{u} = -\frac{\sigma^2}{2}\Delta\hat{u} + \frac{1}{2\mu}(\vec{\nabla}\hat{u})^2 + \gamma\hat{u} + \hat{V}[\hat{m}], \tag{15}$$

$$\partial_t\hat{m} - \vec{s}\cdot\vec{\nabla}\hat{m} = \frac{\sigma^2}{2}\Delta\hat{m} + \frac{1}{\mu}\nabla\cdot(\hat{m}\nabla\hat{u}), \tag{16}$$

whereas the corresponding equations for the ergodic state are

$$0 = -\frac{\sigma^2}{2}\Delta\hat{u}^e + \frac{1}{2\mu}(\vec{\nabla}\hat{u}^e)^2 + \vec{s}\cdot\vec{\nabla}\hat{u}^e + \gamma\hat{u}^e(x) + \hat{V}[\hat{m}^e], \tag{17}$$

$$0 = \frac{\sigma^2}{2}\Delta\hat{m}^e + \frac{1}{\mu}\nabla\cdot(\hat{m}^e\nabla\hat{u}^e) + \vec{s}\cdot\vec{\nabla}\hat{m}. \tag{18}$$

## 3 Parameter space of the model

In [1], it was shown that when $\gamma = 0$, the agents' dynamics is entirely characterized by two parameters, a length scale

$$\xi = \sqrt{\left|\frac{\mu\sigma^4}{2gm_0}\right|},$$

that by analogy with the non-linear Schrödinger context we refer to as the *healing length*, and a velocity scale

$$c_s = \sqrt{\left|\frac{gm_0}{2\mu}\right|},$$

that, for the same reason, we refer to as the *sound velocity*. Their physical meaning can be understood by imagining that the pedestrian crowd is subjected to a local perturbation. The healing length would then be the distance up to which the density would deform, and the sound velocity the speed at which the density would return to its initial unperturbed state when the perturbation is removed. If we then include the parameters $R$ and $s$ characterizing the intruding cylinder, we see that when $\gamma = 0$, our MFG model is entirely characterized by two dimensionless quantities, $\tilde{R} \equiv R/\xi$ and $\tilde{s} = s/c_s$.

As shown in Appendix D, the inclusion of a non-zero discount factor $\gamma$, which has the dimension of the inverse of a time, implies that the MFG model is now characterized by three dimensionless quantities, $\tilde{R}$, $\tilde{s}$ and a third one that we can take as either $\tilde{\gamma}^{(1)} \equiv (\xi/c_s)\gamma$ or $\tilde{\gamma}^{(2)} \equiv (R/s)\gamma$ (Note $\tilde{\gamma}^{(2)} = (\tilde{R}/\tilde{s})\tilde{\gamma}^{(1)}$). The first option, $\tilde{\gamma}^{(1)}$, compares the time scale associated with anticipation to the one of the crowd dynamics, while $\tilde{\gamma}^{(2)}$ measures it in terms of the time scale characterizing the cylinder.

Fig. 2 shows the numerical solution of the stationary equations (17) and (18) (see appendix C for a brief description of the numerical implementation) for four choices of $(\tilde{R}, \tilde{s})$ and different values of $\gamma$. Note that in the $(\tilde{R} \gg 1, \tilde{s} \gg 1)$ and $(\tilde{R} \ll 1, \tilde{s} \ll 1)$ quadrants, we have assumed $\tilde{R} \sim \tilde{s}$, so that $\tilde{\gamma}^{(1)} \sim \tilde{\gamma}^{(2)}$, and both of them are therefore either large together or small together. However in the quadrant $(\tilde{R} \gg 1, \tilde{s} \ll 1)$, we have $\tilde{\gamma}^{(2)} = (\tilde{R}/\tilde{s})\tilde{\gamma}^{(1)} \gg \gamma^{(1)}$, so we have distinguished the three possible cases $(\tilde{\gamma}^{(1)} \ll 1, \tilde{\gamma}^{(2)} \ll 1)$, $(\tilde{\gamma}^{(1)} \ll 1, \tilde{\gamma}^{(2)} \gg 1)$, and $(\tilde{\gamma}^{(1)} \gg 1, \tilde{\gamma}^{(2)} \gg 1)$; and in the same way in the quadrant $(\tilde{R} \ll 1, \tilde{s} \gg 1)$ where $\tilde{\gamma}^{(2)} \ll \gamma^{(1)}$ we distinguish the three cases $(\tilde{\gamma}^{(1)} \ll 1, \tilde{\gamma}^{(2)} \ll 1)$, $(\tilde{\gamma}^{(1)} \gg 1, \tilde{\gamma}^{(2)} \ll 1)$, and $(\tilde{\gamma}^{(1)} \gg 1, \tilde{\gamma}^{(2)} \gg 1)$.

Let us consider for instance the III quadrant, where both $\tilde{s}$ and $\tilde{R}$ are small. The fact that $\tilde{s}$ is small means that from the point of view of the crowd the cylinder is perceived as nearly immobile, which explains the rotational invariant shape of the solution. For small values of $\gamma$, the distance at which an immobile perturbation is felt by the crowd is, as mentioned above, given by the healing length $\xi$. As $\gamma$ increases this length should be compared to $d_{c_s} = c_s/\gamma$, the length scale related to the finitude of the anticipation horizon. Hence, from figure 3 we see that the scale of the density perturbation around the obstacle is given by the smallest between the $d_{c_s}$ and $\xi$. In this case, a large $\gamma$ does not, however, modify the qualitative aspect of the density distribution, which remains rotationally invariant.

Figure 4 then focuses on the I quadrant where both $\tilde{R}$ and $\tilde{s}$ are large. Because $\tilde{s}$ is large, the agents feel that the cylinder moves significantly more rapidly than the speed they can themselves maintain comfortably within the crowd. For low $\gamma$, they would therefore tend to anticipate the obstacle arrival by moving sideways quite early, which explains the low density corridor extending rather far in front of the cylinder in that case, typically at a distance of order $l_s = s\xi/c_s$. The density profile is in this case essentially symmetric, as for $\gamma = 0$ the system is invariant under the symmetry $(t \mapsto -t, y \mapsto -y)$. When $\gamma$ increases, $l_s$ should be compared with $d_s = s/\gamma$, which measure how far from the cylinder agents can foresee its motion. As illustrated on Figure 4 , we see that when $d_s < l_s$, the size of the perturbation in front of the

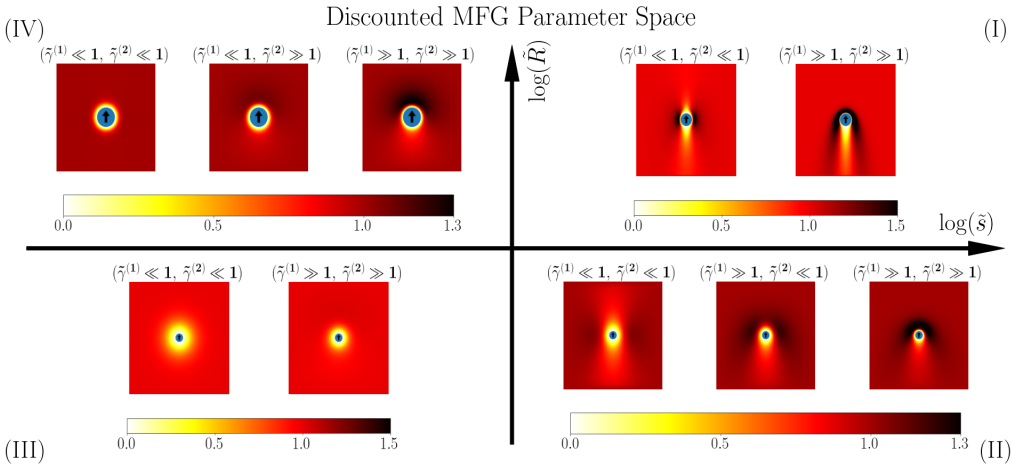


Figure 2: Exploration of parameter space of the MFG model. Each sub-figure represents the discounted stationary MFG density obtained solving (18) and (17). The axis represent the dimensionless quantities $\tilde{R} \equiv R/\xi$ and $\tilde{s} = s/c_s$. Each quadrant shows different values of $\tilde{\gamma}^{(1)} \equiv (\xi/c_s)\gamma$ (or $\tilde{\gamma}^{(2)} \equiv (R/s)\gamma$). We note that the choice of parameters best representing the experimental conditions lies in quadrant I, except for the case of Fig. 1c which lies at the boundary between quadrants I and II. Parameters of the sub-figures in each quadrant in format $\left(\tilde{s}, \tilde{R}; [\tilde{\gamma}^{(1)}]\right)$ [with $\tilde{\gamma}^{(2)} = (\tilde{R}/\tilde{s})\tilde{\gamma}^{(1)}$]: quadrant I $(3, 3; [.25, 5])$, quadrant II $(3, 0.3; [0.5, 5, 40])$, quadrant III $(0.3, 0.3; [0.25, 5])$, quadrant IV $(0.3, 3; [0, 0.45, 1.8])$.

cylinder is given by $l_s$. Contrarily to what happens in the third quadrant however, this change of scale qualitatively alters the solution, with a density blob forming in front of the cylinder and on the other hand a density profile behind the cylinder which is much less affected.

The variations of the density plots seen on quadrant II and IV are somewhat more complex since the four length scales $(\xi, l_s, d_{c_s}, d_s)$ are involved, but the mechanisms observed in Figure 3 and Figure 4 can be seen to be at work there too.

## 4 Comparisons with experiment

We now turn to the analysis of the experimental settings previously discussed. We will deal with the three different experimental configurations showed in Figure 1 separately. Our claim is that we can describe the three scenarios as the stationary state of our MFG model. This is already true for the frontal configuration, as was shown in [1]. Our goal is therefore to demonstrate that this is also true for the other two configurations. We will compare the experimental data to the density field $\hat{m}_e$ and to the velocity field $v(\vec{x}) = -[\mu^{-1}\nabla\hat{u}^e + \sigma^2(\nabla\hat{m}^e)/(2\hat{m}^e)]$ derived from the system Eqs. (18)-(17). For completeness, we have also solved the time dependent MFG equations (HJB)-(KFP) and in appendix C we compare their solution at intermediate times $t \simeq T/2$ to $\hat{m}_e$, and verify that they are as expected identical, the ergodic approach being however significantly faster and more precise.

### 4.1 Pedestrians facing the obstacle

In [1] we studied the case where pedestrians were facing the arriving cylinder. Under these circumstances, people could efficiently estimate the cylinder's size and velocity, thus the time it would take for the obstacle to reach them. We model such scenario by taking $\gamma = 0$, and the

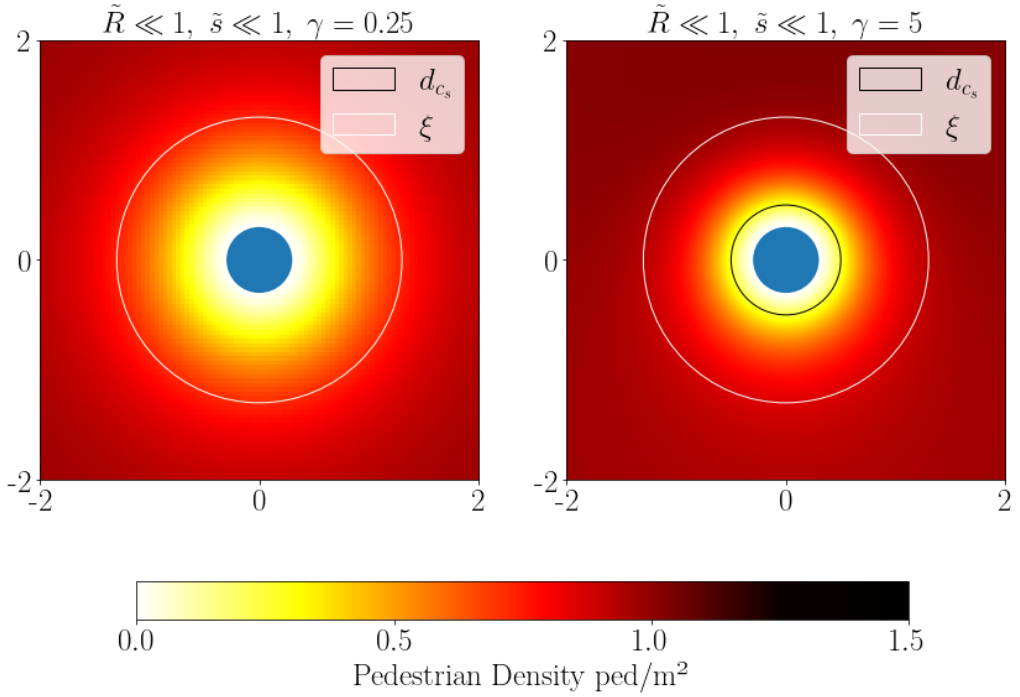


Figure 3: Focus on the quadrant III of Figure 2 with details about the size of the perturbation. The white circle has radius $R + \xi$ whereas the black circle has radius $R + d_{c_s}$, with $d_{c_s} \equiv c_s/\gamma$ (note that the left panel's black circle is not visible since $d_{c_s} = 4$). We observe how the smallest of the circles is the one governing the distance at which the perturbation due to the cylinder is felt.

simulation is shown on the left column of Figure 5. Here we see how striking the resemblance to the experiment is. Starting from the density plot, we clearly see the vertically symmetric distribution of pedestrians, with a depletion prior and posterior to the obstacle passage and with an increase on the sides. Moreover, the velocity field obtained from the MFG model correctly displays the lateral motion of pedestrians stepping aside to make room for the intruder. We believe MFG good performances should be attributed to an element that, as already discussed in [1], many pedestrian dynamics models, such as granular and social force models, struggle accounting for. This is the long term anticipatory behavior of individuals clearly captured in the experiment and naturally present in the very structure of MFG, namely by means of the backward-solved HJB equation (HJB). The back-propagation of information allows MFG agents to optimally anticipate the obstacle's arrival, and most notably *without prescribing an anticipation time*, contrarily to many models for crowds motion. Indeed, solving the MFG equations gives the Nash equilibrium velocity an agent should adopt for any given point in the simulated space, i.e. the strategy of motion which, in the spirit of (2), is best suited to avoid the obstacle and high density areas.

### 4.2 Pedestrians randomly oriented

In the experimental configuration where participants were asked to orient themselves randomly we see, from the right column of Figure 6, that the main difference with the frontal case is in the decrease of the depletion in front of the obstacle, meaning that participants anticipate less. We can imagine that, when participants were placed randomly, only some of them could gather information about the obstacle visually, whereas the rest had to resort to all their other senses to decide how to react. This impacts the global anticipatory behavior and

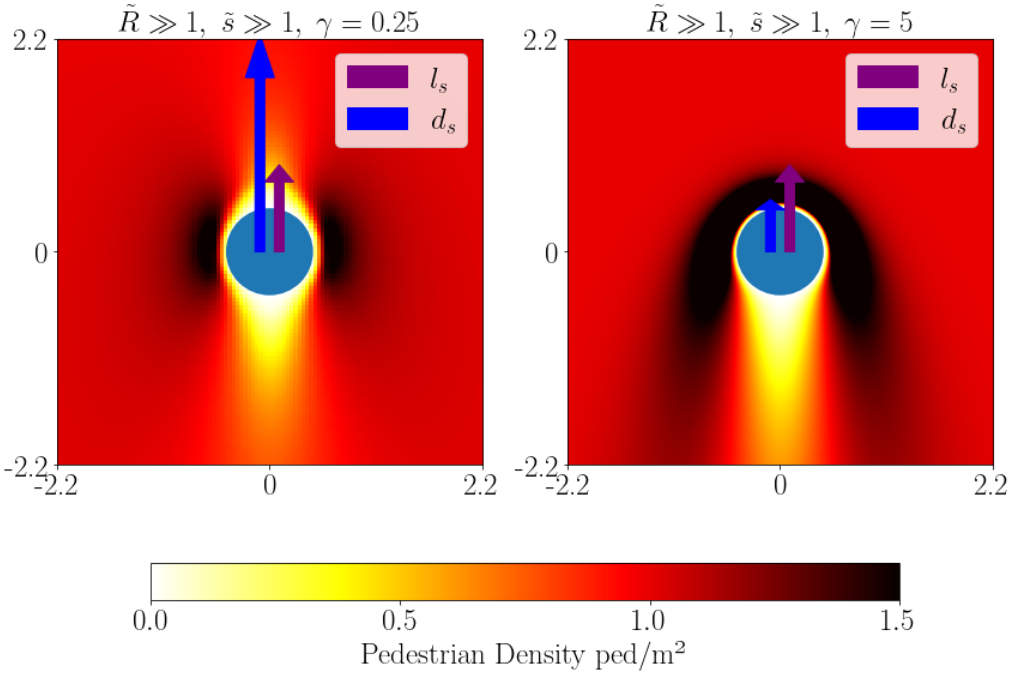


Figure 4: Focus on the quadrant I of Figure 2 with details about the size of the perturbation. The purple arrow's length is $R + l_s$, with $l_s \equiv s\xi/c_s$ the scale of the length at which agents should start moving to optimally avoid impact, whereas the blue arrow's length is $R + d_s$, where $d_s = s/\gamma$ represents how far the cylinder travels during time $1/\gamma$. It is apparent how a congestion in front of the cylinder appears when $d_s < l_s$, because the agents optimize only on a small portion of cylinder's trajectory.

causes a later reaction to the obstacle arrival. The inclusion of the discount factor $\gamma$ in our MFG is enough to describe the change in the crowd's avoidance strategy. The left column of Figure 6 shows the numerical solution of the MFG system for $\xi$ and $c_s$ as for the frontal case and with $\gamma = 0.5$. We can indeed observe that turning on the discount factor produces the desired effects, by reducing the crowd's displacement in front of the obstacle but still conserving the accumulation on the sides and the density depletion after its passage. Moreover, the simulated velocity field shows an increase in escaping dynamics in front of the cylinder and slight circulation around it.

### 4.3 Pedestrians giving their back to the obstacle

Finally, when participants in the experiment had to give their back to the obstacle and were asked not to anticipate, the observed behavior changed decisively. As the right panel of Figure 7 shows, having lost the visual information, it was harder to estimate the obstacle's velocity and direction of motion, resulting in pedestrians being pushed along by the intruder, and behaving like granular material [1]. Behind the cylinder, on the other hand, no significant depletion is shown, and this we believe is due to the diffusivity of the crowd, given the pedestrians' intention to have as much space as possible. The left column of Figure 7 shows the MFG simulation for $\xi = 0.4$, $c_s = 0.2$ and $\gamma = 6$. Here we recover the accumulation in front of the obstacle and the smaller depletion behind it. By looking at the velocity plots we clearly see that pedestrians in front of the cylinder are pushed by the intruder along the direction of its motion. Then, we also remark the agreement with the rotational motion around the obstacle, analogously to what would happen for granular inert matter, under purely mechanical forces. We managed to recover the experimental behavior mainly by means of the discount factor, slightly modifying

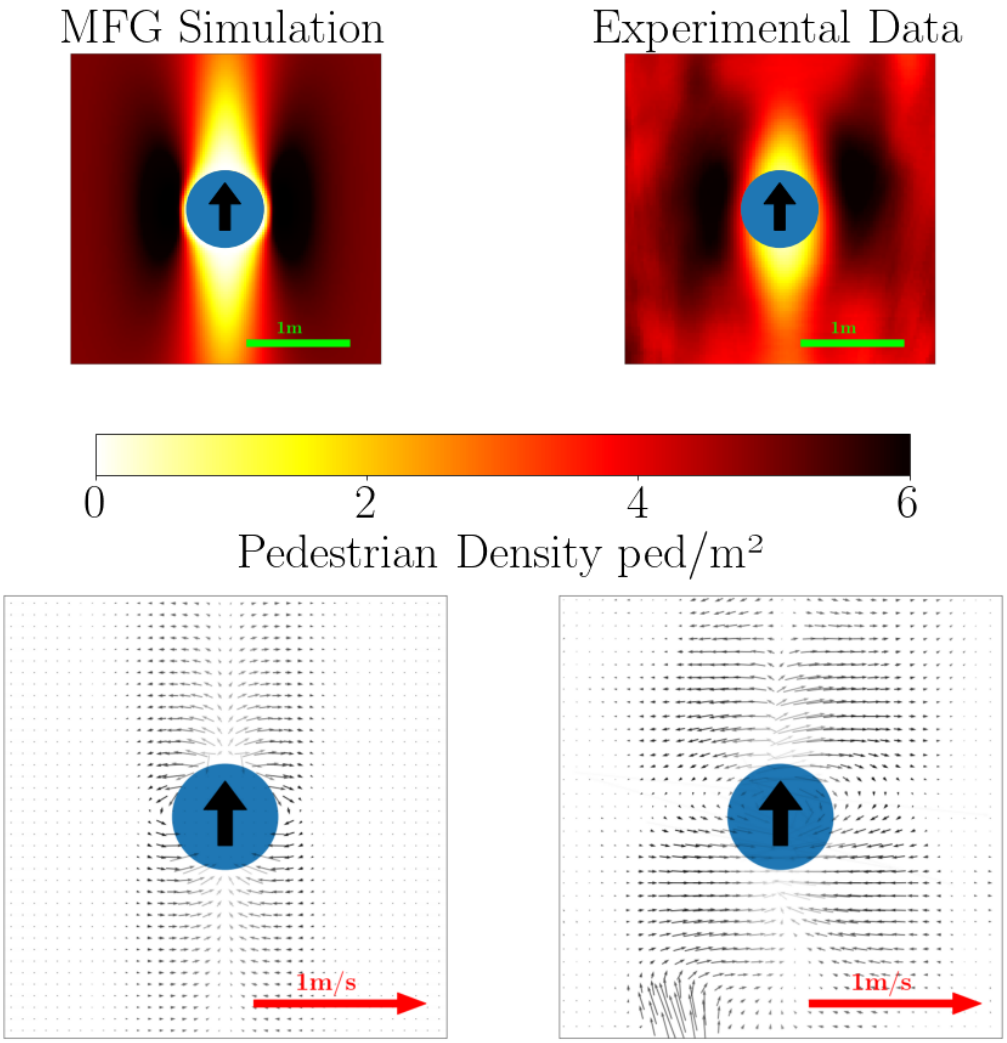


Figure 5: Qualitative comparison between density, first row, and velocity plots, second row, between the experiment, right column, and the ergodic state of the MFG model, with parameters $\xi = 0.2$, $c_s = 0.1$ and $\gamma = 0$, left column, for the case where all pedestrians were facing the incoming intruder. The green segment and the red arrow are a scale for distance and velocity respectively.

$\xi$ and $c_s$ to better fit the data, placing the solution at the boundary between quadrants I and II. This means that the discounting term correctly reproduces losses in anticipatory abilities.

## 5 Conclusion

In the present work we have provided a detailed description of the consequences of adding to the Mean-Field Games model used in [1] a term representing agents anticipation's horizon. Moreover, we have shown that such term helps modulating the simulated anticipatory behavior, making it possible to reproduce a wider range of crowd dynamic scenarios, as the comparison with the different experimental configurations has shown. This is all the more remarkable since we used the most simple and first ever proposed Mean-Field Game model [8], to which we just added a parameter, the discount factor. By using our MFG to describe, both quantitatively and qualitatively, the human behavior observed in this particular experiment,

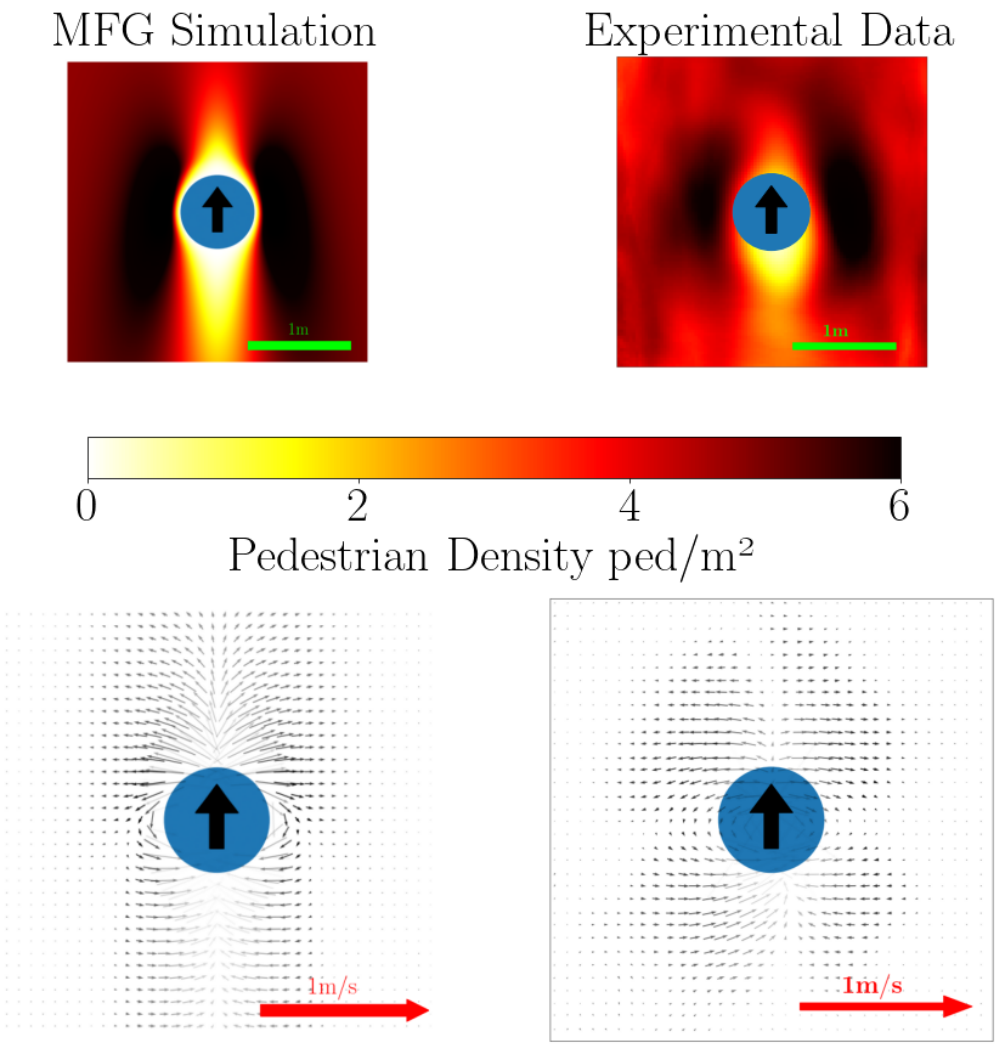


Figure 6: Qualitative comparison between density, first row, and velocity plots, second row, between the experiment, right column, and the ergodic state of the MFG model, with parameters $\xi = 0.2$, $c_s = 0.1$ and $\gamma = 0.5$, left column, for the case where pedestrians were oriented randomly.

we do not wish to imply that pedestrians solve a system of coupled differential equations while walking, but we highlight that at least in simple cases, individuals have internalized some basic anticipation mechanisms allowing them to rapidly coordinate with others and efficiently avoid eventual obstacles.

## Acknowledgements

We acknowledge the precious help of Alexandre Nicolas who prepared and provided the experimental data with the conventions used in this Paper. We thank Alberto Rosso for the discussions about this work and useful comments about the manuscript.

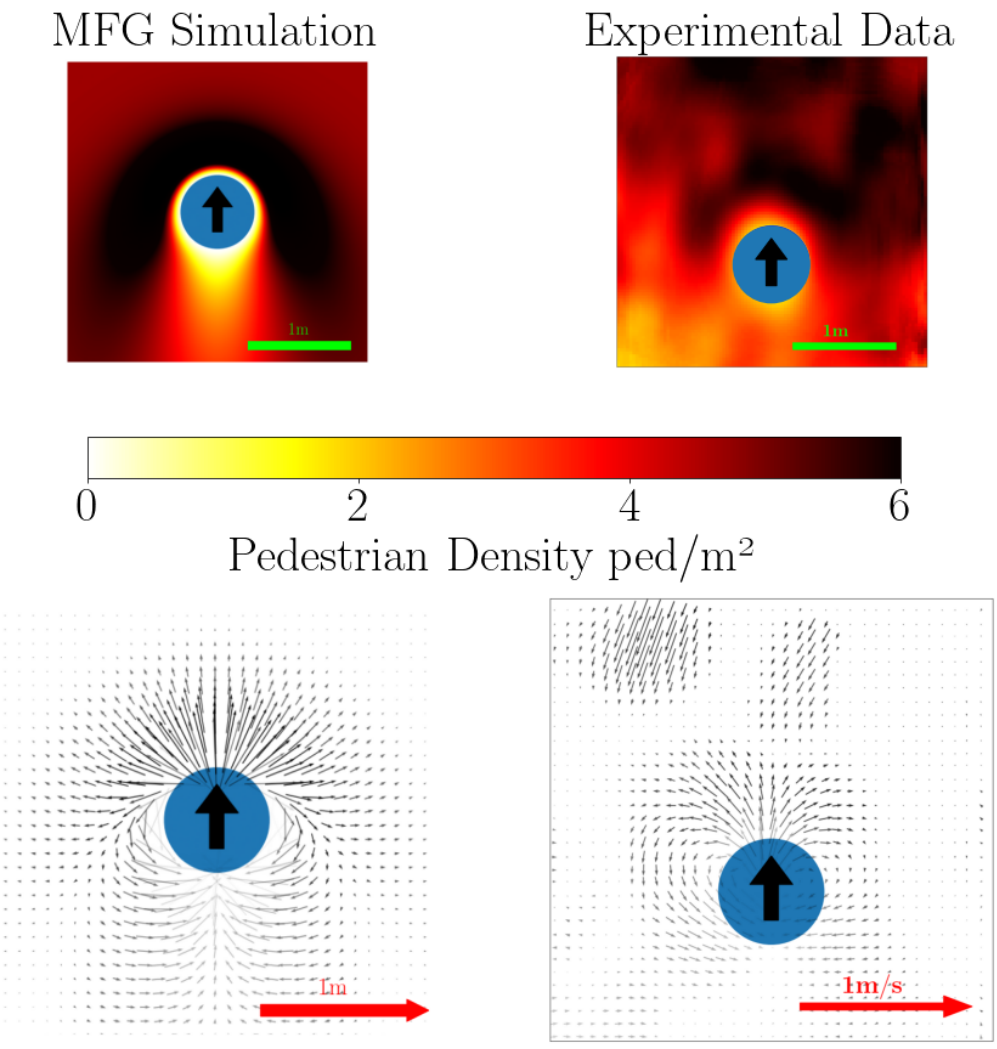


Figure 7: Qualitative comparison between density, first row, and velocity plots, second row, between the experiment, right column, and the ergodic state of the MFG model, with parameters $\xi = 0.4$, $c_s = 0.2$ and $\gamma = 6$, left column, for the case where pedestrians were giving their back to the incoming cylinder and were asked not to anticipate.

## A Derivation of the discounted HJB

Starting from the definition of the cost functional (2) we have

$$\begin{aligned} u(\vec{x},t) &= \inf_{\vec{a}} \mathbb{E}\left\{\int_t^T \mathcal{L}(\vec{x},\tau)[m]e^{\gamma(t-\tau)}d\tau + e^{\gamma(t-T)}c_T(\vec{x}_T)\right\} \\ &= \inf_{\vec{a}} \mathbb{E}\left\{\int_t^{t+dt} \mathcal{L}(\vec{x},\tau)[m]e^{\gamma(t-\tau)}d\tau + e^{-\gamma dt} \right. \\ &\qquad \left. \times \left(\int_{t+dt}^T \mathcal{L}(\vec{x},\tau)[m]e^{\gamma(t+dt-\tau)}d\tau + e^{\gamma(t+dt-T)}c_T(\vec{x}_T)\right)\right\}. \end{aligned}$$

Making use of the *dynamic programming principle* [19], this can be written as

$$\begin{aligned} u(\vec{x},t) &= \inf_{\vec{a}}\left[\mathcal{L}(\vec{x},t)[m]dt + e^{-\gamma dt}u(\vec{x}+d\vec{x},t+dt)\right] \\ &\overset{\text{Ito}}{=} \inf_{\vec{a}}\left\{\mathcal{L}(\vec{x},t)[m]dt + (1-\gamma dt)\left[u(\vec{x},t) + dt\left(\partial_t u + \vec{a}\cdot\vec{\nabla}u + \frac{\sigma^2}{2}\Delta u\right)\right]\right\}, \end{aligned}$$

where in the last passage the Ito chain rule has been used to calculate the total time derivative of the value function. Then, by keeping only terms of order one in $dt$ we obtain

$$0 = \partial_t u - V[m] + \frac{\sigma^2}{2}\Delta u - \gamma u + \inf_{\vec{a}}\left\{\frac{\mu}{2}\vec{a}^2 + \vec{a}\cdot\vec{\nabla}u\right\}. \tag{A.1}$$

At this point, by minimizing the term in the curly brackets with respect to $\vec{a}$ we find that the optimal velocity is given by

$$\vec{a}^* = -\frac{\vec{\nabla}u}{\mu}. \tag{A.2}$$

Finally, (A.2) is plugged back in (A.1) to obtain (HJB).

## B Alternative formulation of MFG

In [1], we took advantage of the fact that by applying the Cole-Hopf transformation

$$u(\vec{x},t) = -\mu\sigma^2\log\Phi(\vec{x},t), \tag{B.1}$$

one can cast the MFG equation in a form more familiar to physicists. Now, substituting (B.1) into equation (HJB) we obtain

$$\mu\sigma^2\partial_t\Phi = -\frac{\mu\sigma^4}{2}\Delta\Phi - V[m]\Phi + \gamma\mu\sigma^2\Phi\log\Phi. \tag{B.2}$$

The second part of this transformation amounts to defining $\Gamma(\vec{x},t) = \frac{m(\vec{x},t)}{\Phi(x,t)}$ which, when plugged inside the KFP equation (KFP) yields

$$\mu\sigma^2\partial_t\Gamma = \frac{\mu\sigma^4}{2}\Delta\Gamma + V[m]\Gamma - \gamma\mu\sigma^2\Gamma\log m + \gamma\mu\sigma^2\Gamma\log\Gamma. \tag{B.3}$$

The stationary equations are

$$-\frac{\mu\sigma^4}{2}\Delta\Phi^e - V[m^e]\Phi^e + \gamma\mu\sigma^2\Phi^e\log\Phi^e = 0, \tag{B.4}$$

$$\frac{\mu\sigma^4}{2}\Delta\Gamma^e + V[m^e]\Gamma^e - \gamma\mu\sigma^2\Gamma^e\log\Phi^e\Gamma^e + \gamma\mu\sigma^2\Gamma^e\log\Gamma^e = 0. \tag{B.5}$$

When passing to the moving frame, as in 2.3, the time dependent MFG in the Cole-Hopf settings becomes

$$\mu\sigma^2\partial_t\hat{\Phi} - \mu\sigma^2\vec{s}\cdot\vec{\nabla}\hat{\Phi} = -\frac{\mu\sigma^4}{2}\Delta\hat{\Phi} - V[m]\hat{\Phi} + \gamma\mu\sigma^2\hat{\Phi}\log\hat{\Phi}\,, \tag{B.6}$$

$$\mu\sigma^2\partial_t\hat{\Gamma} - \mu\sigma^2\vec{s}\cdot\vec{\nabla}\hat{\Gamma} = \frac{\mu\sigma^4}{2}\Delta\hat{\Gamma} + V[m]\hat{\Gamma} - \gamma\mu\sigma^2\hat{\Gamma}\log m + \gamma\mu\sigma^2\hat{\Gamma}\log\hat{\Gamma}\,, \tag{B.7}$$

whereas from (B.4) and (B.5) we get the corresponding equations for the stationary state

$$-\frac{\mu\sigma^4}{2}\Delta\hat{\Phi}^e - V[m_0]\hat{\Phi}^e + \gamma\mu\sigma^2\hat{\Phi}^e\log\hat{\Phi}^e + \mu\sigma^2\vec{s}\cdot\vec{\nabla}\hat{\Phi}^e = 0\,, \tag{B.8}$$

$$\frac{\mu\sigma^4}{2}\Delta\hat{\Gamma}^e + V[m_0]\hat{\Gamma}^e - \gamma\mu\sigma^2\hat{\Gamma}^e\log m + \gamma\mu\sigma^2\hat{\Gamma}^e\log\hat{\Gamma}^e + \mu\sigma^2\vec{s}\cdot\vec{\nabla}\hat{\Gamma}^e = 0\,. \tag{B.9}$$

Now, if $\gamma = 0$, we see that these equations are similar to the Non-linear Schrödinger equation in a moving frame, and in [1] we explain that casting the problem in this form is beneficial to the development of efficient numerical schemes, especially for the stationary state of MFG. Unfortunately the presence of the logarithmic term does pose significant problems for the numerical implementation when $\gamma > 0$, if one tries to solve for the stationary state in this formulation. However, as explained in appendix C, this form of the MFG equations is instrumental in curing the divergences occurring near the obstacle in the original $(m,u)$ formulation of the MFG equations.

## C Brief description of the numerical scheme

Figures 5, 6 and 7 compare the stationary state of our MFG model to the experimental data collected in [7]. The stationary states shown there, as well as in Fig. 2, are obtained solving directly equations (17) and (18), using an algorithm which at its core is related to the one used in [1] for the stationary state. This consists in choosing a grid representing the space, in this case the 2d area where the experiment took place. Then, for each site $i$, both $\hat{m}^e_i$ and $\hat{u}^e_i$ are expressed as functions of neighboring sites. By starting from an initial guess, the values of $\hat{u}^e$ and $\hat{m}^e$ are updated until convergence.

Within the $(\hat{u}^e, \hat{m}^e)$ variables, this approach fails however near hard walls, or here near the cylinder, where the value function $u$ shows a logarithmic divergence. This is why in [1] we applied this method to the equations in their NLS form (i.e. with the variables $(\hat{\Phi}^e, \hat{\Gamma}^e)$). Unfortunately, as explained in appendix B, when $\gamma \neq 0$ the MFG equations in the $(\hat{\Phi}^e, \hat{\Gamma}^e)$ variables imply a logarithm, and this logarithm makes this approach unfeasible.

For finite $\gamma$, it is therefore necessary to mix the solution of the equations in both formulations, and more specifically to solve the problem expressed in the $(\hat{\Phi}^e, \hat{\Gamma}^e)$ variables near the obstacles, and in its original $(\hat{u}^e, \hat{m}^e)$ form away from it. This has proven to be a very reliable and fast algorithm, allowing us to directly compute the solution of the ergodic state. More details on this method will be provided in a future publication.

As a check of coherence, we also have solved the time dependent MFG system, to verify that the solution we obtain solving (18) is the same to what we get by taking the solution of (16) at $t = T/2$. We solved the time dependent problem using the Matlab routine ode45. Figures 8 and 9 show the results of this comparison for the choice of parameters used in Figs. 6 and 7 demonstrating that the two approaches indeed give the same result. The ergodic approach is, however, significantly faster and more precise, in particular because the time-dependent approach, being performed in the lab reference frame, requires a large system.

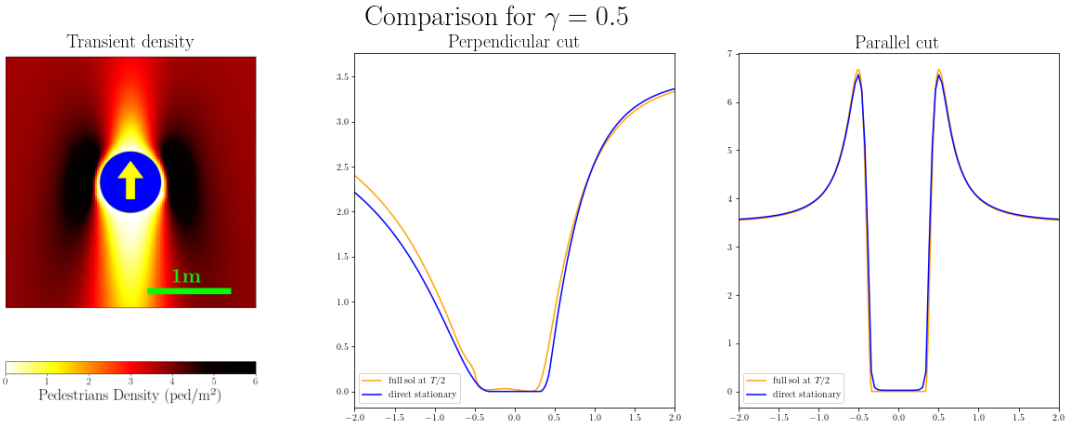


Figure 8: Middle and right panels: density profiles of the discounted MFG stationary state along a vertical (middle) and horizontal (right) cut passing through the center of the cylinder. The curves compare the solution obtained solving directly Eqs. (18)-(17) (blue line) and the one obtained from the time dependent Eqs. (HJB)-(KFP) and taking the solution at $T/2$ (orange line). Left panel: density plot obtained from the time dependent Eqs. (HJB)-(KFP). The parameters of the simulations are the same as in Fig. 6 (corresponding to $\gamma = 0.5$).

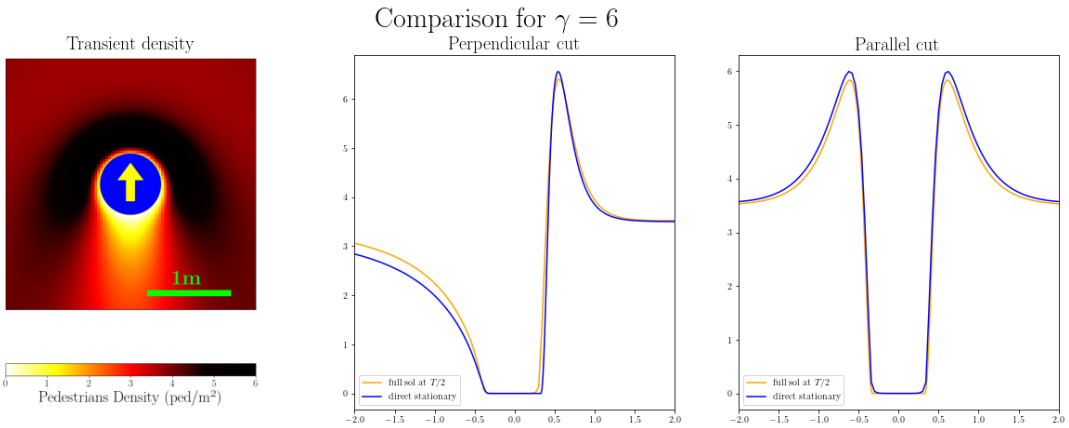


Figure 9: Same as in Fig. 8, but for the parameters of Fig. 7(corresponding to $\gamma = 6$).

## D Dimensionless equations

In section 3 we have introduced the length scale $\xi$ and velocity scale $c_s$, which are such that at $\gamma = 0$, the solution of the MFG equations are entirely determined by the dimensionless ratio $\tilde{R} = R/\xi$, and $\tilde{s} = s/c_s$.

Considering now $\gamma \neq 0$, let us introduce the scaled variables $\tilde{x} = x/\xi$, and $\tilde{t} = t/\tau$, where $\tau$ is the characteristic time scale of the system obtained as $\tau = \xi/c_s$. Substituting these in (15) we get

$$\frac{\partial_{\tilde{t}} u}{\tau} = -\frac{\sigma^2}{2\xi^2}\Delta_{\tilde{x}\tilde{x}} u + \frac{(\vec{\nabla}_{\tilde{x}} u)^2}{2\mu\xi^2} + \gamma u + \frac{c_s}{\xi}\vec{\tilde{s}} \cdot \vec{\nabla}_{\tilde{x}} u + gm + U_0(\tilde{x}\xi, \tilde{R}\xi)\,. \tag{D.1}$$

Introducing now $\tilde{a}^* = a^*/c_s$ the scaled optimal velocity, we see that if we want to define it as $\tilde{a}^* = -\partial_{\tilde{x}}\tilde{u}$ this implies to define the scaled value function as $\tilde{u} = u/(\mu\xi c_s) = 2u/(\mu\sigma^2)$. Noting furthermore than the definition Eq. (13) of $U_0$ implies $U_0(\tilde{x}\xi, \tilde{R}\xi) = U_0(\tilde{x}, \tilde{R})$, Eq. (D.1)

reads

$$\partial_{\tilde{t}}\tilde{u} = -\Delta^2_{\tilde{x}\tilde{x}}\tilde{u} + \frac{(\vec{\Delta}_{\tilde{x}}\tilde{u})^2}{2} + \tilde{\gamma}^{(1)}\tilde{u} + \vec{\tilde{s}}\cdot\vec{\nabla}_{\tilde{x}}\tilde{u} + \frac{m}{m_0} + U_0(\tilde{x},\tilde{R})\,, \tag{D.2}$$

with $\tilde{\gamma}^{(1)} = \gamma\tau$ is the scaled discount ratio. Applying the same scaling to Eq. (16) we obtain the dimensionless KFP equation

$$\partial_{\tilde{t}} m = \Delta_{\tilde{x}\tilde{x}} m + \vec{\nabla}_{\tilde{x}}\cdot(m\vec{\nabla}_{\tilde{x}}\tilde{u}) + \vec{\tilde{s}}\cdot\vec{\nabla}_{\tilde{x}} m\,. \tag{D.3}$$

Up to a scaling, the solution of our model is therefore entirely determined by the scaled quantities $\left(\tilde{R},\tilde{s},\tilde{\gamma}^{(1)}\right)$, or equivalently $\left(\tilde{R},\tilde{s},\tilde{\gamma}^{(2)}\right)$ where $\tilde{\gamma}^{(2)} = (\tilde{R}/\tilde{s})\tilde{\gamma}^{(1)}$.

## References


[1] T. Bonnemain, M. Butano, T. Bonnet, I. Echeverría-Huarte, A. Seguin, A. Nicolas, C. Appert-Rolland and D. Ullmo, *Pedestrians in static crowds are not grains, but game players*, Phys. Rev. E **107**, 024612 (2023), doi:10.1103/PhysRevE.107.024612.

[2] S. P. Hoogendoorn and P. H. L. Bovy, *Pedestrian route-choice and activity scheduling theory and models*, Transp. Res. B: Methodol. **38**, 169 (2004), doi:10.1016/S0191-2615(03)00007-9.

[3] D. Helbing and P. Molnár, *Social force model for pedestrian dynamics*, Phys. Rev. E **51**, 4282 (1995), doi:10.1103/physreve.51.4282.

[4] F. Zanlungo, T. Ikeda and T. Kanda, *Social force model with explicit collision prediction*, Europhys. Lett. **93**, 68005 (2011), doi:10.1209/0295-5075/93/68005.

[5] I. Karamouzas, B. Skinner and S. J. Guy, *Universal power law governing pedestrian interactions*, Phys. Rev. Lett. **113**, 238701 (2014), doi:10.1103/PhysRevLett.113.238701.

[6] I. Echeverría-Huarte and A. Nicolas, *Body and mind: Decoding the dynamics of pedestrians and the effect of smartphone distraction by coupling mechanical and decisional processes*, Transp. Res. C: Emerg. Technol. **157**, 104365 (2023), doi:10.1016/j.trc.2023.104365.

[7] A. Nicolas, M. Kuperman, S. Ibañez, S. Bouzat and C. Appert-Rolland, *Mechanical response of dense pedestrian crowds to the crossing of intruders*, Sci. Rep. **9**, 105 (2019), doi:10.1038/s41598-018-36711-7.

[8] J.-M. Lasry and P.-L. Lions, *Jeux à champ moyen. I - Le cas stationnaire*, C. R. Acad. Sci. Paris **343**, 619 (2006), doi:10.1016/j.crma.2006.09.019.

[9] J.-M. Lasry and P.-L. Lions, *Jeux à champ moyen. II - Horizon fini et contrôle optimal*, C. R. Acad. Sci. Paris **343**, 679 (2006), doi:10.1016/j.crma.2006.09.018.

[10] M. Huang, R. P. Malhamé and P. E. Caines, *Large population stochastic dynamic games: Closed-loop McKean-Vlasov systems and the nash certainty equivalence principle*, Commun. Inf. Syst. **6**, 221 (2006).

[11] P. Cardaliaguet, *Notes on mean field games*, Collège de France, Paris, France (2013), https://www.ceremade.dauphine.fr/~cardaliaguet/MFG20130420.pdf.

[12] D. A. Gomes and J. Saúde, *Mean field games models — A brief survey*, Dyn Games Appl **4**, 110 (2013), doi:10.1007/s13235-013-0099-2.

[13] A. Bensoussan, J. Frehse and S. C. P. Yam, *The master equation in mean field theory*, J. Math. Pures Appl. **103**, 1441 (2015), doi:10.1016/j.matpur.2014.11.005.

[14] P. Cardaliaguet, F. Delarue, J.-M. Lasry and P.-L. Lions, *The master equation and the convergence problem in mean field games*, Princeton University Press, Princeton, USA, ISBN 9780691193717 (2019), doi:10.23943/princeton/9780691190716.001.0001.

[15] R. Carmona and F. Delarue, *Probabilistic analysis of mean-field games*, SIAM J. Control Optim. **51**, 2705 (2013), doi:10.1137/120883499.

[16] A. Lachapelle and M.-T. Wolfram, *On a mean field game approach modeling congestion and aversion in pedestrian crowds*, Transp. Res. B: Methodol. **45**, 1572 (2011), doi:10.1016/j.trb.2011.07.011.

[17] D. Ullmo, I. Swiecicki and T. Gobron, *Quadratic mean field games*, Phys. Rep. **799**, 1 (2019), doi:10.1016/j.physrep.2019.01.001.

[18] P. Cardaliaguet, J.-M. Lasry, P.-L. Lions and A. Porretta, *Long time average of mean field games with a nonlocal coupling*, SIAM J. Control Optim. **51**, 3558 (2013), doi:10.1137/120904184.

[19] R. E. Bellman, *Dynamic programming*, Princeton University Press, Princeton, USA, ISBN 9780691146683 (2010), doi:10.1515/9781400835386.